MORPHOMETRICS AND ORIENTATION OF *FRACTOFUSUS* DOMINATED ASSEMBLAGES FROM THE EDIACARAN OF NEWFOUNDLAND

By © Jenna Neville

A Thesis submitted to the School of Graduate Studies in partial fulfillment of the requirements

for the degree of

Master of Science

Department of Earth Sciences

Memorial University of Newfoundland

December 2023

St. John's, Newfoundland and Labrador

Abstract

The rangeomorph genus *Fractofusus* inhabited marine benthic environments during the Ediacaran period. These frondlike organisms with fractal-like branching are believed to be among the earliest multicellular animals. Studying their paleobiology, paleoecology and interactions with their paleoenvironment is crucial for understanding early animal evolution. This study compared morphometric and orientation data of *Fractofusus misrai* (from Mistaken Point, NL) and *Fractofusus andersoni* (from Little Catalina, NL) in order to better understand population structure and paleoecology. Statistical analyses were conducted to infer size and shape classes, and to determine any significant orientation differences between the shape groups. This work indicates that the *F. misrai* assemblage on the E surface likely resulted from aseasonal continuous reproduction following a single spatfall event while the *F. andersoni* assemblage on the H14 surface is comprised of two spatfall events. Previous studies have suggested that *Fractofusus* is randomly oriented, key evidence used to infer a reclining mode of life. This study has revealed orientation trends based on shape, with proportionally wider specimens oriented to the southeast and more elongated specimens being oriented towards the northeast. These findings suggest that some aspect of the paleobiology of *Fractofusus* may have been controlled by current-related phenomena (possibly oxygen or nutrient capture).

Co-Authorship Statement

The design of the research topic of this Master's thesis was determined in collaboration with Dr. Duncan McIlroy as an expansion of my Undergraduate Honours Thesis. The large undertaking of field work and data collection were completed with the assistance of members of Dr. Duncan McIlroy's research group: Daniel Pérez Pinedo, Giovanni Passinetti, Christopher Mckean, and Hayley Fitzgerald. The statistical analyses performed in R were completed with the support of Daniel Pérez Pinedo. I completed statistical interpretation and thesis writing with editorial support from Dr. Duncan McIlroy, as well as Dr. Rod Taylor and Dr. Suzanne Dufour. While I am lead author, due to their contributions to this project, Dr. Duncan McIlroy and Daniel Pérez Pinedo are co-authors.

Acknowledgements

I would like to thank my supervisor, Dr. Duncan McIlroy, for the vast amount of time, support and encouragement given for this project. Thank you to my committee members, Dr. Rod Taylor and Dr. Suzanne Dufour. Thank you to the members of Dr. Duncan McIlroy's research group, Daniel Pérez Pinedo, Giovanni Passinetti, Christopher Mckean, and Hayley Fitzgerald, for all of the assistance given to this project, and companionship provided along the way.

Thank you to my parents and my fiancé, for always encouraging me through my academic journey.

Table of Contents

List of Tables

List of Figures

List of Abbreviations and Symbols

BIC   Bayesian information criterion

DCA   detrended correspondence analysis

EM   expectation maximization

NMDS   non-metric multidimensional scaling

PCA   principal component analysis

PCoA   principial coordinate analysis

r   correlation coefficient

List of Appendices

1. Introduction

The Ediacaran biota (~575-542 Ma) represents a critical point in life evolution encompassing the appearance of the first large complex organisms, and is considered to include three main time-related assemblages: The Avalon, White Sea and Nama assemblages (Waggoner, 2003; Narbonne, 2005). The Avalon Assemblage is the oldest, consisting of unique deep-marine—predominantly non-motile—frondlike organisms, and has been found in Avalonia (e.g. Newfoundland and England) and Laurentia (e.g. western Canada) (Waggoner, 2003). Many of the Avalon Assemblage taxa are frondose fossils, consisting of one or more fronds that were either reclining or attached to the seafloor by a holdfast. In the Rangeomorpha the fronds are made up of self-similar branches, and commonly include a stem and disc (e.g. Brasier et al., 2012), while other frondose taxa such as the Arboreomorpha and other *incertae sedis* have less complex morphologies. Even within Newfoundland, the Avalon Assemblage differs slightly between the fossil localities, for example, the biota of Mistaken Point is dominated by *Fractofusus misrai* and has a number of taxa unknown on the Bonavista Peninsula, where the most common taxon is *Fractofusus andersoni* (e.g. Hofmann et al., 2008; Matthews et al., 2021).

Ediacaran fossils were first discovered at Mistaken Point in 1967 (Anderson and Misra, 1968) and not reported from the Bonavista Peninsula until much later (O'Brien and King, 2005). The Mistaken Point biota contains twenty-two species, while eighteen species are currently reported from the Bonavista Peninsula. The two regions share several taxa—many of which belong to the extinct clade Rangeomorpha—but have differing stratigraphic ranges in the two regions (Hofmann et al., 2008; Mason et al., 2013; Matthews et al., 2021). The Rangeomorpha is a clade of frondose multicellular soft-bodied organisms with fractal-like self-similar branching whose affinities have been much debated and variously attributed to the Metazoa, the Protozoa or the

Holomycota, though ultimately, their phylogenetic position has yet to be unequivocally determined (Seilacher et al., 2003; Peterson et al., 2003; Narbonne, 2005; Gehling and Narbonne, 2007; Liu and Matthews, 2017; Dunn et al., 2018). The rangeomorph genus *Fractofusus* (*F. misrai and F. andersoni*) is one of the few taxa that is universally accepted as having been a bottom-dwelling recliner. The genus is likely endemic to Newfoundland, since the only other report is from northwestern Canada of a poorly preserved fusiform Ediacaran fossil (Narbonne et al., 2014), however it lacks rangeomorph branching and is considered dubious herein. *Fractofusus* was chosen as the primary focus of this study because of its high abundance on some large highly fossiliferous horizons making it ideal for a variety of statistical analyses. Since *F. misrai* is the most abundant species on the E surface at Mistaken Point, Avalon Peninsula (e.g. Gehling and Narbonne, 2007), and *F. andersoni* is the most abundant species on the H14 surface at Little Catalina, Bonavista Peninsula (e.g. O'Brien and King, 2005; Hofmann et al., 2008; Mitchell et al., 2015; Fig. 1.1), these surfaces were chosen for detailed integrated morphometric and paleocurrent analysis.

Previous studies of *Fractofusus* have used: 1) morphology to infer modes of growth (e.g. Gehling and Narbonne, 2007; Brasier and Antcliffe, 2009; Brasier et al., 2012); 2) specimen orientation to make inferences about paleoenvironment (e.g. Seilacher, 1999; Gehling and Narbonne, 2007; Mitchell et al., 2015; Vixseboxse et al., 2021; Pérez-Pinedo et al., 2023); and 3) spatial distribution within assemblages to infer paleoecology (e.g. Clapham et al., 2003; Mitchell et al., 2015). The purpose of this study was to analyze morphometric and orientational data derived from fossil specimens of *Fractofusus* on the E surface at Mistaken Point and the H14 surface at Little Catalina in an integrated way to explore the effects of paleocurrents on morphology and growth. The work undertaken allowed conclusions to be made concerning population structure and

2

assessment of possible modes of reproduction, and—when combined with orientation trends—it allowed determination of how *Fractofusus* may have grown in response to paleoenvironmental conditions.
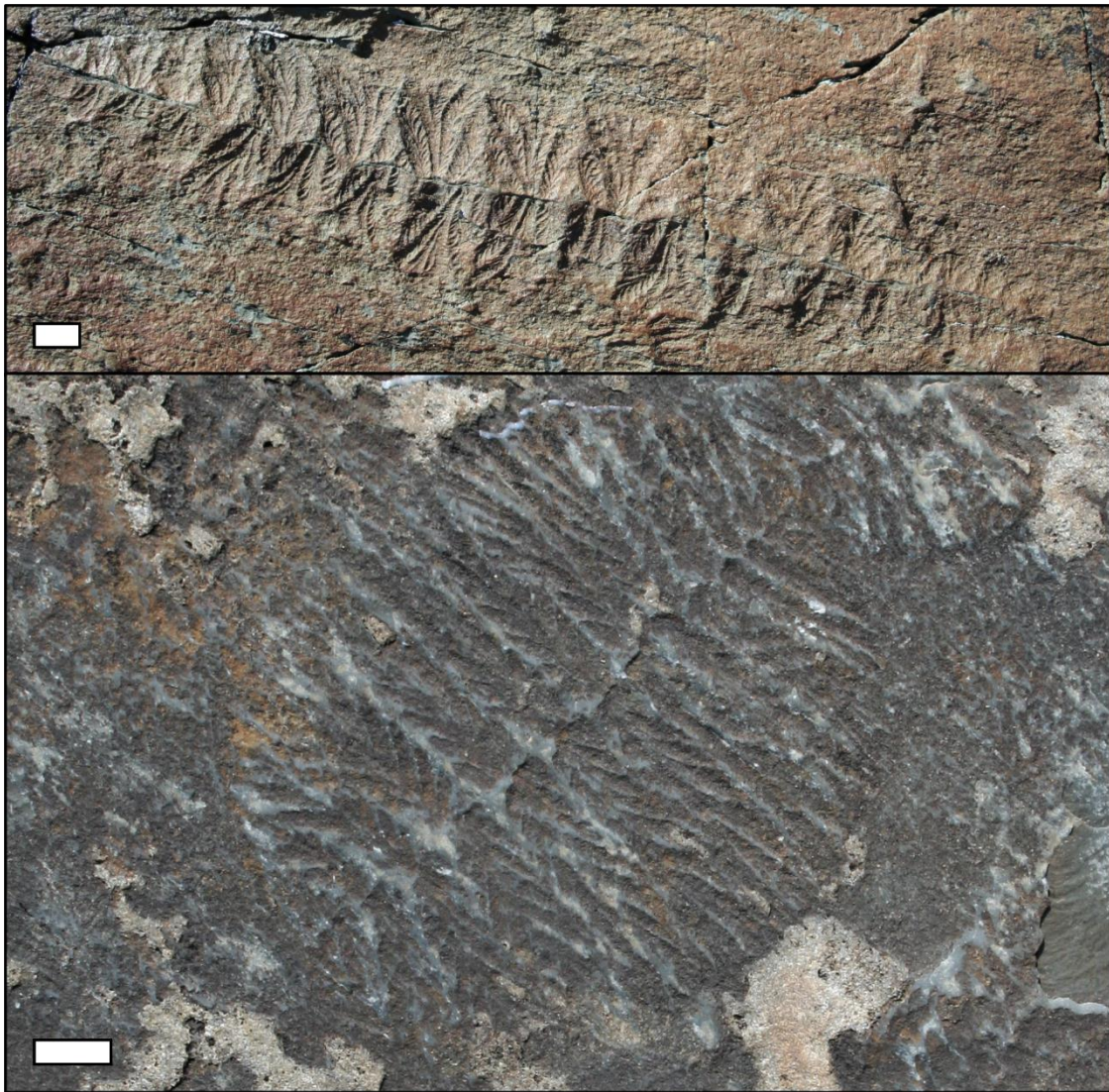
Fig. 1.1. *Fractofusus misrai* from the E surface at Mistaken Point (top) and *Fractofusus andersoni* from the H14 surface at Little Catalina (bottom). Scale: 1 cm.

1.1 Geologic Setting

The Avalon Zone of the island of Newfoundland is well known for its Ediacaran fossils, which have been found in the Conception and St. John's Groups, a deep marine slope to basin floor turbidite-dominated volcano-sedimentary stratigraphic section, interpreted to have been deposited in a broadly upward shallowing basin adjacent to a volcanic arc (Benus, 1988; Wood et al., 2003; Matthews et al., 2021). This stratigraphic succession has been lithostratigraphically correlated between the Catalina Dome of the Bonavista Peninsula and Mistaken Point, though the stratigraphic succession is thinner, and many of the shared species persist to stratigraphically higher levels, in the Catalina Dome (Narbonne, 2005; Hofmann et al., 2008; Mason et al., 2013; Fig. 1.2). This lithostratigraphic correlation is in urgent need of geochronologic corroboration as there is no biostratigraphical rationale for the correlations.

This study focused partly on *Fractofusus misrai*, best known from the E surface at Mistaken Point but also known from two other levels in the ~290m thick Mistaken Point Formation, and has also been reported from the underlying Briscal Formation (Gehling and Narbonne, 2007; Matthews et al., 2021; Fig. 1.2). Also considered was an assemblage of the abundant *F. andersoni* on the H14 surface at Little Catalina, from the ~80m thick Catalina Member of the Trepassey Formation, the only formation on the Bonavista Peninsula known to have this species (O'Brien and King, 2005; Gehling and Narbonne, 2007; Hofmann et al., 2008).

The volcanic ash bed overlying the E surface at Mistaken Point has been re-dated to 565 +/- 0.64 Ma (Matthews et al., 2021), and lithostratigraphic correlation suggests that the H14 surface might be approximately the same age (Hofmann et al., 2008).
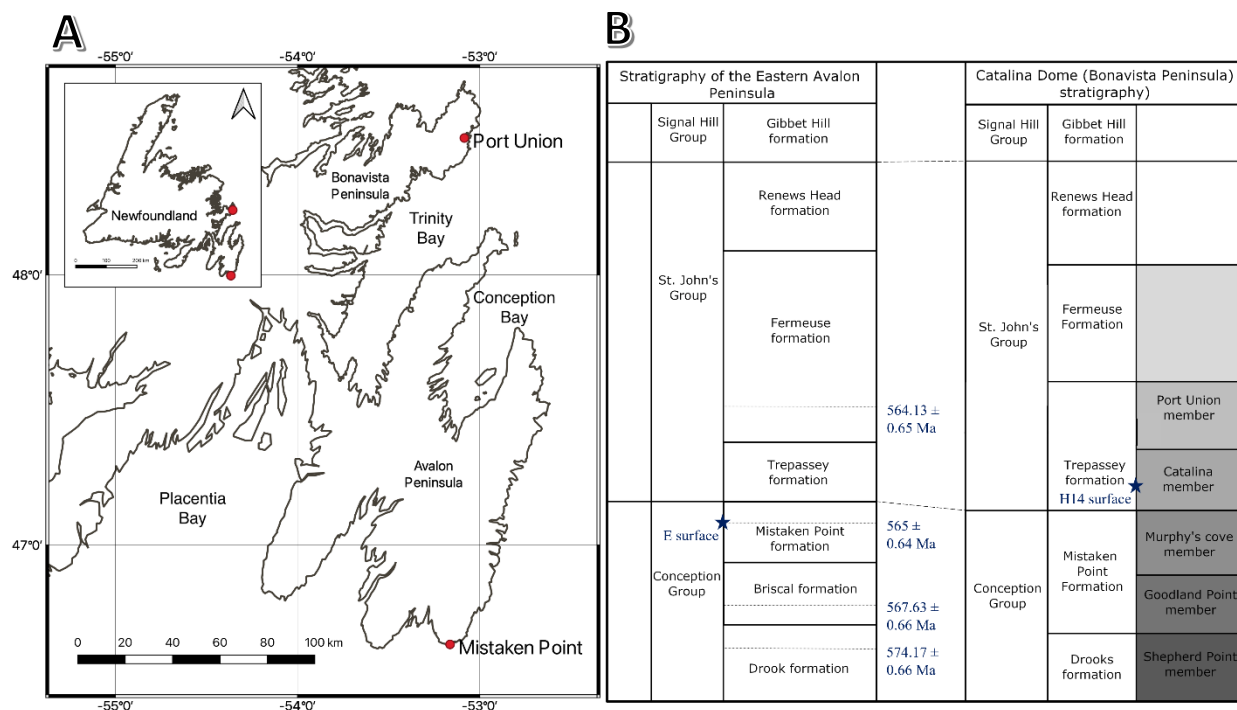
Fig. 1.2.A, Location map of Southeastern Newfoundland; **B**, Lithostratigraphy of the Mistaken Point area (Matthews et al., 2021) and the Bonavista Peninsula (Hofmann et al., 2008).

1.2 Paleoenvironment

The stratigraphic section containing the Avalon Assemblage in Southeastern Newfoundland has been interpreted as having been deposited in a turbidity/density flow dominated slope to basin floor system adjacent to a volcanic arc (Benus, 1988; Wood et al., 2003; Matthews et al., 2021). Deposition is considered to have occurred below the photic zone, supporting the idea that these Ediacaran organisms were not photoautotrophic (Seilacher, 1992; Wood et al., 2003). Sedimentological study of the area suggests that the Conception Group accumulated in the basin floor and lower slope settings, while the St. John's Group documents regional shallowing to the shelf-slope break (Wood et al., 2003). The stratigraphic range of *F. misrai* suggests that it may have favored toe of slope settings, while *F. andersoni* may have favored the slope and basin floor settings (Gehling and Narbonne, 2007). However, the recent documentation of *F. misrai* in the

Fermeuse Formation of the Catalina Dome (Peréz-Pinedo et al., 2023) would seem to contradict that assertion.

A two-phase tectonic model for Southeastern Newfoundland suggests that deposition began in a forearc basin east of the volcanic arc and west of a subduction zone, which then transitioned to a strike-slip dominated pull-apart basin (Wood et al., 2003; Ichaso et al., 2007; Mason et al., 2013). The greater abundance and frequency of tuffs/tuffites in the stratigraphy of the Bonavista Peninsula area suggests that the area might have been closer to the volcanic arc than Mistaken Point (Ichaso et al., 2007; Mason et al., 2013).

Ediacaran fossils from Conception Bay (O'Brien and King, 2005; Hofmann et al., 2008) are associated with unusually thick, muddy turbidites (possibly ponded turbidites) and paleocurrent directions different from Mistaken Point; these differences have been explained in two ways: 1) strike-slip movement may have brought the two basins closer together than they were at the time of deposition; or 2) the areas were separated by a topographic high within the forearc basin, termed the "Harbour Main High", with Conception Bay on the western side closest to the volcanic arc and Mistaken Point on the eastern side (Ichaso et al., 2007; Fig 1.3). It is suggested that the topographic high may have been subaerial and therefore might have constituted as sediment source for the slope deposits at Mistaken Point (Ichaso et al., 2007). The inferred presence of ponded turbidites in the Bonavista Peninsula stratigraphy has been used to suggest that it was also on the western side of the Harbour Main High (Mason et al., 2013).
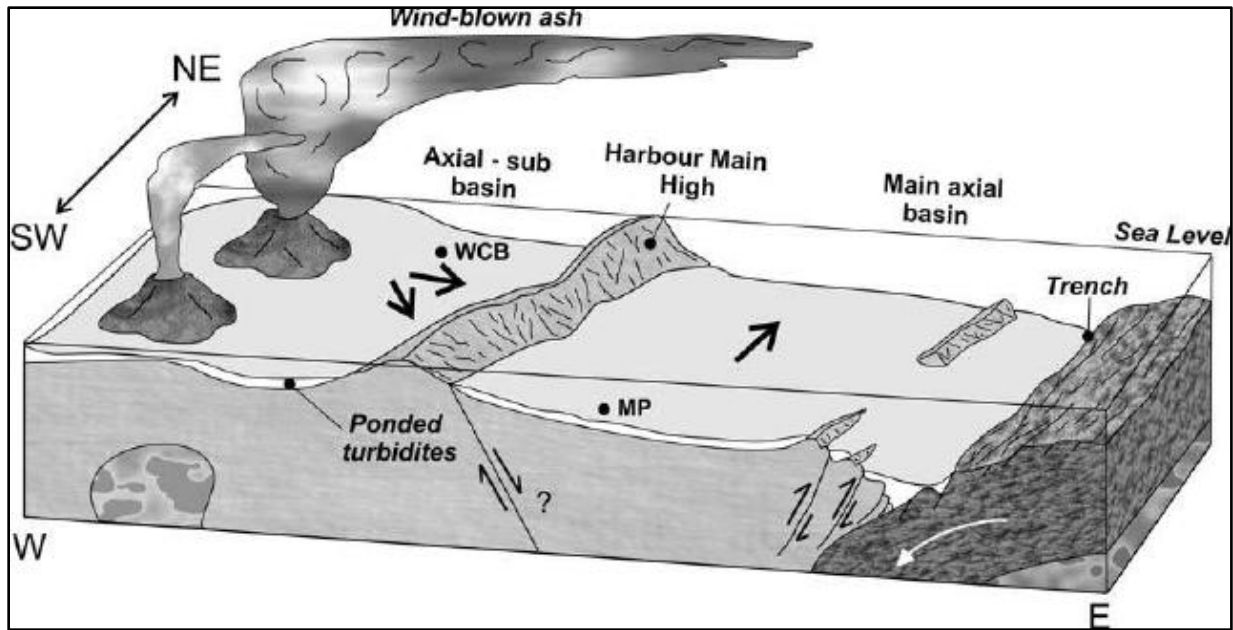
Fig. 1.3. Fore-arc basin setting for the Conception Bay and Mistaken Point area illustrating the ponded turbidites, differing paleocurrent directions and "Harbour Main High" (from Ichaso et al., 2007).

The orientation of frondose taxa on the Ediacaran fossil surfaces across eastern Newfoundland has been used to directly interpret paleoflow directions (Seilacher, 1992; Wood et al., 2003; Ichaso et al., 2007; Vixseboxse et al., 2021). At Mistaken Point, the majority of fronds are oriented towards the northeast, perpendicular to the inferred, southeasterly dipping, paleoslope direction as determined by physical sedimentary structures in the turbidites (similarly in Bonavista Peninsula turbidites (Mason et al., 2013)); from this it has been suggested that frondose taxa were "felled" by northeasterly contour currents (Wood et al., 2003; Ichaso et al., 2007; Liu and Matthews, 2017). However, it is noted here that contour currents are generally slow (less than 20 cm/s) and non-episodic in nature (Zhao et al., 2015). It has been inferred that the Bonavista Peninsula area experienced a contour current flow direction similar to that inferred for Mistaken Point, though weaker and intermittent, with other bottom currents also affecting the orientation of erect frond species as well (Mason et al., 2013). Ash-laden turbidity currents have been considered

to be responsible for preservation at Mistaken Point, inferring that the orientation of some fronds represent the turbiditic flow direction rather than that of a contour current (Matthews et al., 2021). Most recently it has been noted that—since many fronds are also oriented into the inferred turbiditic flow direction (Vixseboxse et al., 2021)—it may have been a background clear-water current (perhaps related to a submarine canyon) that controlled their orientation (McIlroy et al., 2022).

The apparently random orientation of *Fractofusus* on the Mistaken Point E surface has been used to suggest that they were not affected by the same currents that oriented erect organisms, and as such were reclining, not living erect in the water column like other rangeomorphs (Seilacher, 1992, 1999; Gehling and Narbonne, 2007). This inference of a reclining mode of life has been further supported by the lack of any strong orientation trends displayed by *F. andersoni* on the Little Catalina H14 surface (Mitchell et al., 2015).

1.3 Taphonomy

Two preservation styles can be found at Mistaken Point and on the Bonavista Peninsula: 1) Conception-style preservation- in which diverse Avalon Assemblage populations were preserved by volcanic ash, and 2) Fermeuse-style preservation- in which assemblages of mainly *Aspidella* fossils are preserved by sand-rich turbidites (Narbonne, 2005). It has also been proposed that the formation of a pyritic veneer produced by sulfate reducing bacteria was key to Conception-style preservation, along with the presence of volcanic ash (Liu, 2016). This broadly supports the 'death mask' model of preservation, in which seafloor microbial mats aided in soft-bodied organism preservation (Gehling, 1999). On both the Avalon and Bonavista peninsulas, there is a stratigraphic shift in mode of preservation from Conception-style to Fermeuse-style preservation

interpreted to reflect a gradual decrease in the abundance of volcanic ash depositing events towards the top of the St. John's Group (Narbonne, 2005). At Mistaken Point, the taphonomic shift occurs within the Trepassey Formation, while at the Bonavista Peninsula, Conception-style preservation persists into the Fermeuse Formation; this has been interpreted as being due to the Bonavista Peninsula's closer proximity to the volcanic arc (Narbonne, 2005; Mason et al., 2013).

The E surface at Mistaken Point and the H14 surface at Little Catalina both have Conception-style preservation, in which the fossils are preserved atop a hemipelagic siltstone and are cast by an overlying volcanic ash or tuffite (Wood et al., 2003; Narbonne, 2005; Gehling and Narbonne, 2007; Hofmann et al., 2008; Matthews et al., 2021). At both localities, *Fractofusus* is considered to have decomposed before the volcanic ash fully lithified, allowing the ash to settle onto their lower surface impressions on the seafloor, preserving them in negative epirelief (Seilacher, 1992; Narbonne, 2005; Gehling and Narbonne, 2007; Fig. 1.4). The high fidelity of preservation has been linked to the very early diagenetic induration of the sediment due to the life activity of the reclining organism (cf. Dufour & McIlroy 2017; McIlroy et al. 2021; Taylor et al. 2023). While both *Fractofusus* bearing surfaces have Conception-style preservation, the fossil assemblage on the H14 surface is much less diverse, compared to the high diversity on the E surface (Hofmann et al., 2008, Matthews et al., 2021). The E surface assemblage in particular is thought to have included both biomass and necromass in an obrution type preservation style (Liu et al., 2011; Antcliffe et al., 2015; McIlroy et al., 2021). The presence of necromass is inferred by the variable state of preservation of recognizable taxa varying from the obliterated biomass of ivesheadiomorphs through variably detailed effaced preservation of recognizable taxa (Liu et al., 2011). Building upon, and in support of this concept, Antcliffe et al., (2015) created a decay index

to quantify the differing preservation states, ranging from grade one (high fidelity) to five (effaced).
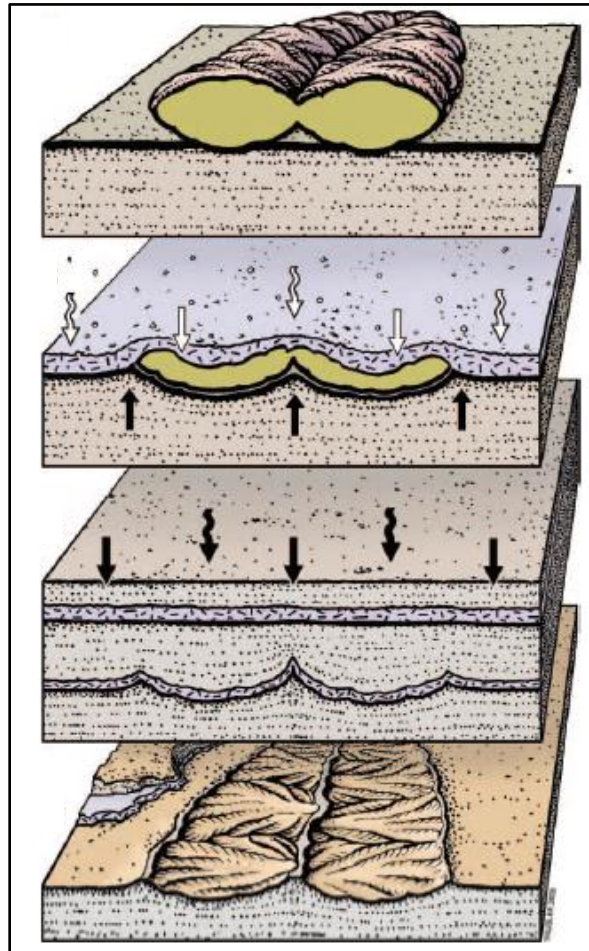
Fig. 1.4. The taphonomy of *Fractofusus* (from Gehling and Narbonne, 2007), in which the organisms were buried by a turbid flow of volcanic ash causing quick decay and ash lithification in their lower impression.

Several studies have proposed different ways in which Conception-style (ash) preservation occurred, with all scenarios being due to either ash-laden turbidity currents from the nearby volcanic arc (Seilacher, 1992; Matthews et al., 2021) or water-lain ash fall (Wood et al., 2003; Ichaso et al., 2007; Mason et al., 2013), elaborated below.

1.3.1 Turbidity Current Scenario

At Mistaken Point, the normally graded layers of volcanic ash with ripple cross lamination that overlay the fossil beds (Seilacher, 1992), as well as current ripples in stratigraphically adjacent turbidite beds of the Mistaken Point Formation (Wood et al., 2003) have been used to infer a southwardly directed ash-laden downslope current triggered by a volcanic ash fall event. The southward current is inferred to have "felled" erect frondose organisms (e.g. *Charniodiscus*), and then a "back surge" bent their fronds and folded several reclining *F. misrai* (Seilacher, 1992; Fig. 1.5). Though we note that, if correct, this back flow must have happened before any deposition in order to preserve the frond on the seafloor rather than within the turbidite which seems unlikely. The inferred instantaneous burial and preservation is considered to have created "fossil snapshots", in which population structure and standing biomass on the day of the depositional event were recorded (Seilacher, 1992; Gehling and Narbonne, 2007). A further complication to this felling model is the observation that several reclining *F. misrai* overlie the stems of *Charniodiscus procerus*, which has been explained by a complex taphonomic model which invokes "relief inversion", in which the *F. misrai* were initially overlain by the *Charniodiscus* and impressed onto the tuff following decay of the stem (Seilacher, 1992; Fig. 1.5). However, it has been considered that the stem of *C. procerus* lay beneath the matground in life, and only the frondose portion was erect (Pérez-Pinedo et al., 2022), allowing for colonization of the matground overlying the stem by *Fractofusus* during life of the *C. procerus*.

More recently, it has been suggested that the sediment overlying the fossil horizon was a tuffite formed by a turbidity current that reworked and redeposited tuff from higher on the slope (Matthews et al., 2021). This report similarly concludes that a turbidity current felled erect frondose organisms, and thus that the fossil orientations record paleocurrent directionality.

The sedimentologic/taphonomic model is somewhat contentious: 1) the invoking of a "back surge" current before deposition (Seilacher, 1992) does not find support in flow mechanics of density currents (McIlroy et al., 2022); 2) there are competing models invoking either a volcanic ash fall event triggering an immediate downslope current (Seilacher, 1992), versus volcanic ash remobilization of previously sedimented ash in the form of a turbidity current (Matthews et al., 2021); and 3) it has been considered that the existence of the Harbour Main High (Ichaso et al., 2007) would not have allowed directly arc-derived turbidity currents to reach Mistaken Point (Seilacher, 1992; Matthews et al., 2021).
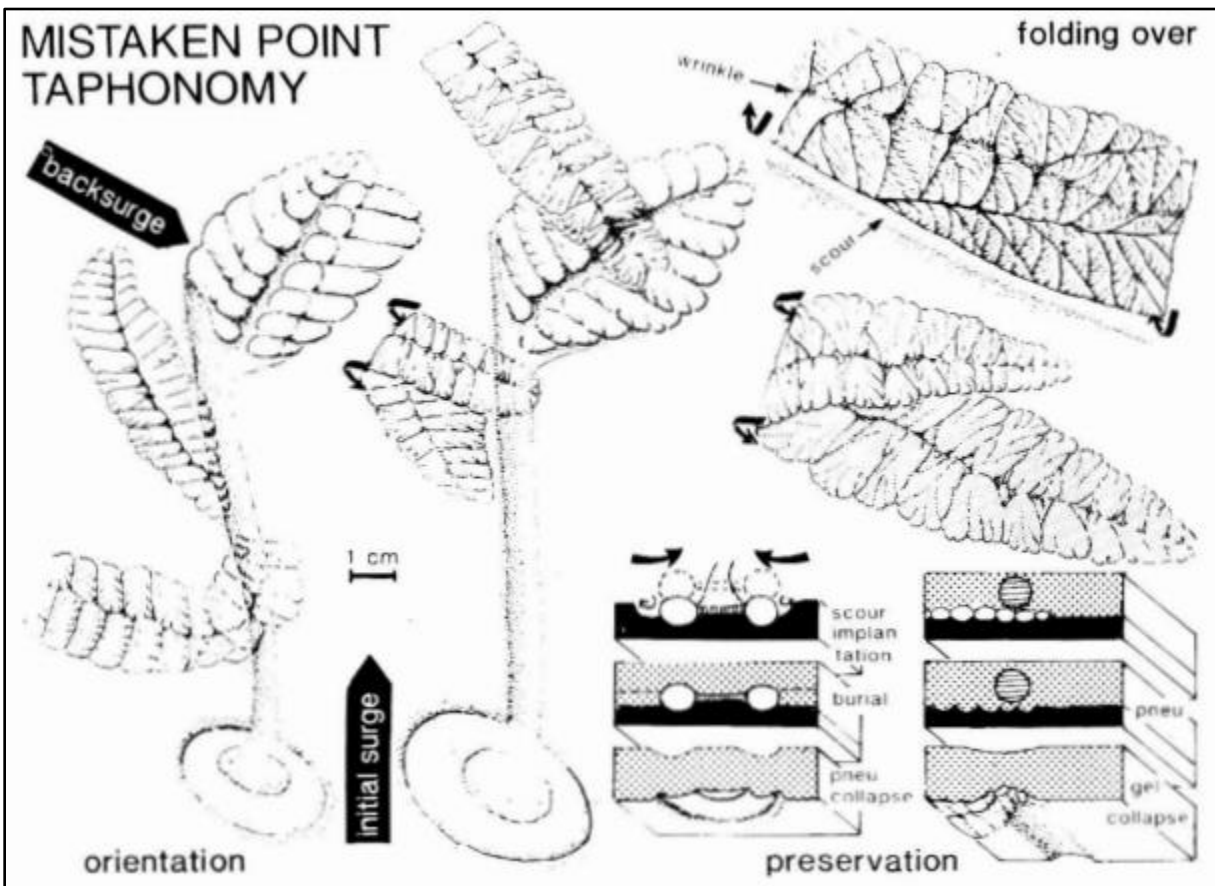
Fig. 1.5. Mistaken Point taphonomy in which a southward ash-laden downslope current felled *Charniodiscus* then a "back surge" bent their fronds and folded several *F. misrai*, and the complex relief inversion model to account for how *F. misrai* can appear to overlie *Charniodiscus* by being impressed onto the overlying tuffite after decay of the stem (from Seilacher, 1992).

1.3.2 Water-lain Ash Scenario

Paleoenvironmental study of the Mistaken Point area (Wood et al., 2003) and the Bonavista Peninsula area (Mason et al., 2013) has additionally proposed that geostrophic contour currents existed in the periods between turbidity current events, and the contour currents inclined erect frondose organisms into a recumbent position. Once in that recumbent position, volcanic ash settled from suspension smothering the erect organisms, thereby collapsing them onto the seafloor, and also smothering reclining species in their life position. In this scenario, the frondose organisms record contour current directionality rather than that of an ash-rich turbidity current (Wood et al., 2003; Mason et al., 2013). It does however not account for the observation that portions of the necromass on the surface also share the same orientation, but at periods long prior to the inferred smothering event (Antcliffe et al., 2015).

It has been noted that the majority of Mistaken Point surfaces have frondose organisms with northeasterly orientations, which is orthogonal to the inferred southeasterly oriented depositional slope/turbidity current direction (Wood et al., 2003). This model therefore invokes a northeasterly directed contour current, but also noted that a small number of surfaces—including the E surface—have fronds with southeasterly orientations, implying that they were oriented by density currents before burial (Wood et al., 2003; Fig 1.6), but not explaining the lack of sedimentation associated with those inferred earlier currents. The variability of frond orientations on the fossiliferous surfaces in the Bonavista Peninsula area has been used to support the influence of contour and other bottoms currents (Mason et al., 2013).
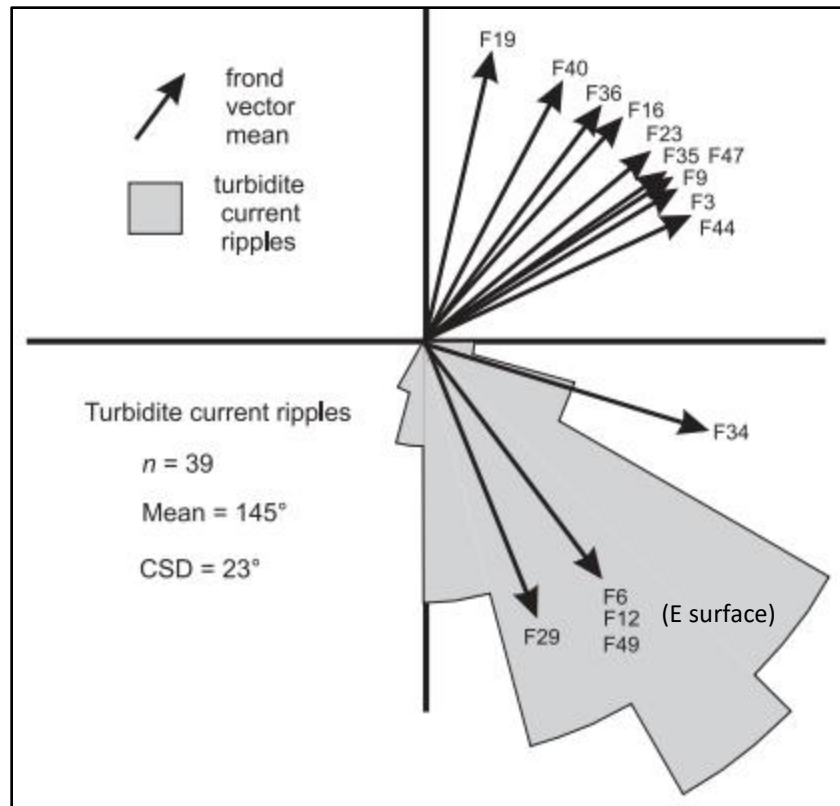
Fig. 1.6. Paleocurrent data for the Mistaken Point succession, showing two frond orientations, with many of the southeasterly directed fronds being from the E surface (from Wood et al., 2003).

Later paleoenvironmental study of the Conception Bay and Mistaken Point areas (Ichaso et al., 2007) provided a semi-regional basin reconstruction (Fig. 1.3). This model inferred different contour paleocurrent directions in the two regions (southwesterly in Conception Bay and northeasterly in Mistaken Point). These opposing current directions cannot be part of global thermohaline circulation, which suggests complex (non-geostrophic) flow directions or deeply penetrating surface currents that may have been responsible for some frond orientations (Ichaso et al., 2007). The model is predicated on the inference that fronds are oriented by slope-parallel contour currents, that are presumably too weak to transport sand-grade material capable of making ripples (following Wood et al. (2003)). The strongest currents in the region are southeasterly directed sediment-laden density currents that deposit turbidites with ripple cross lamination, which

have been inferred to represent the orientation of the basin slope. It is considered here that the possibility of the presence of routed/confined axial turbidites (e.g. Lomas and Joseph, 2004) has not been adequately explored.

1.3.3 Taphonomy Hydrodynamics and Paleobiology

Recent studies have used statistical methods and flow models to relate fossil orientation and paleoflow direction (Vixseboxse et al., 2021, McIlroy et al., 2022; Pérez-Pinedo et al., 2023). Understanding the mode of preservation of the fronds that are commonly used as paleocurrent indicators in the Mistaken Point Formation goes hand-in-hand with understanding fossil orientation.

Statistical analysis of fossil orientation distributions on the Mistaken Point E surface has demonstrated that most taxa are oriented parallel to the inferred southerly turbidity paleocurrent (Vixseboxse et al., 2021). The exceptions to the downslope orientation of unipolar taxa being *Bradgatia* and *Thectardis* which exhibit bidirectional orientations (north and south), and the bipolar *Fractofusus* was found to have no preferential directionality (Vixseboxse et al., 2021). In order to account for the upslope orientations of some fronds, Vixseboxse et al. (2021) invoked an upslope flow in the turbulent head of the turbidity current, which they proposed felled the upright *Bradgatia* and *Thectardis*. This was inferred to have been followed by laminar flow which felled the remaining upright organisms in the downslope southerly direction (Vixseboxse et al., 2021). *Fractofusus misrai*, a reclining species, was found not to be reoriented by the turbidity current (Vixseboxse et al., 2021).

Previous studies have suggested the occurrence of tuffite deposition via a density current at Mistaken Point (Matthews et al., 2021). However, the Mistaken Point E surface ash layer is

normally graded indicating that the ash could be a water-lain tuff (Wood et al., 2003; McIlroy et al., 2022). Contrary to the Vixseboxse et al. (2021) interpretation, there are no published occurrences (experimental or field evidence) of near-bed, upslope-directed flow in density flows relative to substrate, therefore, a turbidity current cannot be responsible for organism felling in an upstream direction (McIlroy et al., 2022). This appears to have been a misunderstanding that flow vectors in turbidity flow models are instantaneous velocities within a flow that is moving much faster than the turbulence within it (McIlroy et al., 2022). The remaining issue of upslope orientation of unipolar fossils was explained by McIlroy et al., (2022) to be due to rheotropic growth of epibenthic reclining organisms that grew in response to a persistent clear water bottom current (McIlroy et al., 2022). This is comparable to bidirectional growth of epifaunal bryozoans in unidirectional currents (Ryland, 1977). In order to have a more robust interpretation and understanding of fossil frond orientation and paleocurrent influence, there is a need to consider fossil orientation data relative to a paleocurrent direction that is derived from independent sedimentologic current indicators (McIlroy et al., 2022; i.e. paleocurrent data not inferred from frond orientation).

Our recent study, Pérez-Pinedo et al., (2023), presented a new integrated approach in order to further statistically analyze the relationship between fossil orientations and paleocurrents, using fossil orientation data and paleocurrent direction (SE) derived from climbing ripple foresets. This study focused on an outcrop of the Fermeuse Formation at Melrose, in the Catalina Dome of the Bonavista Peninsula in eastern Newfoundland (Pérez-Pinedo et al., 2023; Fig. 1.2). The fossil assemblage on this surface consists primarily of *F. misrai*, with a few *Bradgatia* and *Pectinifrons* (Pérez-Pinedo et al., 2023). The study focused on statistical analyses of *F. misrai* and includes some qualitative conclusions regarding *Bradgatia* and *Pectinifrons* (Pérez-Pinedo et al., 2023).

Using a series of modified polythetic and monothetic clustering techniques, it was found that the *F. misrai* specimens are oriented in two orthogonal principal directions, NE-SW and NW-SE (Pérez-Pinedo et al., 2023). The results were interpreted to support a rheotropic response in order to either increase dissolved organic matter absorption or reduce the risk of being swept away by the current (Pérez-Pinedo et al., 2023). Due to the apparently random distribution of *Bradgatia* and *Pectinifrons*, it was suggested such random orientations may reflect reclining life modes, unlike traditional interpretations of specimens being upright and aligned by paleocurrents (Pérez-Pinedo et al., 2023).

1.4 Ediacaran Biotas of the E and H14 Surfaces

Species belonging to the clade Rangeomorpha make up the majority of the Avalon Assemblage in Newfoundland along with elements of Arboreomorpha, Porifera (e.g. *Thectardis avalonensis*; Clapham et al., 2004), and Protista (e.g. *Palaeopascichnus*; Hawco et al., 2019), as well as other *incertae sedis* (Erwin et al., 2011), including possible triradialomorphs (e.g. *Triforillonia*; Gehling et al., 2000), "Blackbrookia" (cf. Dufour and McIlroy, 2017), *Hadrynichorde catalinensis* (Hofmann et al., 2008)*, Hadryniscala avalonica* (Hofmann et al., 2008)*, Hiemalora stellaris* (Fedonkin, 1980)*, Parviscopa bonavistensis* (Hofmann et al., 2008)*, and *Broccoliforma alta* (Mason and Narbonne, 2016).

While the Rangeomorpha and Arboreomorpha are both clades of frondose organisms, they differ in that rangeomorphs have several orders of self-similar (fractal-like) branching while it has been proposed that arboreomorphs have spherical or hemispherical secondary branches and lack high order self-similar branch subdivisions (Dececchi et al., 2017). Rangeomorphs have been described using inconsistent morphologic terminologies. Attempts have been made to unify the

17

morphologic terms, but different authors follow different terminology models; due to this, the morphologic terminology of Brasier et al., (2012) was followed here.

The Porifera have a body plan consisting of a pinacoderm with pores (ostia and oscula) and an aquiferous system which is used for filter feeding. The reconstructed body plan of *Thectardis*, for example, meets the criteria for such a feeding system (Sperling et al., 2011; Suarez and Leys, 2022). The unassigned taxa on both surfaces all show morphologies different from each other and the clades (Table 1; Erwin et al., 2011).

Table 1.1. Descriptions and interpretations of Ediacaran taxa not yet assigned to any higher groupings or clades, found on the E surface at Mistaken Point and/or the H14 surface at Little Catalina.

Taxa	Morphological Description	Interpretation
Hadrynichorde	Smooth, slender, string-like structure attached to a disc	Benthic tethered organisms, resembling algae (Hofmann et al., 2008)
Hadryniscala	Smooth, flat, band-like structure with transverse ridges (ladder-like)	Impressions of flat soft-bodied organisms, resembling algae (Hofmann et al., 2008)
Hiemalora	Disc with appendages attached to the outer ring	Holdfasts of different kinds of frondose organisms (e.g. rangeomorphs and/or arboreomorphs; Shao et al., 2019)
Broccoliforma	Irregular lobate frond with a stem and a disc	Taphomorph of *Primocandelabrum* or a frondose organism belonging to a new Ediacaran clade (Mason and Narbonne, 2016)

1.5 *Fractofusus* Morphology

Fractofusus is a flat-fusiform to ovate organism with no attachment organ and having two vanes composed of several fractally-branched modules that meet at a straight to weakly zigzagged commissure (Gehling and Narbonne, 2007; Taylor et al., 2023; Fig. 1.7A). The overall frond shape of *F. misrai* is elongate fusiform while *F. andersoni* is ovate (Gehling and Narbonne, 2007). In standardizing nomenclature used to describe Rangeomorpha, Brasier et al., (2012) refer to: vanes as rows; modules as primary or first-order branches; and the commissure as suture or growth axis. Modules (primary branches) consist of fractally branching "principal frondlets" (*F. andersoni*) or "principal frondlets" and "subsidiary frondlets" (*F. misrai*) (Gehling and Narbonne, 2007; Fig. 1.7B). This architectural detail was not addressed by Brasier et al., (2012), but has been considered by Taylor et al., (2023), who consider that "principal frondlets" should be referred to as primary branches and "subsidiary frondlets" referred to as subsidiary branches. *Fractofusus misrai* specimens typically contain an obovate to triangular primary branch flanked by asymmetrical subsidiary branches whereas *F. andersoni* primary branches widen toward the periphery (Gehling and Narbonne, 2007). Several orders of branching have been described, with *Fractofusus* showing up to third-order branching (Gehling and Narbonne, 2007; Brasier et al., 2012). However, third order branching may not be true branching but rather invaginations on the second-order branches (Taylor et al., 2023). First and second order branching are usually displayed and may be either furled or unfurled, in which the branching details are visible and either obscured or not obscured by branch folding/curling or dishevelment (Brasier et al., 2012; Fig. 1.7C). The same concept of furling can be applied to the growth axis, as furling of row margins along the growth axis can conceal a possible stem/rachis above the plane of preservation, producing a straight to zigzag midline suture (Brasier et al., 2012; Fig. 1.7D).
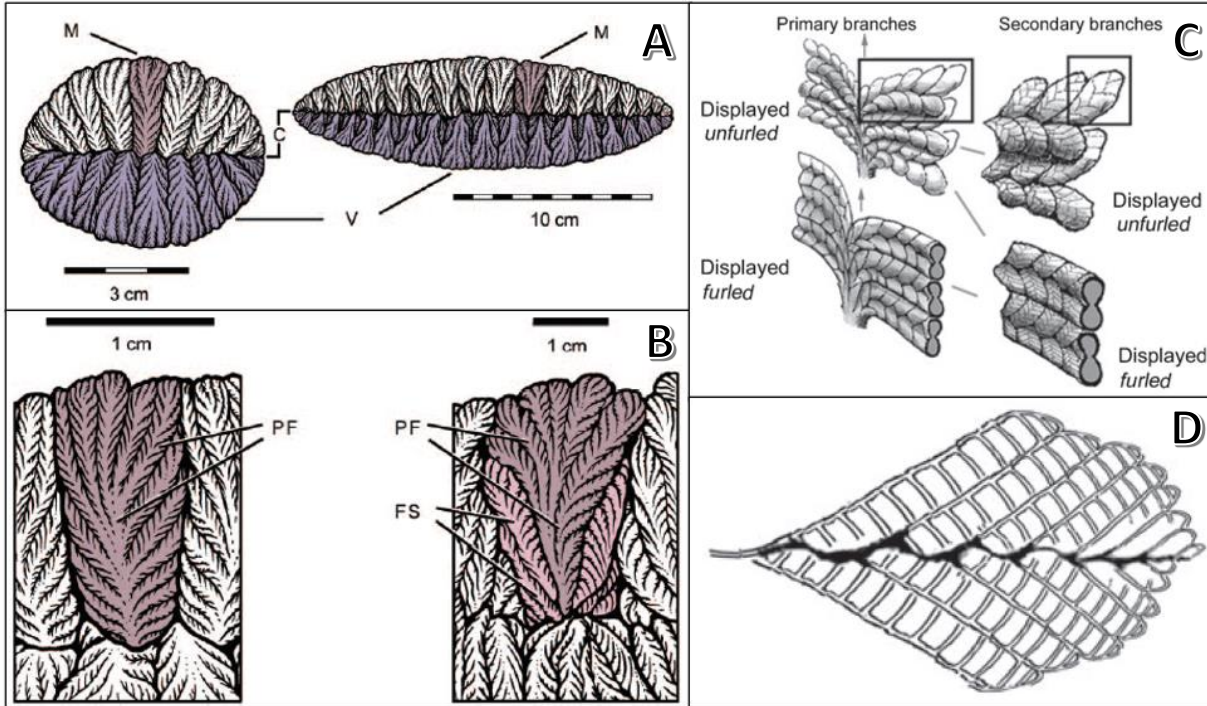
Fig. 1.7. *Fractofusus* morphology. **A**, *Fractofusus* original illustration (from Gehling and Narbonne, 2007) showing the morphologic features: M: module, C: commissure, and V: vane, or primary branch, suture/growth axis, and row (Brasier et al., 2012), for *F. andersoni* (left) and *F. misrai* (right); **B**, *F. andersoni* modules contain PF: principal frondlets, and *F. misrai* modules contain PF and SF: subsidiary frondlets (from Gehling and Narbonne, 2007), or primary branches and subsidiary branches (Taylor et al., 2023); **C**, displayed and unfurled branching versus displayed and furled branching (from Brasier et al., 2012); **D**, A concealed growth axis due to furling producing a zigzag suture (from Brasier et al., 2012).

It has been suggested that in *Fractofusus*, primary branches of a row show no consistent opposite or alternate arrangement relative to those in the opposite row (Gehling and Narbonne, 2007). This was further supported by the description of glide plane symmetry (Brasier et al., 2012) but it has also been suggested that *Fractofusus* has bilateral symmetry (Hofmann et al., 2008). *Fractofusus misrai* specimens consist of 15 to 25 primary branches per row compared to 8 to 13 branches in *F. andersoni*, although it is not specified whether both rows in a specimen contain the same number of primary branches (Gehling and Narbonne, 2007; Brasier et al., 2012; Fig. 1.8). Primary branches have been referred to as pairs, suggesting equal primary branches on both rows

(Hofmann et al., 2008). The contradictions regarding primary branch symmetry have recently been addressed, describing some *F. misrai* specimens as having equal primary branches in both rows, while others, in agreeance with glide plane symmetry (Brasier et al., 2012), have asymmetrical arrangement of primary branches due to anomalously sized branches or having a different number of primary branches per row due to ecological/environmental stimuli (Taylor et al., 2023). *Fractofusus andersoni* is characterized by alternate secondary branching, whereas *F. misrai* specimens show primary branches with secondary branches that are generally symmetrical (Gehling and Narbonne, 2007).
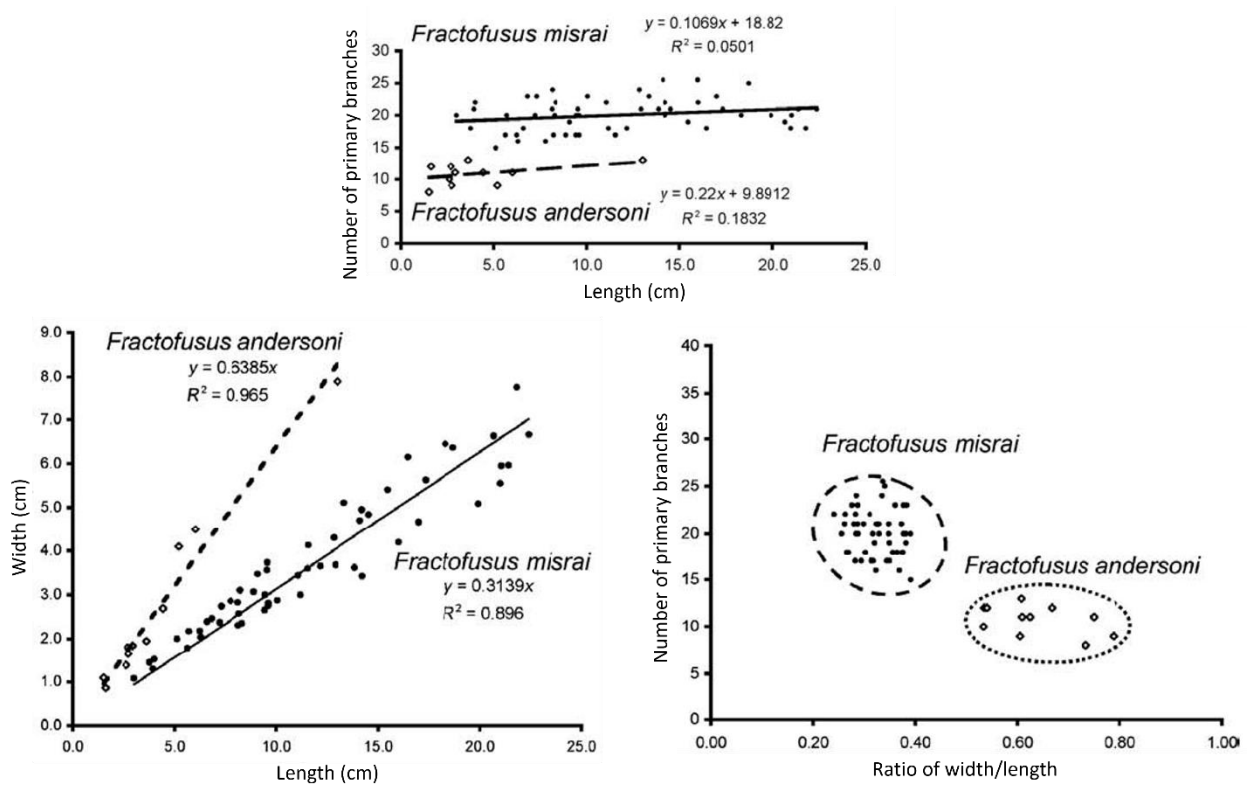
Fig. 1.8. Morphometric graphs for both *Fractofusus* species (from Gehling and Narbonne, 2007).

Morphometric data for *Fractofusus* demonstrate *F. misrai* specimen lengths of 3 to 22 cm, widths of 1 to 8 cm, and the presence of 15 to 25 primary branches per row. In contrast, *F. andersoni* specimens have lengths of 1.5 to 13 cm, widths of 0.8 to 8 cm and 8 to 13 primary branches per row (Gehling and Narbonne, 2007). By graphing the morphometric measurements of *F. misrai* and *F. andersoni* (Fig. 1.8), it has been demonstrated that there is a relationship between length and width, but no relationship between length or width and number of primary branches (Gehling and Narbonne, 2007).

Fractofusus fossils are preserved impressions of the bottom of the organism in the underlying sediment, meaning that there is little to no evidence for the morphology of the top of the organism. A few fossils of *F. misrai* are believed to be impressions of folded organisms, showing part of the bottom and top surface, and have been used to conclude that both surfaces of the organisms were identical (Gehling and Narbonne, 2007). This is consistent with *Fractofusus* consisting of two rows, though it has been suggested that *Fractofusus* may have also had one or more rows not in contact with the underlying sediment, however, this cannot be cogently demonstrated without the discovery of three-dimensionally preserved specimens (Gehling and Narbonne, 2007; Fig. 1.9). Based on extensive study of current-damaged *Fractofusus* specimens, a recent reconstruction has demonstrated *Fractofusus* to have been relatively flat, with a concave upper surface and a convex lower surface (Taylor et al., 2023; Fig. 1.10) rather than biconvex (Gehling and Narbonne, 2007).
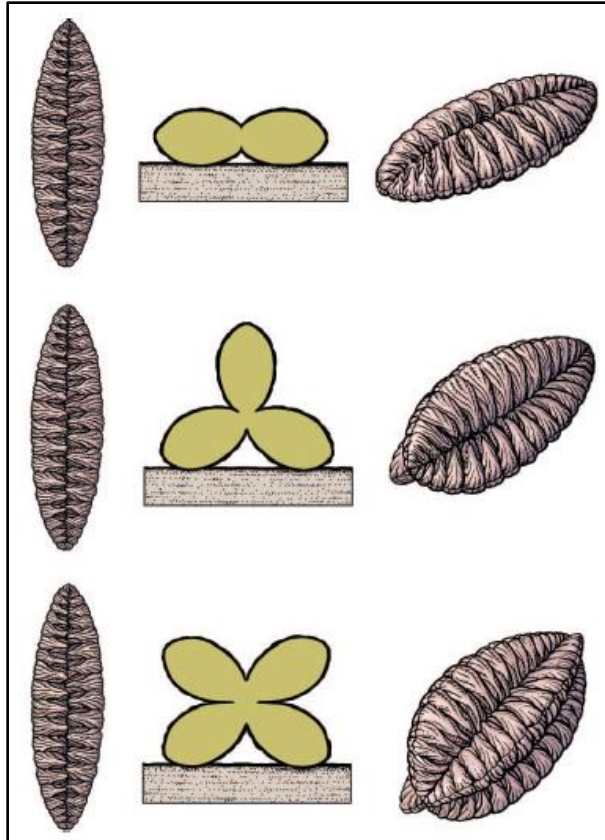
Fig. 1.9. *Fractofusus* models with two, three and four rows (from Gehling and Narbonne, 2007).

Fractofusus misrai specimens were originally described as straight or bent while *F. andersoni* specimens are generally straight, lacking further description of their general shape variation (Gehling and Narbonne, 2007). An emended diagnosis described *F. misrai* specimens as straight, curved or kinked, with such shape variation likely due to intrinsic growth (Taylor et al., 2023). Some *F. misrai* specimens that appear to be torn from being bent show a gap between primary branches suggesting that primary branches were attached to the growth axis/rachis but not to each other (Gehling and Narbonne, 2007; Taylor et al., 2023; Fig. 1.10).

Fig. 1.10. 3-D reconstructions of *F. misrai* (left) and *F. andersoni* (right) (from Taylor et al., 2023).

1.6 Rangeomorph Growth

The established taxonomic framework for Rangeomorpha describes the rules, or concepts, of growth in rangeomorphs (Brasier et al., 2012); these include polarity, insertion, inflation, deterministic versus non-deterministic growth and furling. Frondose organisms possess growth tips, or poles, the main generative zones in most taxa. Fronds are thus classified as being unipolar, bipolar, or multipolar (Brasier et al., 2012). Once a branch is formed, subsequent growth is due to insertion of up to four orders of branching, and/or inflation of the branches (Brasier et al., 2012). This pattern of growth may be deterministic (i.e. growth that is programmed to stop at a specific state, e.g. *Fractofusus*) or non-deterministic (i.e. growth which continues indefinitely, e.g. some *Bradgatia*; Brasier et al, 2012). The states of rangeomorph branches may be furled (in which

24

branch tips are not seen, e.g. *Charnia*) or unfurled (in which branch tips are fully seen, e.g. *F. misrai*; see Brasier et al., 2012).

1.7 *Fractofusus* Growth

Fractal-like branching in *Fractofusus* has been interpreted as originating from two growth tips at the termini of a central growth axis, with branch addition in two directions 180° apart (i.e. bipolar growth; Brasier et al., 2012; Fig. 1.11A). It has been considered that subsidiary branches grew to fill the space between primary branches close to the central axis (Gehling and Narbonne, 2007). The lack of a simple relationship between specimen length and number of primary branches suggests that the insertion of primary branches was completed early in ontogeny and then growth continued through the life of the organism by inflation of those branches (Gehling and Narbonne, 2007). Once the number of primary branches was established, it has been considered that inflation of first-order branches was proximal while inflation of second-order branches was usually distal (Brasier et al., 2012). The displayed and unfurled nature of branching suggests an adaptation to maximize surface area, either in contact with the sediment for nutrition, or with the water column for solute exchange (Dufour and McIlroy, 2017). The gap between primary branches seen in bent specimens (Fig. 1.11B) not only supports growth from the central growth axis but could also suggest that primary branches grew by fractal quilting rather than by independent branches clustering together (Gehling and Narbonne, 2007).
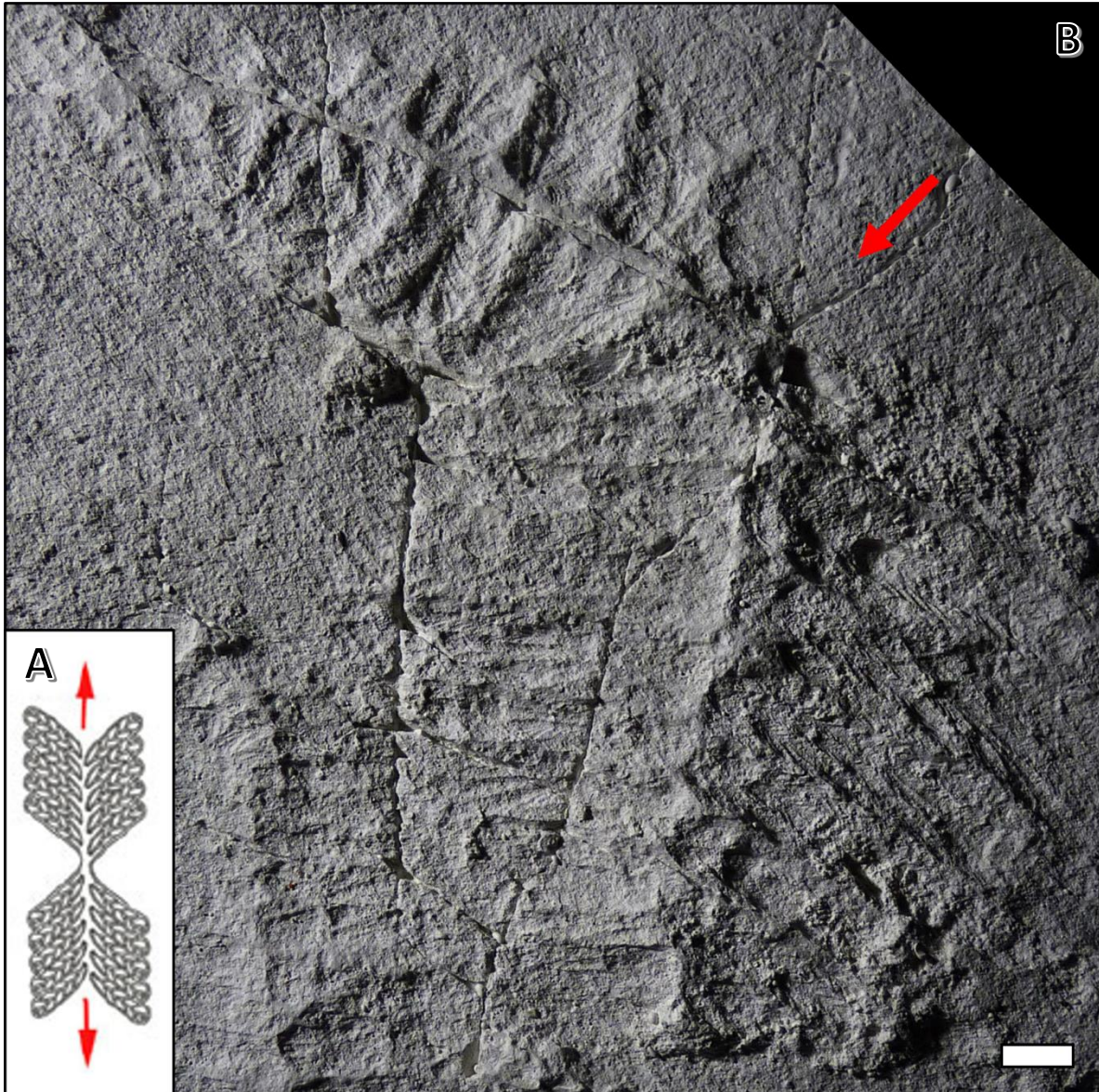
Fig. 1.11. A, Bipolar growth illustration (from Brasier et al., 2012); **B**, *Fractofusus misrai* specimen with a gap between primary branches due to bending, scale: 1 cm.

1.8 Paleoecology

One of the first studies to interpret the paleoecology of the Mistaken Point assemblage concluded that Mistaken Point communities were tiered and ecologically structured in a manner similar to modern suspension feeding communities (Clapham et al., 2003). The ecological interpretations of Clapham et al. (2003) were based on the inference that the Mistaken Point assemblage represents an all-living community at the time of burial (Seilacher, 1992), and this interpretation has been challenged based on the recognition of both biomass and necromass (dead organisms on the preserved seafloor) in the assemblage (Liu, 2011; Antcliffe et al., 2015; Fig. 1.12). When fossils considered to be necromass are included in the community structure, it becomes clear that the Mistaken Point communities were likely structured differently to modern communities in metrics such as species richness and diversity (Liu, 2011). Notwithstanding the challenges of making such calculations with an incomplete taxonomic framework (McIlroy et al., 2022).
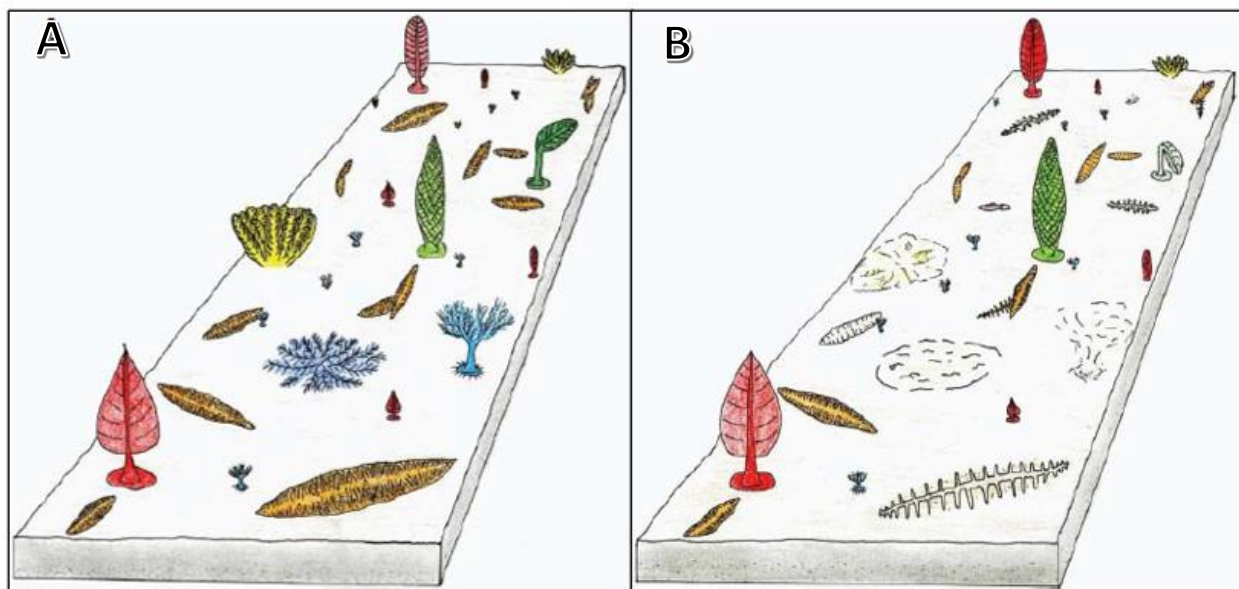
Fig. 1.12. A, A community of all living organisms; **B**, A community containing biomass and necromass (from Liu, 2011).

It was further proposed that the Mistaken Point E surface assemblage includes multiple generations, with living and dead organisms being preserved at various stages of decay (Antcliffe et al., 2015; Fig. 1.13). Based on revised criteria for determining standing crop it was also proposed that only 15-40% of the community was alive at the time of burial, suggesting that *Fractofusus* may have been so abundant due to large proportions of dead organisms available for their nutrition (Antcliffe et al., 2015). Therefore, it was concluded that instead of the total biota being alive at the same time and being a tiered community of filter feeders, they were time-averaged communities of organisms that obtained nutrients from underlying microbial mats as well as dead and decaying organisms nearby (Antcliffe et al., 2015).
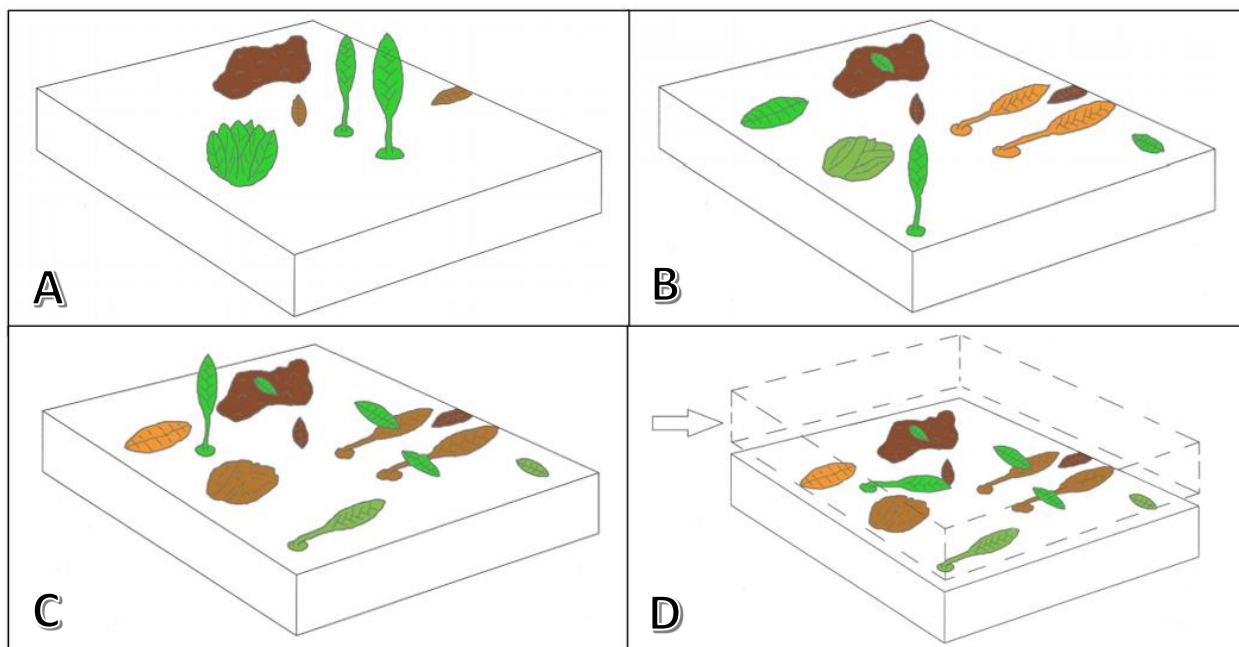
Fig. 1.13. A, Surface colonization; **B**, Death and decay of fronds fallen in alignment with contour current flow and new organism colonization; **C**, Further death, decay and colonization; **D**, Influx of volcanic ash aligned fronds in influx direction, preserving a snapshot of the community at several stages of life (from Antcliffe et al., 2015).

Several paleoecological aspects of *Fractofusus* and other Ediacaran taxa found on the E and H14 surfaces have been investigated, such as their reproduction, feeding strategies and interactions with their environment (Liu et al., 2015; Mitchell et al., 2015; Dufour and McIlroy, 2017). Examination of the population structure of four taxa (*Fractofusus, Beothukis, Pectinifrons and Thectardis*) on several of the Mistaken Point fossil surfaces has been used to suggest that these taxa underwent sexual reproduction and reproduced continuously (Darroch et al., 2013). While there is no direct fossil evidence (apart from abundant filamentous structures on some surfaces that rarely—and possibly accidentally—connect different rangeomorph taxa that are also present in high abundance; Liu and Dunn, 2020), sexual reproduction by waterborne propagules and asexual stolons has been suggested by statistically analyzing the distribution of *Fractofusus* on the D and E surface at Mistaken Point and the H14 surface at Little Catalina (Mitchell et al., 2015; Fig. 1.14A). These differing suggestions regarding reproduction for *Fractofusus* are possibly due to the different population structure results; one study found a unimodal distribution of *Fractofusus* on the E surface at Mistaken Point (Darroch et al., 2013) while the other found a trimodal distribution (Mitchell et al., 2015). However, subsequent work has agreed with Darroch et al. (2013) that there is a unimodal distribution of *Fractofusus* preserved on the E surface (Mitchell and Butterfield, 2018).

There is also no direct fossil evidence regarding feeding strategies of the Rangeomorpha, although several have been proposed (Antcliffe et al., 2015; Dufour and McIlroy, 2017; McIlroy et al., 2021). Early work mainly considered rangeomorphs as filter feeders, although fossil material mostly lacks filter feeding structures (Jenkins, 1985; Clapham and Narbonne, 2002; Liu et al., 2015). Theoretical modeling and surface-area-to-volume ratios (assuming truly fractal branching) have been used to support osmotrophic feeding for several Ediacaran taxa, including *Fractofusus*

(Laflamme et al., 2009; Hoyal Cuthill and Conway Morris, 2014). Though most authors would not support the inference of truly fractal branching, and the presence of such giant osmotrophs seems highly unlikely (McIlroy et al., 2021). It has also been proposed that *Fractofusus* could have obtained nutrition from underlying microbes by combined phagotrophy and chemosymbiosis, which is a hypothesis in need of biogeochemical testing (Dufour and McIlroy, 2017; Fig. 1.14B). There is however no general consensus in the literature.
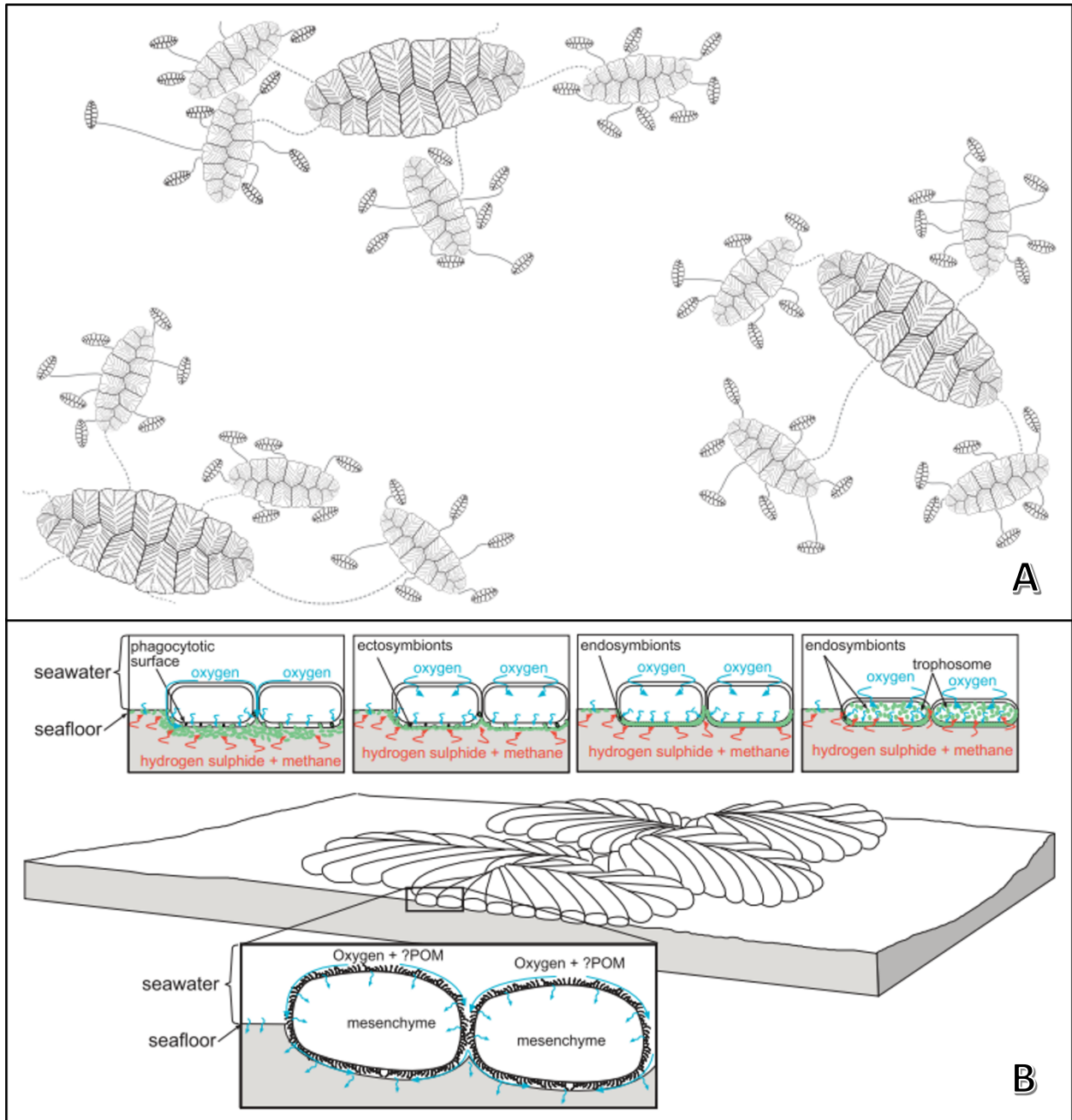
Fig. 1.14. A, illustration of the inferred *F. andersoni* stolon-like reproduction on the H14 surface at Little Catalina, NL (from Mitchell et al., 2015); **B**, *Fractofusus misrai* substrate interaction (oxygenation by ciliary action) and feeding (phagotrophy, ectosymbiosis and endosymbiosis) (from Dufour and McIlroy, 2017).

1.9 Relevance of Study / Objectives

Much of the literature regarding the Ediacaran paleobiology contains a degree of uncertainty and competing interpretations. The phylogeny of the rangeomorphs of the Ediacaran biota has long been debated and is still uncertain (Seilacher et al., 2003; Peterson et al., 2003; Narbonne, 2005; Gehling and Narbonne, 2007); further study of these extinct organisms is important as it may provide insight into broader topics such as animal evolution. This study of *Fractofusus* worked towards quantitatively resolving two main paleobiological problems:

1) Determine *Fractofusus* population structure and infer reproductive modes.

2) Combine *Fractofusus* morphometrics and orientation to infer interactions with the paleoenvironment.

2. Methods

Photographs of *F. misrai* specimens from the Mistaken Point E surface and *F. andersoni* specimens from the Little Catalina H14 surface were taken using a grid system (Fig. 2.1), photographing specimens within each quadrat. The photographed specimens were examined using the image processing and analysis software ImageJ (Rasband, 1997-2018) to record quantitative morphometric and orientational data, as well as qualitative morphological data. Specimens in which measurements/data could not be determined due to poor detail preservation (e.g. specimen incompleteness, ash cover, or cracking) were excluded from the data set. This data was graphically and statistically analyzed and compared to determine possible trends in morphology and orientation, that could be used to make inferences about paleoecology and paleoenvironment.

Fig. 2.1. Grid sampling of the H14 surface at Little Catalina. String used for gridding divided the surface into ~1m squares.

2.1 Data Collection

The shape of *F. misrai* can be straight, curved or kinked, while *F. andersoni* specimens are generally straight (Gehling and Narbonne, 2007; Taylor et al., 2023). Field photographs from the gridded surfaces were analyzed to determine which specimens were straight, curved or kinked (Fig. 2.2A-C). Specimen maximum length and width were measured in centimeters. For straight specimens, maximum length was measured along the midline suture, and maximum width was measured perpendicular to the suture at the widest part (Fig. 2.2D). For curved and kinked specimens, maximum length was measured in two increments, and maximum width was measured at the widest part of the fossils (Fig. 2.2E).

To determine specimen orientation relative to (magnetic) north, all specimen photographs contain a compass. For straight specimens, the general shape was compared to the compass to determine two measurements 180° apart (Fig. 2.2F). For curved and kinked specimens, both segments of the specimens opposite the curve/kink were compared to the compass to determine a measurement for each of the two specimen segments (Fig. 2.2G). This method of measuring specimen orientation differs from that used by Gehling and Narbonne (2007), in which a vector mean was used for bent specimens. Due to the circular nature of orientation data, of the two measurements per specimen, the measurement below 180° was used in the statistical analyses; therefore, kinked or curved specimens (e.g. Taylor et al., 2023; Pérez-Pinedo et al., 2023) containing both measurements above or below 180° were removed from the statistical analyses.

Retrodeformation is sometimes applied to Ediacaran fossils, in which deformation is estimated by changing elongated holdfast fossils into circles (Jenkins and Gehling, 1978; Wood et al., 2003). Notably, this process is based on the assumption that holdfasts were circular during life which might not always be the case (Liu, 2011). Previous study of the H14 surface did not apply

retrodeformation as the surface shows no obvious directional distortion and lacks suitable deformation indicators (Mitchell et al., 2015). However, aware of implications retrodeformation can have (e.g. data distributions seen in Seilacher, 1999; Gehling and Narbonne, 2007; Vixseboxse et al., 2021), *F. misrai* specimens were retrodeformed following the method of Wood et al. (2003). The results derived from the retrodeformed specimens are reported solely in section 3.5.
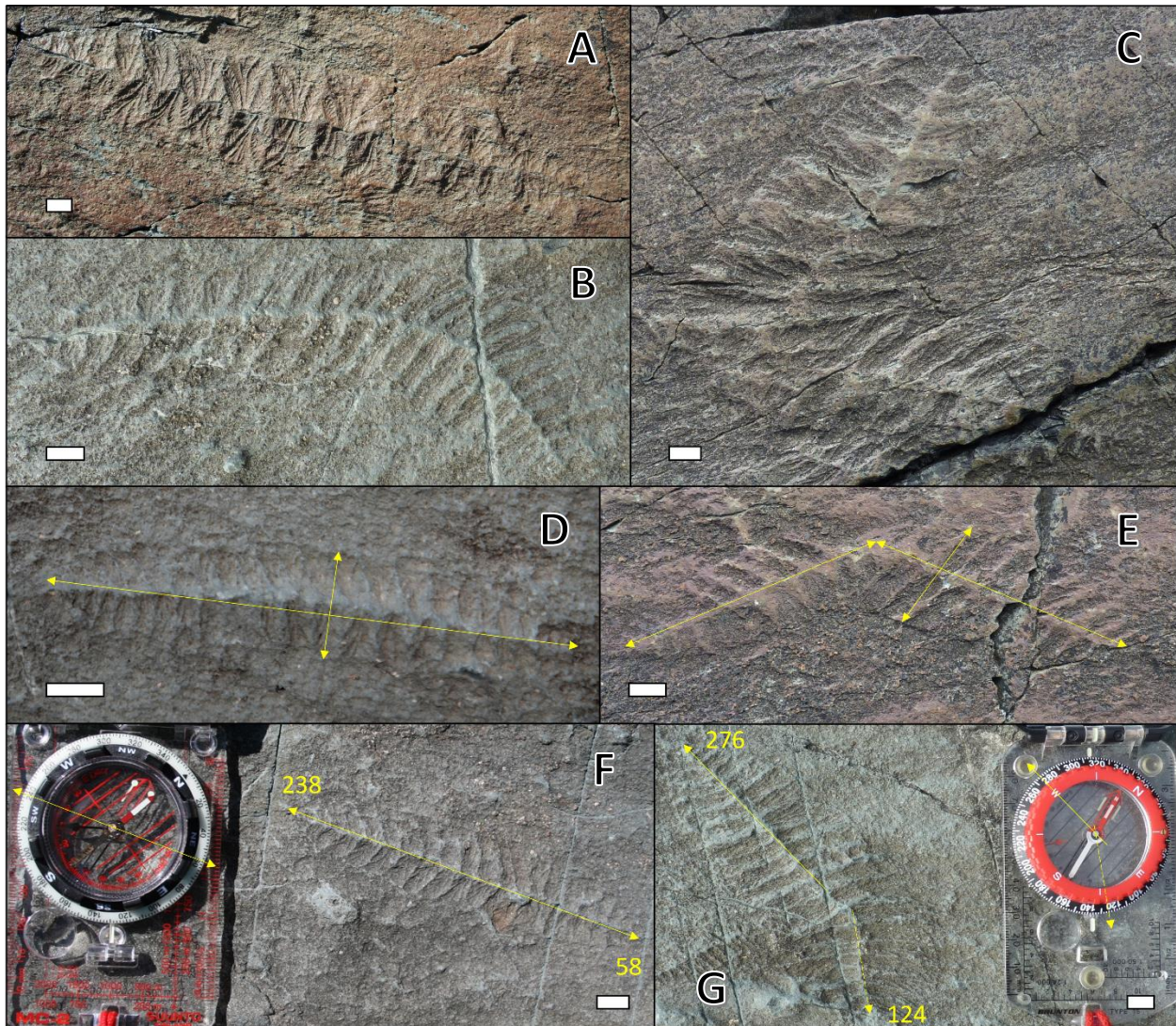
Fig. 2.2. Examples of *F. misrai* shape variation: **A**, straight; **B**, curved; **C**, kinked; **D** and **E**, measuring maximum length and width of straight versus curved/kinked *F. misrai* specimens; **F** and **G**, determining the orientation trend for a straight *F. misrai* specimen versus the orientation of both segments per curved/kinked *F. misrai* specimen. Scale: 1 cm.

2.2 Statistical Analysis

2.2.1 Analyzing Population Structure

To analyze population structure, an approach similar to that demonstrated by Darroch et al. (2013) was used. Analyzing size-frequency distribution is an established technique to investigate population structure in marine benthos (Hallam, 1967; Billet and Hanson, 1982; Darroch et al., 2013); size distribution of logarithmically transformed data better reflects population structure, as demonstrated with scleractinian corals (Bak and Meesters, 1998; Meesters et al., 2001). The normality of the size-frequency (length and width) data was tested by performing the Shapiro-Wilk test on the unlogged and logged length and width data (when logarithmic transformation was needed) for each species in R (R Core Team, 2022). Next, the natural log of the length and width data was used to complete univariate (length data) and multivariate (length and width data) analyses, in which the data was analyzed by comparing different Gaussian finite mixture models fitted by an EM clustering algorithm using the package mclust (Scrucca et al., 2016) in R (R Core Team, 2022). Finally, the best fit model was selected based on the Bayesian Information Criterion (BIC), an index used to choose between alternative models. This approach was designed to find the most likely number of Gaussian components (modes) or clusters in the data, corresponding to the number of inferred size classes in the population. Due to the multivariate analyses finding more clusters than the univariate analyses, the interaction between length and width was further explored by analyzing an additional variable, length:width (L:W), a proxy for specimen shape**.**

2.2.2 Analyzing Shape

As a means of quantitatively analyzing specimen shape, specimen length was divided by specimen width, to create a variable (L:W) for shape (Fig. 2.3). To statistically analyze shape, an approach similar to that used to analyze population structure was used. First, the Shapiro-Wilk test was performed on the unlogged and logged L:W data for each species in R (R Core Team, 2022). Then, using mclust (Scrucca et al., 2016) in R (R Core Team, 2022) to complete a univariate analysis, the data was analyzed to determine the number of clusters selected based on the BIC which were interpreted as different shape types/groups in the population. The Wilcoxon test was utilized in R (R Core Team, 2022) to corroborate the results of the univariate (L:W) analyses. The null hypothesis of the test is the two groups have the same median and mean values (Hammer and Harper, 2006), which was applied to the data to indicate whether the L:W groups identified were statistically different. Due to the population structure and shape analyses both finding multiple clusters, these clusters were then compared by non-metric multidimensional scaling (NMDS) to determine any similarities or differences.
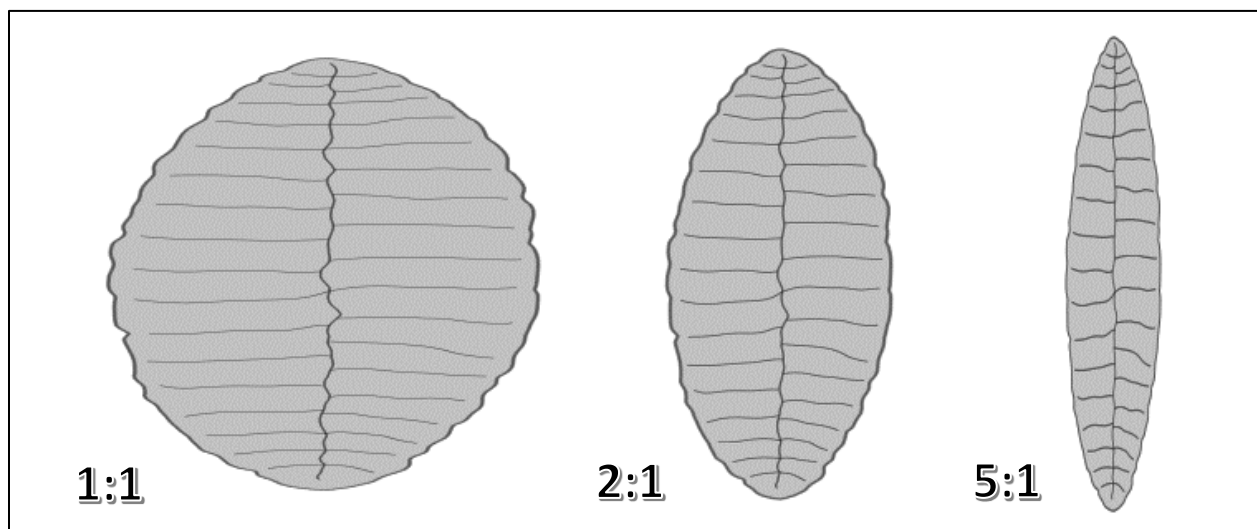
Fig. 2.3. Examples of different *Fractofusus* specimen shapes based on their L:W ratio.

2.2.3 Comparing Size (L&W) and Shape (L:W) Clusters

Non-metric multidimensional scaling is an ordination technique that projects multidimensional data into two dimensions and is used to visualize the level of similarity of data points (*Fractofusus* specimens) based on multiple variables (length, width and orientation) in order to determine any trends or groups within the dataset (Kruskal, 1964; Clarke, 1993; Hammer and Harper, 2006). The ordination orders the data based on a rank-based distance matrix that measures the distance (dissimilarity) between data points, with similar data points being near one another and dissimilar data points widely separated (Kruskal, 1964; Clarke, 1993; Hammer and Harper, 2006). The quality of the NMDS ordination result can be assessed by measuring the "stress", the difference between the ranked distances in the reduced dimension and the multidimensional space, with low stress (>0.2) indicating good representation (Clarke, 1993). The variables can be added to the NMDS plot as fitted vectors (arrows), in which the length of the arrows is proportionate to the variable's significance (Oksanen, 2013). Compared to other ordination techniques (e.g. PCA, DCA, PCoA, etc.) NMDS performs very well with ecological datasets (Laflamme et al., 2011), and thus was the chosen ordination technique used to visualize any trends among the two species in terms of their predetermined size and shape clusters and the significance of the variables. NMDS plots were created using the package vegan (Oksanen et al., 2022) in R (R Core Team, 2022). Due to the findings from the NMDS plots, the orientation displayed by specimens in each shape group was assessed as the final step of the analytical process.

2.2.4 Assessing the Relationship Between Shape and Orientation

The violin plot is a hybrid of the box plot and density trace that depicts information regarding summary statistics and distribution of data. It is useful when assessing data clustering and distribution shape of a variable among groups, making it a valuable data exploration and analysis tool (Hintze and Nelson, 1998). The rose plot is a circular histogram that displays the distribution of directional data, commonly used in various specialties within geology (Oxford University Press, 2008). Therefore, these two plot types were used to preliminarily assess for shape-specific orientation trends.

The Shapiro-Wilk test was performed on the unlogged and logged orientation data for each species in R (R Core Team, 2022). This test was used to determine which test to use to assess whether there is a difference in the dependent variable (orientation) for the two independent groups (shape types) per species, as certain tests assume normal distribution (Hammer and Harper, 2006).

Subsequently the Wilcoxon test was performed in R (R Core Team, 2022). The null hypothesis of the Wilcoxon test is that the two groups have the same median and mean values (Hammer and Harper, 2006), which was applied to the data to indicate whether the shape groups have statistically different orientation trends or not.

3. Results

3.1 Overall Shape

Of the photographed specimens, two hundred and eighty-two complete specimens of *F. misrai* from the E surface and five hundred and eighty-seven complete specimens of *F. andersoni* from the H14 surface were measured and analyzed (Appendices A & B). The *F. misrai* specimens were found to be straight, curved or kinked, whereas the *F. andersoni* specimens were all straight.

3.2 Length and Width

Of two hundred and eighty-two *F. misrai* specimens, the length ranged from 2.67 cm to 33.37 cm and the maximum width ranged from 0.83 cm to 10.28 cm. Of five hundred and eighty-seven *F. andersoni* specimens, the length was found to range from 0.43 cm to 23.53 cm and the maximum width ranged from 0.41 cm to 12.89 cm. The length and width data for each species were graphed to determine their relationship (Fig. 3.1), showing a moderate positive relationship with *F. misrai* data ($r = 0.61$) and a strong positive relationship with *F. andersoni* data ($r = 0.86$).
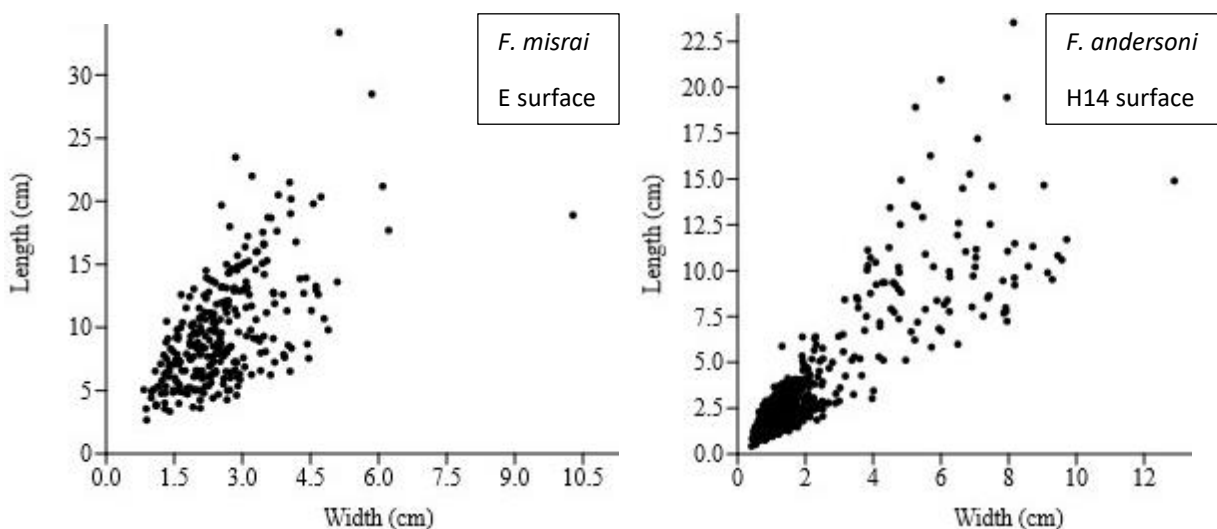
Fig. 3.1. Scatter plots showing the relationship between the length and width of *Fractofusus* spp.

3.3 Orientation

Orientation was determined for three hundred and eight *F. misrai* specimens and five hundred and eighty-seven *F. andersoni* specimens. Curved and kinked *F. misrai* specimens (twenty-six) with both measurements below or above 180° were removed from the statistical analyses. On both surfaces, the specimens show a NE trend, though it is less pronounced on the H14 surface (Fig. 3.2).
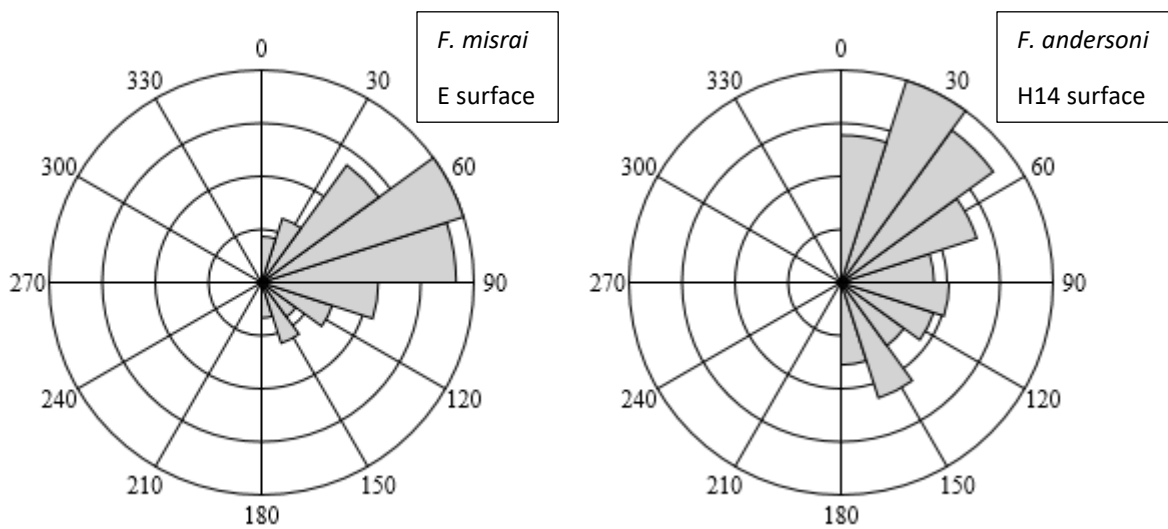
Fig. 3.2. Rose plots showing the orientation of *Fractofusus* specimens from the E surface (note: where stemmed fronds preferential orientation and ripple cross lamination is southeasterly (Seilacher, 1992; Wood et al., 2003)) and the H14 surface.

3.4 Statistical Analysis

3.4.1 Analyzing Population Structure

The size-frequency histograms (length and width) of both the *F. misrai* and *F. andersoni* unlogged data show apparent unimodal positive right skewed distributions (Fig 3.3). Meanwhile, the histograms of *F. misrai* log transformed length and width data appear normally distributed, while those of *F. andersoni* appear to show bimodal distributions (Fig. 3.3). The Shapiro-Wilk test

determined the *F. misrai* length and width data are not normally distributed, therefore requiring

log transformation; the Shapiro-Wilk test determined normal distribution of the log transformed

data. The Shapiro-Wilk test determined the *F. andersoni* length and width data are not normally

distributed before or after log transformation.
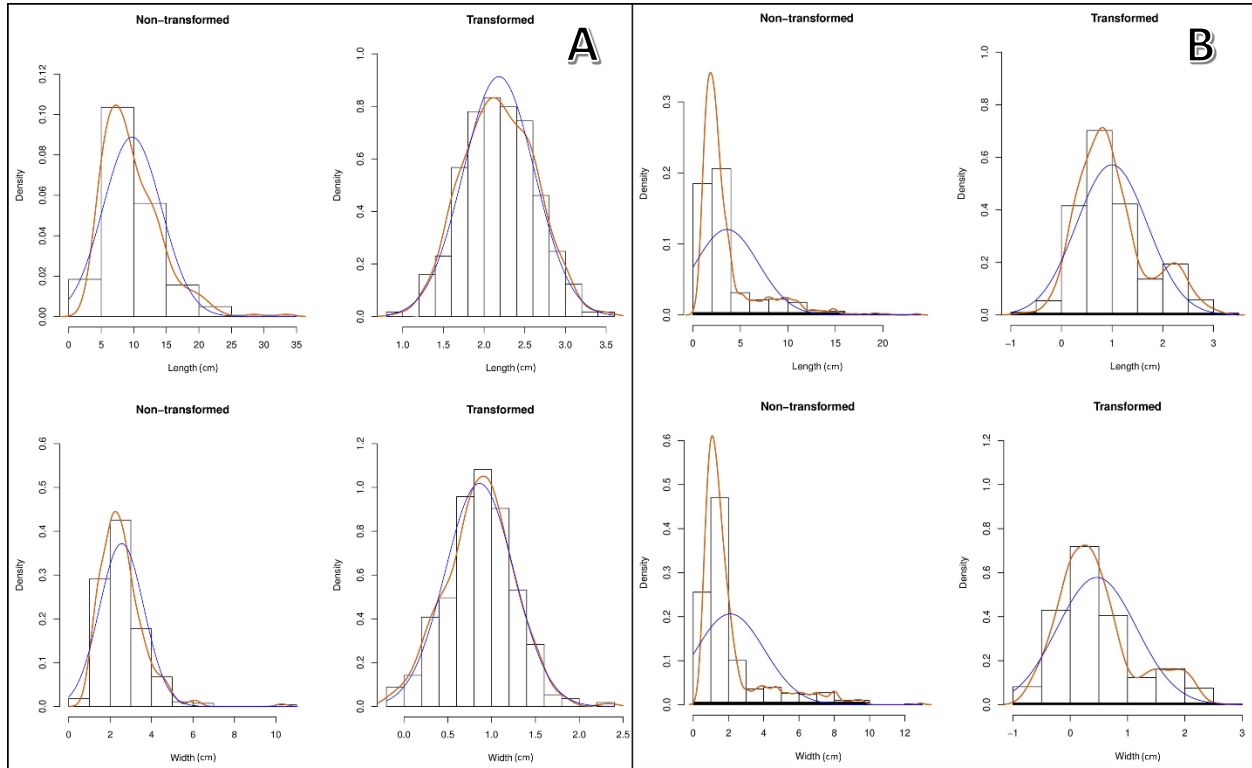
Fig. 3.3. Size frequency histograms (red curves representing data distribution, blue curves representing Gaussian distributions): **A**, *F. misrai* on the E surface; **B**, *F. andersoni* on the H14 surface.

The BIC results of the univariate analyses indicate that the best fit model for the *F. misrai*

length data contained one cluster, while that of *F. andersoni* contained two clusters (Fig. 3.4);

these results are of the models assuming equal variance as they are likely more biologically

realistic than those assuming unequal variance (see Darroch et al., 2013). These results confirm

the size modes seen in the log transformed data for both species (Fig. 3.3.). As size-frequency

distribution is an established indicator of population structure, the univariate results indicate the *F. misrai* population on the E surface contains one size class while the *F. andersoni* population on the H14 surface contains two size classes (also interpreted as representing possible age classes or generations (Darroch et al., 2013; Mitchell et al., 2015)).
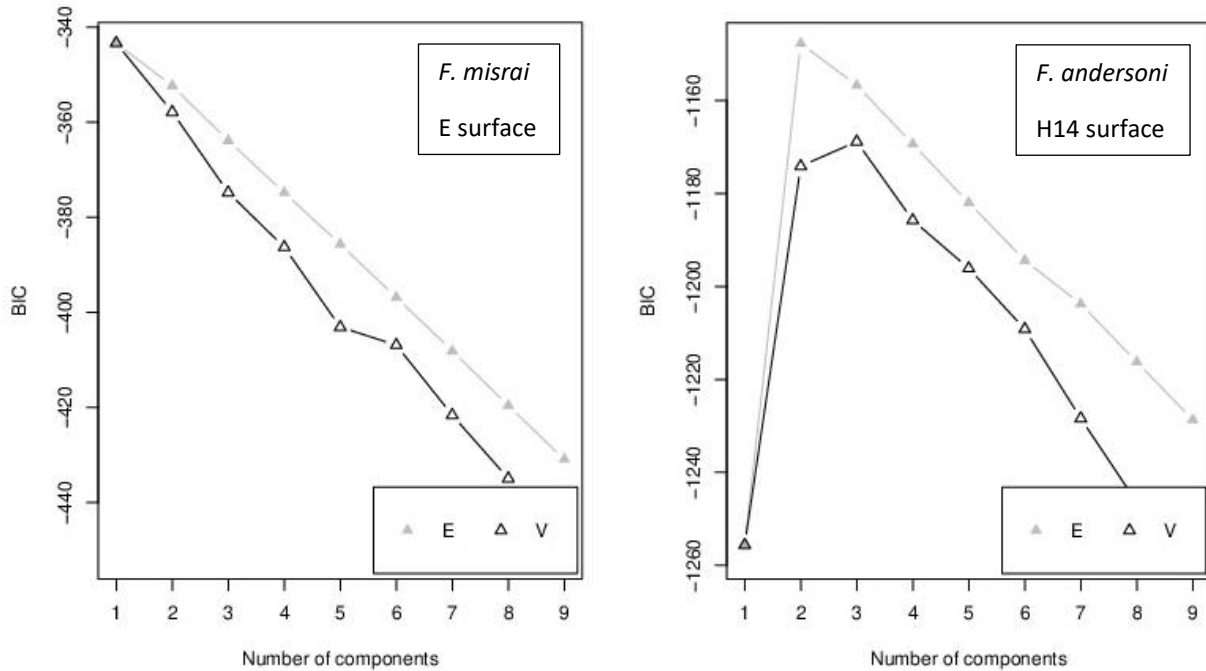
Fig. 3.4. Results of the univariate analyses (length) performed using the mclust package in R.

The BIC results of the multivariate analyses indicate that the best fit model for the *F. misrai* length and width data contained two clusters, while that of *F. andersoni* contained three clusters (Fig. 3.5; see Fraley and Raftery (2007) for details of model assumptions). These results differ from those of the univariate analysis with more clusters when analyzing length and width together rather than length alone, which indicates an important interaction between length and width. To explore this interaction, the length:width dataset was analyzed.
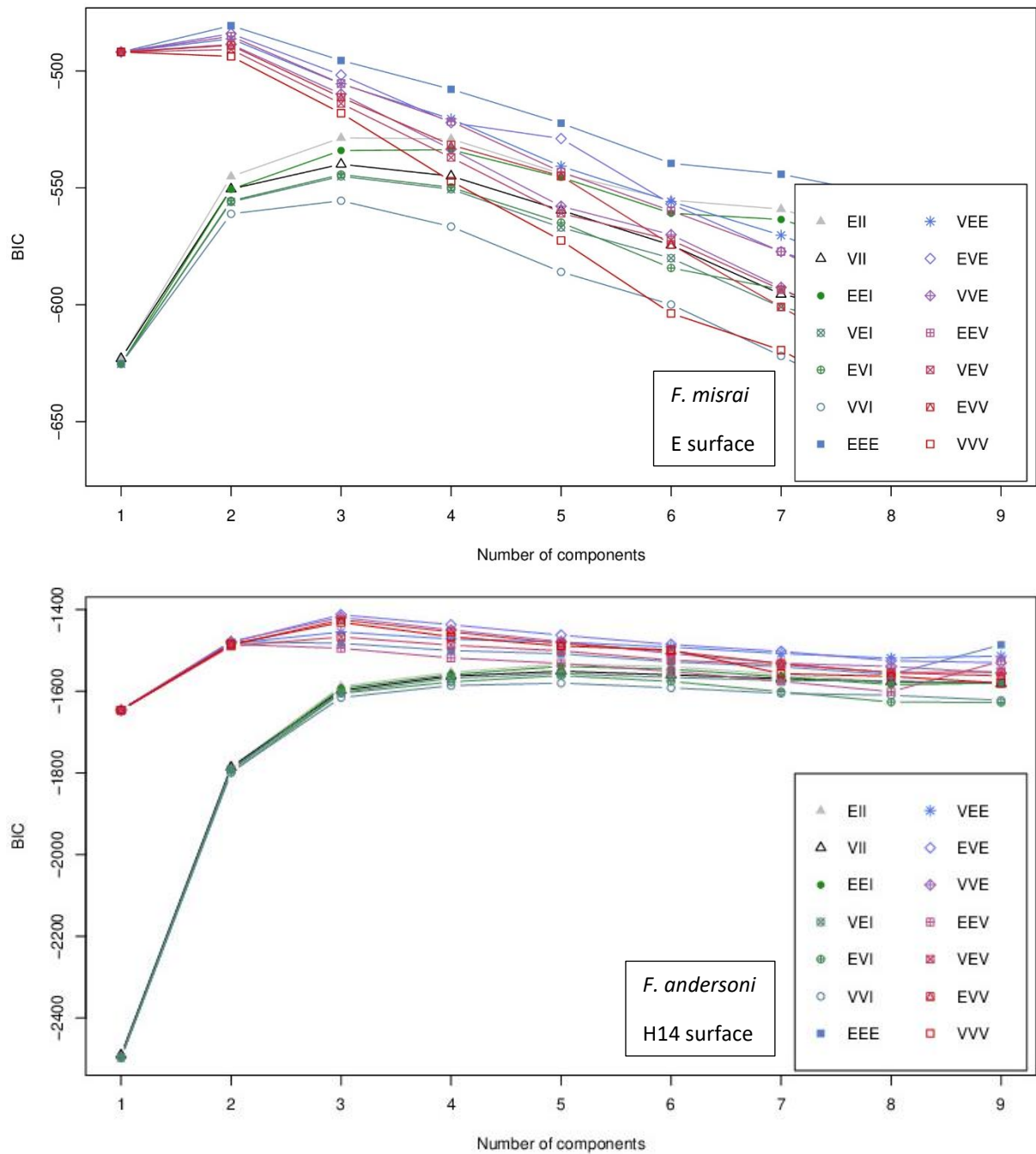
Fig. 3.5. Results of the multivariate analyses (length) performed using the mclust package in R.

3.4.2 Analyzing Shape

Given that the Shapiro-Wilk test determined that the *F. misrai* and *F. andersoni* length:width data are not normally distributed, they therefore required log transformation. The Shapiro-Wilk test determined non-normal distribution of the *F. misrai* and *F. andersoni* log transformed data.

The BIC results of the univariate analyses indicate that the best fit model for *F. misrai* and *F. andersoni* length:width data contained two clusters (Fig. 3.6), indicating two distinct specimen shape types for both species. The Wilcoxon test provided the result of a P-value lower than alpha, rejecting the null hypothesis of the two groups being equal, thus corroborating the result of two distinct shape groups as identified by the univariate analyses. It was found that for both species approximately 40% of specimens belong to shape one and approximately 60% of specimens belong to shape two. For *F. misrai*, the mean length:width values (e.g. Fig. 2.3) per shape group are 2.58 (shape 1) and 4.85 (shape 2), while for *F. andersoni* they are 1.2 (shape 1) and 2.2 (shape 2). Due to these shape-based results and the size-based (length and width) results both indicating multiple clusters, the next step was comparing the clusters by non-metric multidimensional scaling.
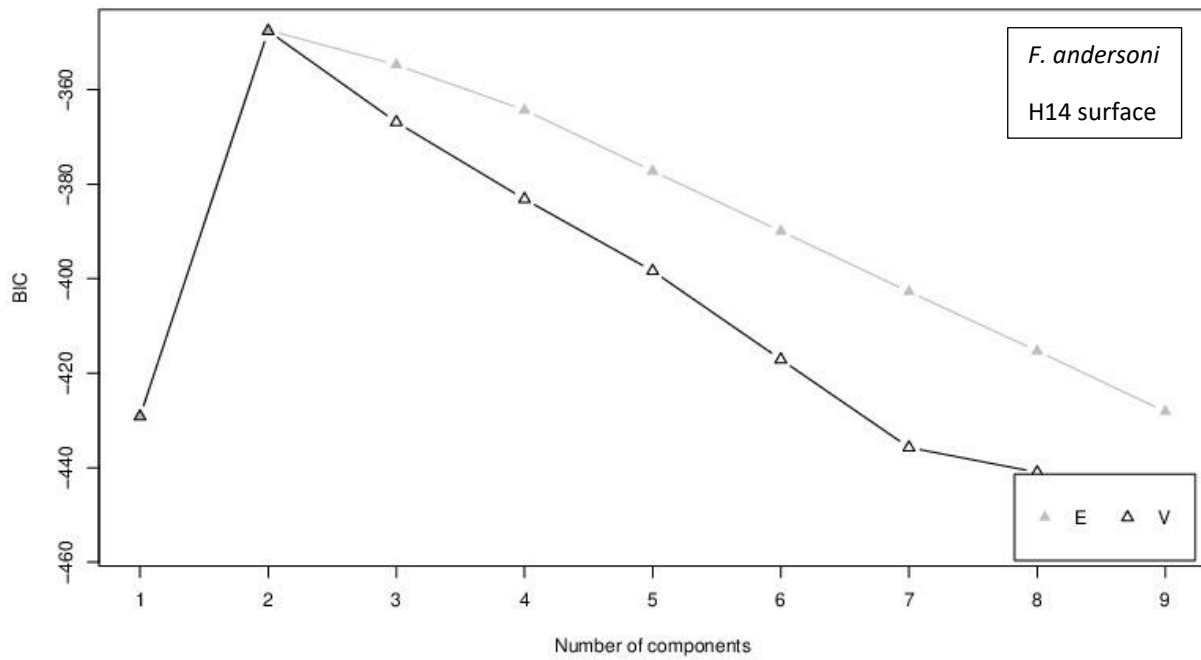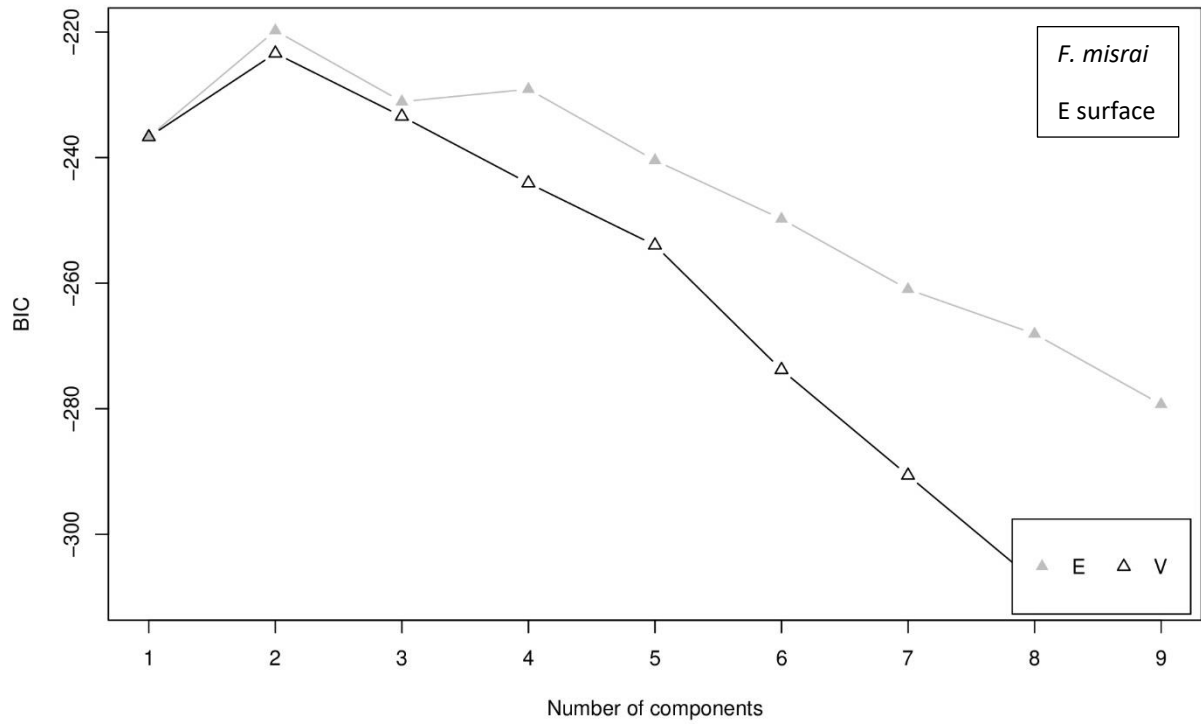
Fig. 3.6. Results of the univariate analyses (length:width) performed using the mclust package in R.

3.4.3 Comparing Size (L&W) and Shape (L:W) Clusters

NMDS plots were created using the vegan package in R as a means of visualizing and determining any differences or similarities between the size and shape clusters of *Fractofusus* found using the mclust package. The stress values of the NMDS plots were 0.029 (*F. misrai*) and 0.015 (*F. andersoni*), indicating good representation. The predetermined clusters are represented in the NMDS plots as different colored polygons (Fig. 3.7), notably showing very little overlap. Both the size and the shape clusters for *F. misrai* are nearly identical (Fig. 3.7A.B), whereas *F. andersoni* has three size clusters (Fig. 3.7C) and two shape clusters (Fig. 3.7D); the NMDS plots show that the third size cluster of F. *andersoni* contains the specimens of larger length and width and that this cluster disappears when the specimens are separated based on the shape metric (Fig. 3.7C,D). The NMDS plots of the shape clusters show comparable trends between the species with the clusters being influenced by the variables in a similar way, though the data for *F. andersoni* are more tightly constrained. It can also be noted from the NMDS plots that the orientation vector is the longest and therefore the most influential variable. Since the NMDS plots show clear similarities among the shape clusters and orientation as the longest vector, the relationship between shape and orientation was investigated next.
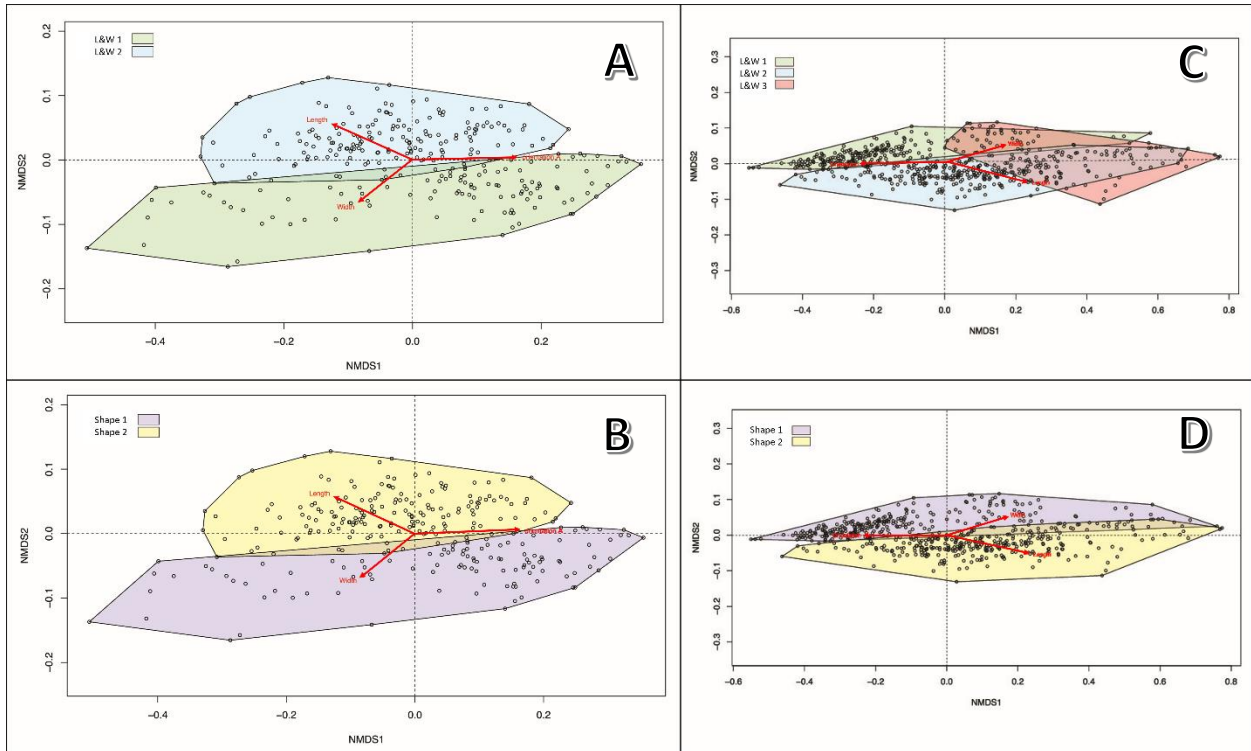
Fig. 3.7. NMDS plots: **A,B**, *F. misrai* on the E surface; **C,D**, *F. andersoni* on the H14 surface.

3.4.4 Assessing the Relationship Between Shape and Orientation

The violin and rose plots present the distribution of orientation data which has a range between 0° and 180°, showing that for both species the specimens in the shape one group are predominately southeasterly oriented and that shape 2 specimens are mostly northeasterly oriented (Fig. 3.8).

To determine whether the trends noted from the violin and rose plots were statistically significant, the Shapiro-Wilk test and the Wilcoxon test were utilized in R. The Shapiro-Wilk test determined that the orientation data are not normally distributed, therefore the Wilcoxon test was chosen (as it does not assume normality like the parametric alternative, the T-test) to determine if there is a statistically significant difference in the orientation variable for the two shape groups for each species. For both species, the Wilcoxon test provided the result of a P-value lower than alpha,

rejecting the null hypothesis of the two groups being equal, thus showing that the shape groups show statistically significant differences in orientation.
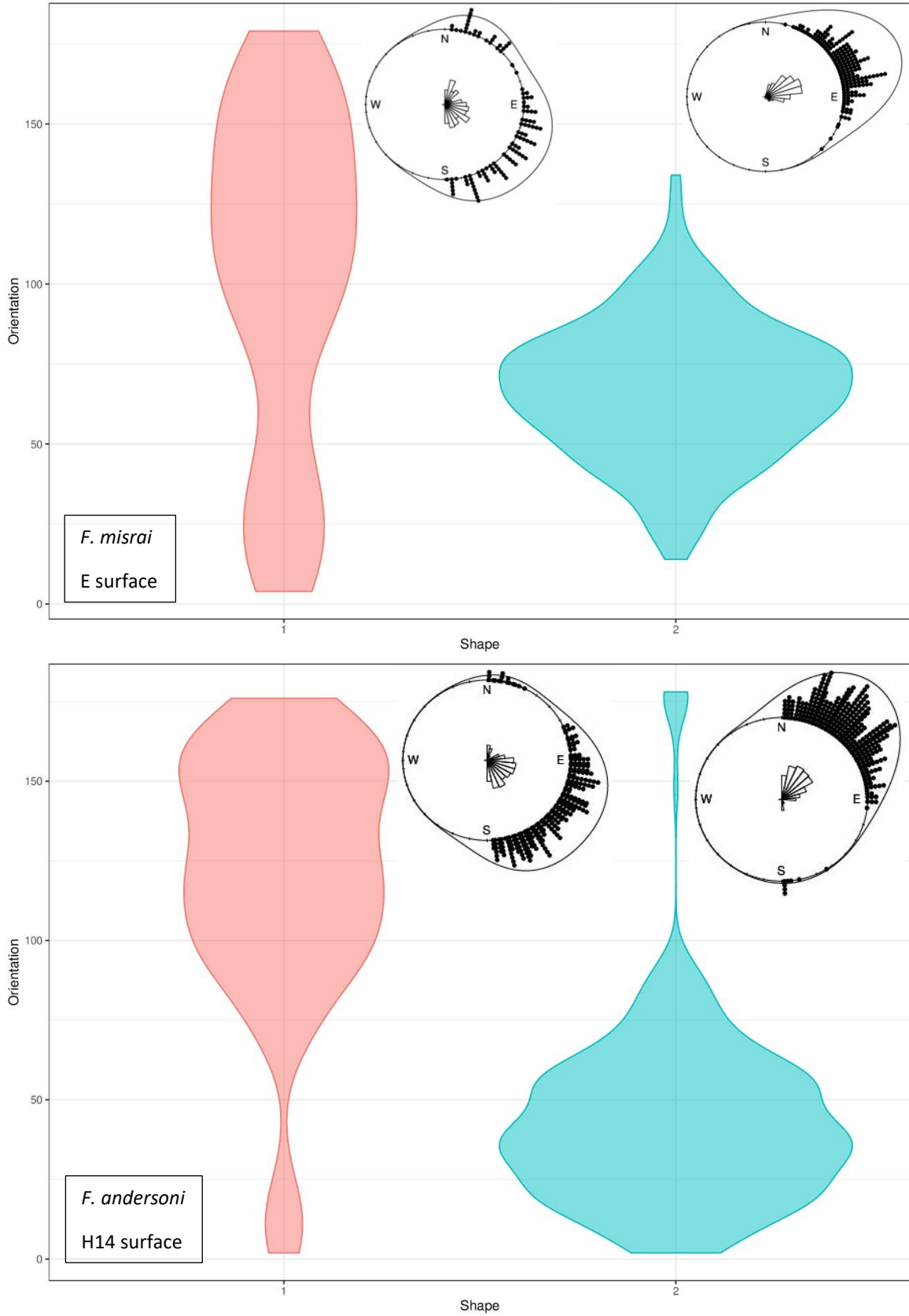
Fig. 3.8. Violin and rose plots showing the orientation of the two *Fractofusus* shape groups.

3.5 Retrodeformation

The *F. misrai* length, width and orientation data were retrodeformed and statistically analyzed in the same manner as the original data, returning similar results: length data contained one cluster, length and width data contained two clusters, length:width data contained two clusters, and similarly shaped violin and rose plots (Fig. 3.9). The most notable difference seen in the results from the retrodeformed data being a more pronounced NE peak in orientation data for the shape one specimens (Fig. 3.8, 3.9).
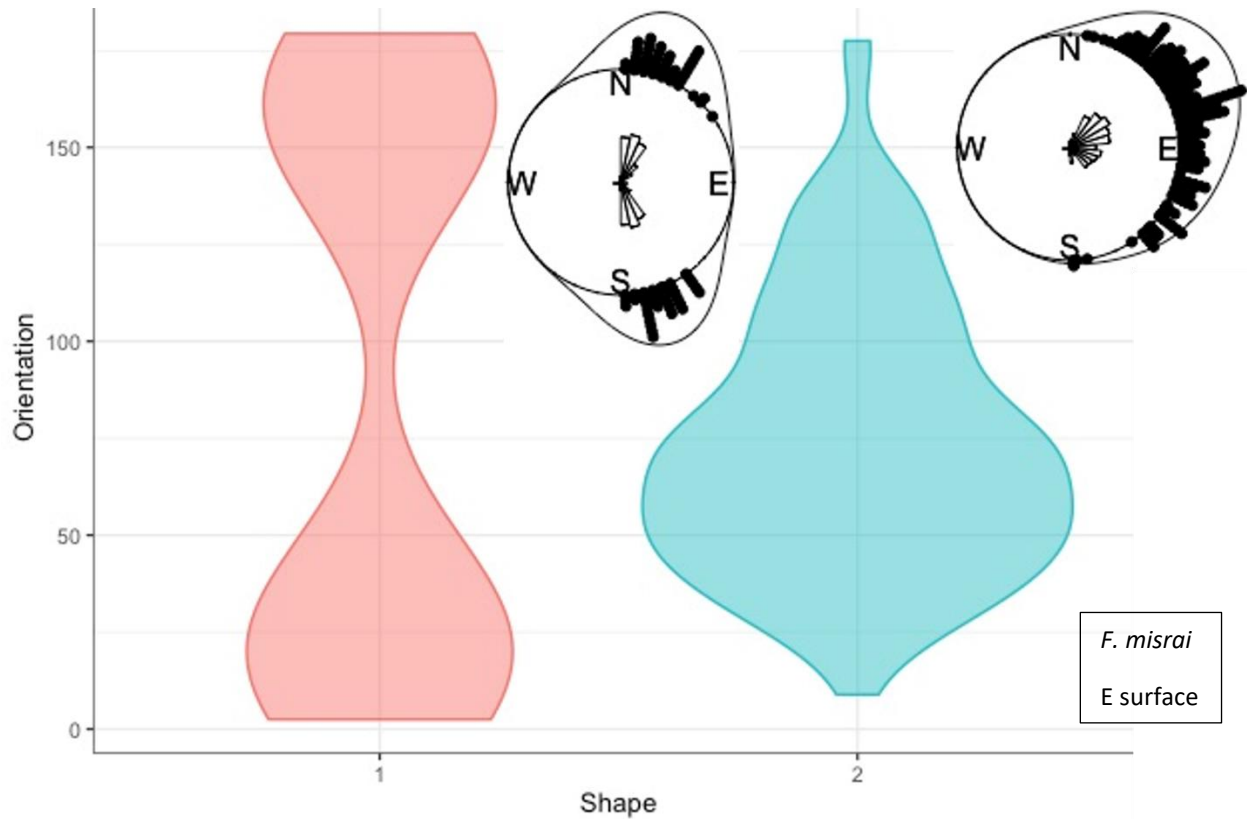
Fig. 3.9. Violin and rose plots showing the orientation of the two retrodeformed *Fractofusus misrai* shape groups.

4. Discussion

4.1 Population Structure and Reproduction

Due to the lack of modern analogues and preserved reproductive structures, the reproductive mode of these organisms is uncertain (Liu et al., 2015). One study reports filamentous organic structures interpreted as stolons, though in the case of *Fractofusus*, no fossils were reported to be actually connected via filaments (Liu and Dunn, 2020). As such, studies regarding reproduction have tended to focus on statistical methods in an attempt to understand population structure and infer reproductive modes (e.g. Darroch et al., 2013; Mitchell et al., 2015; Mitchell and Butterfield, 2018).

Analyzing size-frequency distributions is an established technique used to explore the population structure of marine organisms and has recently been utilized in Ediacaran paleontology (Darroch et al., 2013). An approach shared by two studies to resolve the number of size classes (modes in size metric data also interpreted as possible age classes or generations) in *Fractofusus* populations is fitting size frequency distribution data (specimen length and/or width) to various Gaussian finite mixture models and comparing the BIC values (Darroch et al., 2013; Mitchell et al., 2015). The first study used this approach for *F. misrai* on the E surface, in which the results corresponded to one size class (Darroch et al., 2013). From interpreting a single size class, several reproductive methods were hypothesized, though it was inferred that the results suggest continuous sexual reproduction (Darroch et al., 2013). The second study used a slightly different approach, whereby they also compared Thomas cluster models and used the results to interpret three size classes of *F. misrai* on the E surface, as well as three size classes *of F. andersoni* on the H14 surface; to strengthen this interpretation, BIC values were used to support three size classes of *F. andersoni* (Mitchell et al., 2015). Although, it is important to note that the same was not done for

F. misrai., as BIC values may have provided important additional results. Having interpreted three size classes, opposed to one (Darroch et al., 2013), different reproductive strategies were inferred; it was suggested that the initial population was established via waterborne propagules, and the two later groups were dispersed by stolons (Mitchell et al., 2015). However, in a later study using different statistical analyses (BNI and SPPA), results show inconsistency with multiple size classes on the E surface, and therefore support a single size class of *F. misrai* (Mitchell and Butterfield, 2018), in agreement with Darroch et al. (2013).

Notably, a different approach has been used to analyze the population structure of *F. misrai* on the E surface (Antcliffe et al., 2015). In that work, a decay index created and used solely by this study, was utilized to develop a new taphonomic model for the Mistaken Point surfaces, and to interpret *F. misrai* size frequency distribution (Antcliffe et al., 2015). The first statistical test used, similar to the other studies, is the Shapiro-Wilk test; the specimen length data failed the test, determining it is not normally distributed (Antcliffe et al., 2015). The Shapiro-Wilk test only tests if data is normally or not normally distributed, though the study states that the data forms a multimodal distribution; this claim lacks support without further statistical analyses (i.e. statistical tests created specifically to test for multimodality, such as the clustering methods employed by Darroch et al. (2013) and Mitchell et al. (2015)). The decay index is used to group the specimens into different decay grades, and by employing statistical F tests, it is interpreted that the grades correlate to three different generations within the population, grade 1, grade 2 and grade 3+4 (Antcliffe et al., 2015). Using a qualitative decay index in order to assess the data distribution allows for a certain degree of ambiguity.

Therefore, this study followed the methods described above used by Darroch et al. (2013) and Mitchell et al. (2015), in which size-frequency data was analyzed by comparing different

Gaussian finite mixture models fitted by an EM clustering algorithm using the package mclust (Scrucca et al., 2016) in R (R Core Team, 2022) and the best fit model was selected based on the Bayesian Information Criterion (BIC) values. This approach allows for objective and statistically meaningful results. The univariate (length) analyses indicated one cluster for *F. misrai* and two clusters for *F. andersoni*, whereas the multivariate (length and width) analyses indicated two and three clusters respectively. These results are similar to those described above from previous studies, with the unexpected exception of determining more clusters in the multivariate versus univariate analyses. In all studies, including this study, it is found that there are more size classes in the *F. andersoni* population than in that of the *F. misrai*; as suggested in the literature, this may be due to the different species of *Fractofusus* reproducing by different methods. Alternatively, we suggest that both species may have reproduced sexually, with *F. misrai* having reproduced continuously and *F. andersoni* non-continuously. We interpret the results of the size frequency distribution analyses found in this study as indicating an important interaction between specimen length and width, as such, length:width data (specimen shape proxy) was analyzed next.

Table 4.1. Summary of results from size frequency distribution analyses regarding *Fractofusus* population structure.

Study	Surface & Species	Number of classes
Darroch et al. (2013)	E & *F. misrai*	One
Mitchell et al. (2015)	E & *F. misrai* H14 & *F. andersoni*	Three
Antcliffe et al. (2015)	E & *F. misrai*	Three
Mitchell & Butterfield (2018)	E & *F. misrai*	One
This study (Univariate vs multivariate)	E & *F. misrai* H14 & *F. andersoni*	One or two Two or three

As a means of identifying possible different shapes among specimens, the same approach for analyzing population structure of using the package mclust in R was used, but with the length:width data. The analyses indicated that the length:width data for each species consisted of two clusters, which were interpreted as two distinct specimen shape types. Shape two represents the more elongated specimens whereas shape one is those more circular. Having found multiple clusters from both the size (length and width data) and shape (length:width data) analyses, NMDS plots were used to visualize and compare the clusters (Fig. 3.7). Interestingly, the NMDS plots of the shape clusters are remarkably similar between species and indicate the most important/influential variable as being orientation. Since no previous studies have investigated the relationship between *Fractofusus* shape and orientation, it was determined to be a worthwhile avenue to explore further.

4.2 Orientation Trends and Paleoenvironment / Mode of Life

Until recently, *Fractofusus* orientation analyses and interpretations were based on how data distribution appeared on distribution plots (e.g. histograms and rose plots) without any further quantitative analysis; due to the data appearing to be evenly distributed, showing no clear trends, *Fractofusus* has always been interpreted to be randomly oriented, an inference supporting a reclining lifestyle (Seilacher, 1999; Gehling and Narbonne, 2007; Mitchell et al., 2015). These interpretations have since been statistically supported by analyzing *Fractofusus* orientation data utilizing the clustering algorithms of the package mclust in R, in which no notable directionality was determined (Vixseboxse et al., 2021). The interpretation of random orientation for *Fractofusus* has long been based on either: 1) distribution of orientation data independently (Seilacher, 1999; Gehling and Narbonne, 2007); or 2) in relation to specimen length (Vixseboxse et al., 2021,

Mitchell et al., 2015), all having found no trends or relationships. This is in contrast to a recent study on a fossiliferous surface located near Melrose on the Bonavista Peninsula, which statistically analyzed the orientation of *F. misrai* specimens in relation to both specimen length and width (Pérez-Pinedo et al., 2023). That work found that analyzing these three variables together resulted in two distinct specimen orientation directions (Pérez-Pinedo et al., 2023). In this study, we analyzed *Fractofusus* in similar ways to that of earlier studies, as well as using an additional shape-based methodology not previously employed.

4.2.1 Orientation Data Distribution for F. misrai Specimens on the E Surface

The apparently even distributions found for *F. misrai* orientation data has been for retrodeformed specimens (Seilacher, 1999; Gehling and Narbonne, 2007; Vixseboxse et al., 2021). As mentioned previously, retrodeformation is based on the assumption that the holdfasts of Ediacaran fossils were circular during life (Jenkins and Gehling, 1978; Wood et al., 2003). Though cautious of this methodology, to be consistent with previous studies, retrodeformation was applied to the E surface *F. misrai* specimens of this study. It is clear however that, if there is deformation and the discs were circular, that it is highly heterogenous and a single retrodeformation metric cannot be applied to all specimens (Liu, 2011), therefore both the original and retrodeformed results were analyzed, interpreted and considered.

When comparing the distribution of retrodeformed orientation data versus original data, there is a clear difference, with retrodeformed data appearing more evenly distributed and original data showing an apparent northeast trend (Seilacher, 1999; Gehling and Narbonne, 2007; Vixseboxse et al., 2021). This is also seen with the data used in this study (Fig. 4.1). Since past studies focused on retrodeformed data, an even distribution of data was interpreted as meaning

56

Fractofusus was a group of reclining organisms that were firmly attached to the seafloor matground and not subject to the influence of paleocurrents, unlike other taxa, that have been interpreted as upright organisms felled and oriented by turbidity or contour currents (Seilacher, 1999; Gehling and Narbonne, 2007; Vixseboxse et al., 2021). How data distribution appears should be used as a preliminary measure, and further analyses (e.g. statistical tests) should be applied in order to form meaningful and significant interpretations.
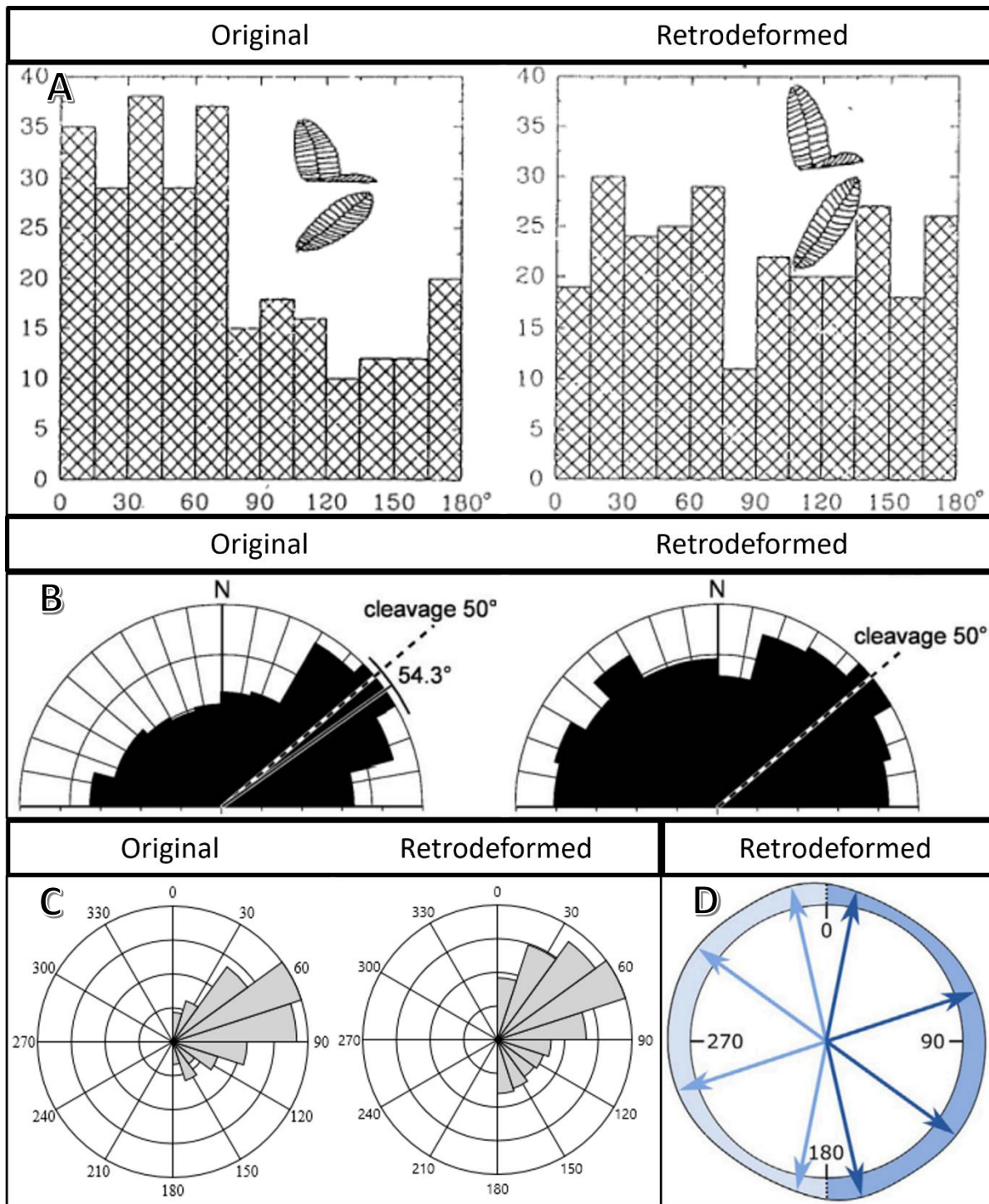
Fig. 4.1. *Fractofusus misrai* specimen orientations, E surface. **A**, from Seilacher, 1999; **B**, from Gehling and Narbonne, 2007; **C**, This study, and **D**, from Vixseboxse et al., 2021.

4.2.2 Orientation Data Distribution for F. andersoni Specimens on the H14 Surface

The orientation of *F. andersoni* specimens is far less studied than *F. misrai*, and to our knowledge has only been analyzed by Mitchell et al. (2015). Unlike the previously discussed studies regarding *F. misrai*, Mitchell et al. (2015) did not apply retrodeformation to *F. andersoni* specimens on the H14 surface as the surface shows no obvious distortion or deformation indicators. Using a statistical clustering technique, *F. andersoni* specimens were determined to fall into three different size classes, and the orientation of specimens in each class were presented in rose diagrams, all showing nearly even distributions (Mitchell et al., 2015). Using the same statistical clustering method, this study found two size classes, and in agreement with Mitchell et al. (2015), an even distribution of orientation data in each size class (fig. 4.2). These findings are similar to those pertaining to *F. misrai*, furthering the idea of reclining organisms not being influenced by paleocurrents (Mitchell et al., 2015). In contrast to earlier studies of *Fractofusus* orientation, this study statistically analyzed specimens based on shape (length:width data). Utilizing the same clustering technique used to determine size classes, two shape groups of *F. andersoni*, as well as *F. misrai*, were determined in this study. The orientation of specimens in each class were presented in rose diagrams showing distinct trends relative to shape (Fig. 3.8), which has not been attempted in prior studies. While *Fractofusus* may not have been influenced by paleocurrents in the way some other taxa were (i.e. felled), they may have been influenced differently, by way of rheotropic growth and ecophenotypism. Here we find the more circular specimens to be oriented parallel to the proposed southeasterly clear-water paleocurrent (McIlroy et al., 2022), and the more elongated specimens being oriented perpendicular to the paleocurrent. In these orientations, specimens appear to have been attempting to expose a wide portion of their body to the paleocurrent, which we interpret as specimens orienting themselves in the most beneficial manner in terms of nutrition,

oxygenation and/or gas exchange (cf. Pérez-Pinedo et al., 2023). Since data distribution is a preliminary measure, these interpretations will be discussed in relation to statistical findings.
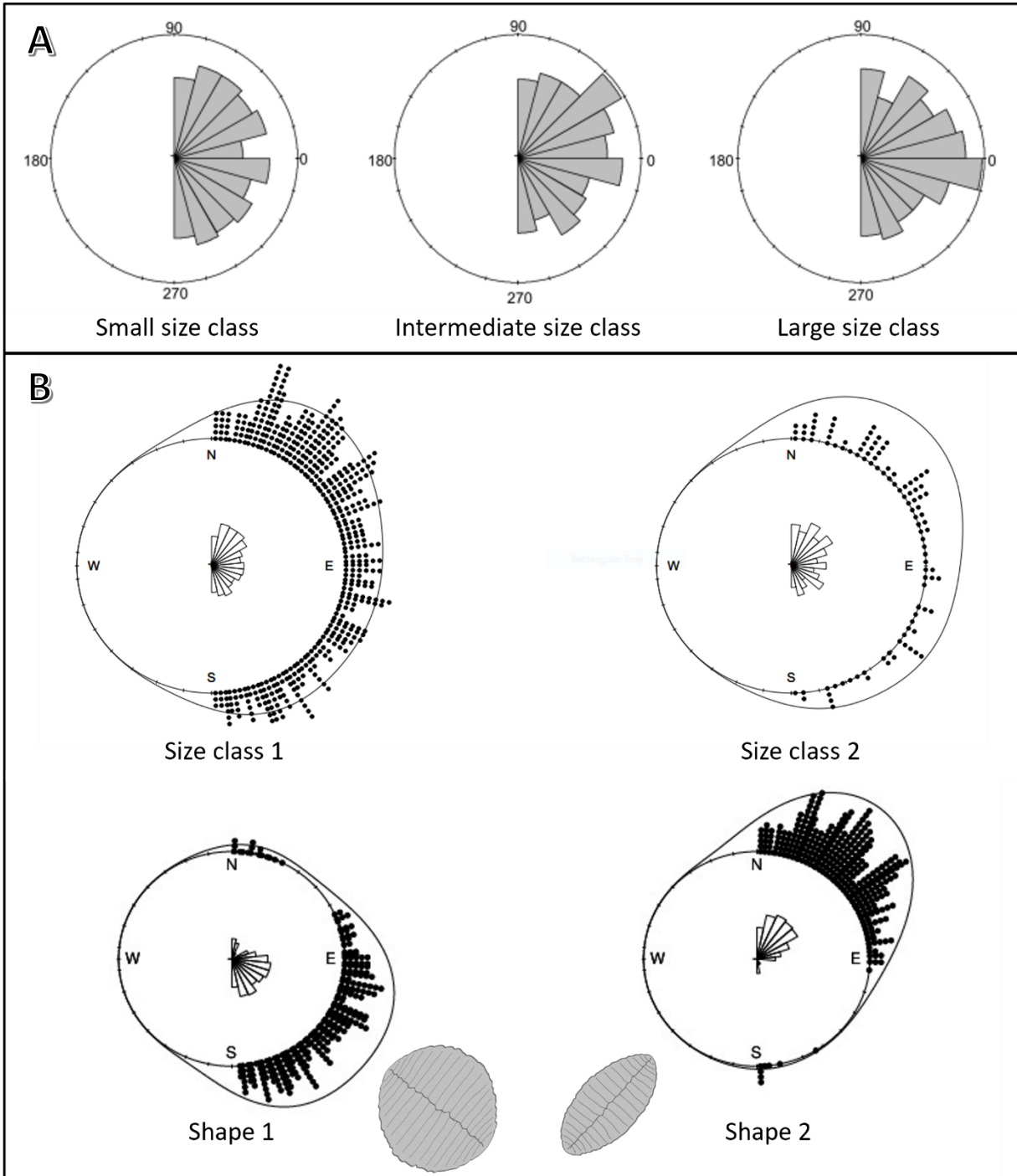
Fig. 4.2. A, Orientation of *F. andersoni* length clusters, H14 surface (from Mitchell et al., 2015); **B**, Orientation of *F. andersoni* length versus length:width clusters, H14 surface (this study).

4.2.3 Comparison of Three Statistical Approaches

Very few studies have statistically analyzed *Fractofusus* orientation data, notably Vixseboxse et al. (2021) and Pérez-Pinedo et al. (2023). By statistically analyzing the distribution of orientation data of *F. misrai* specimens on the E surface, a multimodal distribution was determined, with all mean orientations being evenly distributed thus showing no clear directionality (Vixseboxse et al., 2021). The length of specimens belonging to each orientation mode was statistically tested, finding no significant correlations (Vixseboxse et al., 2021). These statistical findings were interpreted to be in agreement with the traditional idea of *Fractofusus* being a reclining organism that was neither influenced by contour paleocurrents nor disturbed by episodic turbidity paleocurrents (Vixseboxse et al., 2021).

These ideas have recently been challenged and opposed from a conceptual point of view (McIlroy et al., 2022), and by analysis of taxa with respect to independent sedimentological paleocurrent indicators (Pérez-Pinedo et al., 2023). By statistically analyzing the relationship of orientation, length and width data of *F. misrai* specimens on the Melrose Surface by way of modified parallel coordinate plots (PCPs) and polythetic cluster analysis, a bimodal distribution was determined showing clear preferential orientations (Pérez-Pinedo et al., 2023). The findings of Pérez-Pinedo et al. (2023) are important as the study is the first to determine non-random orientation of *Fractofusus*. Consistent with the idea of rheotropic growth of reclining organisms in response to clear-water background currents (McIlroy et al., 2022), it is suggested that *F. misrai* is oriented in two primary directions as a rheotropic response in order to perhaps either maximize adsorption of dissolved organic matter or to reduce risk of being lifted by a current and damaged or transported away (Pérez-Pinedo et al., 2023).

This study is the first to focus on specimen shape; many factors led to this line of investigation. Firstly, due to analyses of total (retrodeformed) *Fractofusus* specimens having always concluded an even distribution of data showing no apparent orientation trends (Seilacher, 1999; Gehling and Narbonne, 2007; Vixseboxse et al., 2021). Additionally, investigation of a relationship between specimen length and orientation has never found any trends (Mitchell et al., 2015; Vixseboxse et al., 2021). The first promising results of any *Fractofusus* specimen orientation trends were found when comparing the three variables of specimen orientation, length and width (Pérez-Pinedo et al., 2023); this shows an important relationship between *Fractofusus* length and width, which we further investigated in this study. The initial clustering analyses of this study found more clusters of specimens when testing specimen length and width together than when considered independently (Fig. 3.4, 3.5), indicating a possible relationship between specimen length and width, which was further explored by analyzing specimen length:width data as a proxy for specimen shape. This relationship was confirmed both by the clustering analyses of the length:width data, which found two clusters for each species (Fig. 3.6, 4.3), and very similar trends in the NDMS plots of the shape clusters for each species, which showed orientation as the most influential variable (Fig. 3.7). Having identified two shape groups and orientation as an influential variable, the orientation of specimens in each shape group was analyzed, finding clear trends that were determined to be statistically significant via the Wilcoxon test (Fig. 3.8, 3.9).
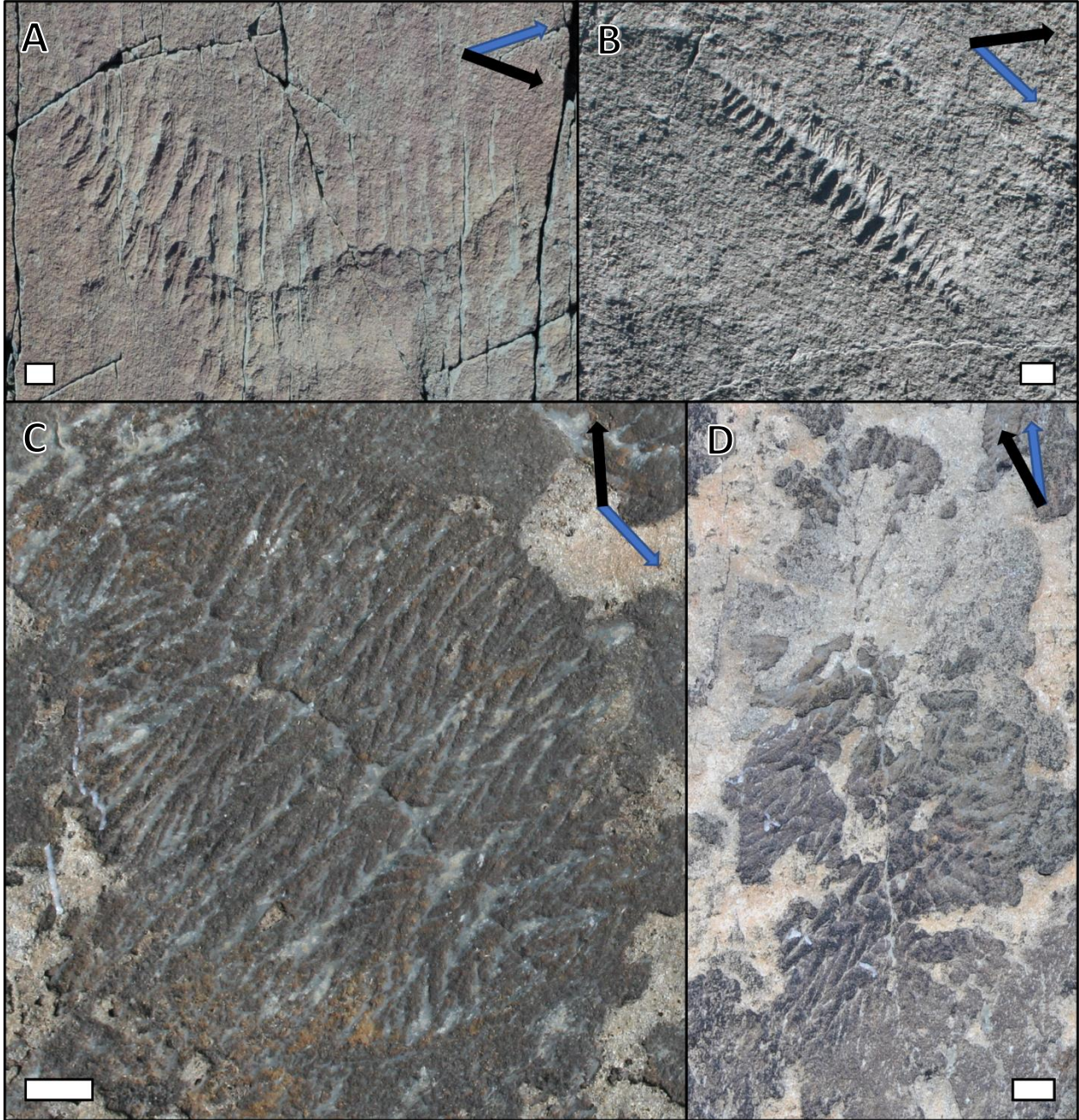
Fig. 4.3. Specimen examples represesting the mean length:width values of the two shape types of **A**, **B**, *F. misrai* and **C**, **D**, *F. andersoni*. Black arrows showing north and blue arrows showing specimen orientation. Scale: 1 cm.

4.2.4 Fractofusus Specimen Shape Analyses Reveal Possible Rheotropic Habits

The results of this study align with the recent interpretations of rheotropic growth in response to deep marine background clear-water currents (McIlroy et al., 2022, Pérez-Pinedo et al., 2023). Having found two main specimen orientation directions, it was interpreted that *F. misrai* might be oriented in such directions as a rheotropic response in order to maximize adsorption of dissolved organic matter or simply to reduce risk of dislocation (Pérez-Pinedo et al., 2023). Our findings of circular specimens oriented near parallel and elongated specimens oriented near perpendicular to a proposed background clear-water (southeasterly) current (McIlroy et al., 2022), suggests that the orientation trends might be due to nutrition being the primary controlling factor. It is considered that based on how the organisms were originally oriented, these nonmotile organisms grew accordingly (longer versus wider) to expose a wide portion of their body to the oncoming current for optional nutrient and/or oxygen uptake. Several lines of evidence lead to this interpretation, notably the low threat of removal by current disturbance and the inferred importance of resources from currents. Mostly negative sedimentological evidence, such as the lack of winnowed horizons, the absence of evidence for uprooting, and the paucity of evidence for tearing of specimens, support relatively weak background currents (Wood et al., 2003). As well, mat-related sedimentary structures may evince microbial mats/matground, which have been suggested as having aided in organism attachment to the seafloor (Seilacher, 1999; Wood et al., 2003). Taphonomic evidence suggests *Fractofusus* was intimately associated with the matground, likely growing partially within it (Taylor et al., 2023). Also, while drag force would have been present, organisms can utilize drag to facilitate feeding and respiration, and flow model experiments demonstrate that organisms with highly textured surfaces, like the fractal-like branching of *Fractofusus*, can reduce drag and capture the oncoming water (Singer et al., 2012). As such, it is

unlikely that the background currents were sufficient to lift *Fractofusus* from the seafloor, therefore, nutrition or oxygen capture was perhaps the driving force behind the rheotropic growth of the reclining organisms like *Fractofusus*.

The Ediacaran organisms of Newfoundland are found in deep marine depositional settings that are generally considered to be well below the photic zone, supporting the idea of these organisms not being photoautotrophs (Wood et al., 2003). In such settings, currents rich in nutrients and oxygen were likely critical to their survival (Wood et al., 2003). Several feeding strategies have been suggested, notably suspension feeding (e.g. Jenkins, 1985; Clapham and Narbonne, 2002), osmotrophy (Laflamme et al., 2009, Hoyal Cuthill and Conway Morris, 2014), and chemoautotrophy (e.g. Durfour and McIlroy, 2017). Rheotropic growth has recently been suggested to be responsible for the orientation of reclining rangeomorphs, as a means to achieve optimal nutrient/oxygen uptake from oncoming currents (McIlroy et al., 2022, Pérez-Pinedo et al., 2023). The findings of computational fluid dynamic simulations have been used to suggest that rangeomorph fronds were employed primarily for respiration and gas exchange rather than feeding (Darroch et al., 2023). Whether it be feeding, respiration or gas exchange, the hydrodynamic regime experienced by the organisms is likely to have been of key importance. As such, it is intuitive that reclining organisms would orient/grow in respect to the oncoming current in manners favorable for these mechanisms. Such habits have been seen in other marine organisms, for example, several species of bryozoans (Ryland, 1977). The orientation trends found in this study show *Fractofusus* organisms generally had their widest point facing the (weak) oncoming southeasterly paleocurrent (e.g. fig. 4.4), supporting rheotropic growth in which the organisms would have optimally exposed more of their branches to potential nutrients and oxygen.
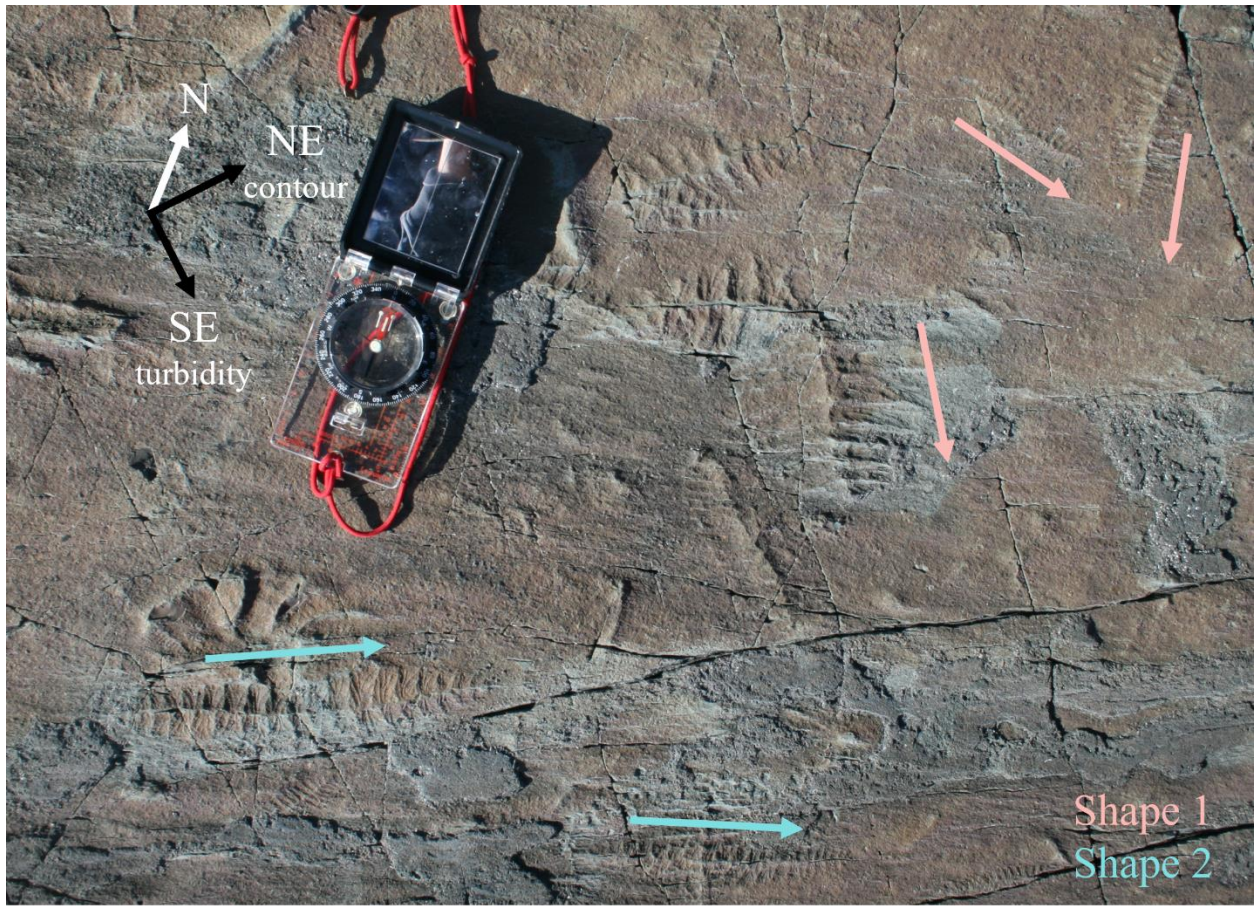
Shape	L:W Mean	Orientation
1	2.58	SE
2	4.85	NE

Fig. 4.4. A portion of the E surface with the *F. misrai* specimen shape and orientation trends found in this study.

4.2.5 Ediacaran Biota, mode of life and rheotropism

The concept that many (but not all, notably *Fractofusus*) Ediacaran taxa—particularly the Rangeomorpha and Arboreomorpha—were immobile organisms living upright in the water column has persisted for over sixty years (e.g. Ford, 1958; Jenkins and Gehling, 1978; Glaessner, 1984), but recently challenged by reclining rheotropic growth (McIlroy et al., 2020, 2021, 2022; Pérez-Pinedo et al., 2023). One of the first significant oppositions to the upright mode of life was that of Seilacher (1992), who interpreted many taxa (i.e. *Fractofusus*, *Beothukis*, and *Hapsidophyllas*) as recliners before they were even formally described. Several taxa have since been reinterpreted as recliners, such as *Bradgatia*, *Pectinifrons abyssalis*, *Charniodiscus procerus*, *Charnia* and *Beothukis*, many of which have also been interpreted as having exhibited a degree of rheotropism (McIlroy et al., 2020, 2022; Pérez-Pinedo et al., 2022, 2023). The results of this study fall in line with recent reinterpretations, in which rheotropism may have been important for the mode of life and cause of orientation trends for *Fractofusus*, and possibly other taxa. Interestingly, the holotype and other specimens of *Beothukis* can be seen oriented near perpendicular to the proposed southeasterly paleocurrent (see figure 1 (McIlroy et al., 2022)); interpreted as having a similar mode of life to *Fractofusus*, implying that perhaps *Beothukis mistakensis* also responded rheotropically to paleocurrents. There are however few clear examples of *B. mistakensis* thus it is difficult to make reliable inferences regarding that taxon (McIlroy et al., 2022), though there are undoubtably other beothukid species on the surface which do appear to be current oriented (Vixseboxse et al. 2022).

5. Conclusion

The reproductive mode of *Fractofusus* has continued to be uncertain due to the lack of modern analogues and preserved reproductive structures (Liu et al., 2015). Previous studies have focused primarily on statistical methods in attempts to understand population structure and infer reproductive modes. Analyzing size-frequency distributions has been a common approach in exploring the population structure of marine organisms, recently including Ediacaran organisms. Notably, Darroch et al. (2013) determined one size class of *F. misrai* on the E surface inferring continuous sexual reproduction, while Mitchell et al. (2015) found three size classes of both *F. misrai* on the E surface and *F. andersoni* on the H14 surface inferring reproduction via waterborne propagules and stolons. Our statistical results and interpretations are similar to previous studies, finding fewer size classes of *F. misrai* (E surface) than *F. andersoni* (H14 surface). The different numbers of discrete size classes between species could indicate species-specific reproductive modes. Overall, the interpretation of reproductive modes in these organisms remains unclear and lacks consensus. The use of statistical analyses provides objective and statistically meaningful results, but different approaches and interpretations (Darroch et al., 2013; Antcliffe et al., 2015; Mitchell et al., 2015; Mitchell & Butterfield, 2018), have led to varying conclusions. Additional studies and data of other surfaces may provide a clearer understanding of the reproductive strategies of *Fractofusus*.

Apart from statistically analyzing *Fractofusus* population structure, this study also utilized statistical analyses to investigate a potential relationship between specimen shape and orientation. Traditionally, *Fractofusus* orientation analyses were based on visual assessments without quantitative analysis, leading to the interpretation of randomly oriented reclining organisms (Seilacher, 1999; Gehling and Narbonne, 2007; Mitchell et al., 2015). However, recent studies

have challenged this interpretation and utilized statistical techniques to analyze *Fractofusus* orientation, finding statistically preferential orientation trends interpreted as organisms growing rheotropically in response to a persistent background current (Pérez-Pinedo et al., 2023). This study further supported this interpretation, by statistically analyzing the relationship between specimen shape and orientation, determining that circular specimens were oriented parallel and elongated specimens were oriented perpendicular to a southeasterly paleocurrent. The findings of this study have important implications for understanding *Fractofusus* paleoecology. The shape-based orientation trends suggest *Fractofusus* may have oriented their widest point into the oncoming current in order to maximize nutrient and/or oxygen uptake. This aligns with recent rheotropic growth interpretations (McIlroy et al., 2022) and challenges the traditional view of reclining organisms in the Ediacaran being randomly oriented and uninfluenced by paleocurrents. Overall, this study provides valuable insights into *Fractofusus* orientation patterns, highlighting the importance of statistical and paleoenvironmental analyses in understanding the ecology of ancient organisms. Further statistical analyses of this nature applied to other species and fossiliferous surfaces may contribute to a more comprehensive understanding of how the Ediacaran biota adapted to their marine paleoenvironment.

References

Anderson, M.M., and Misra, S.B. 1968. Fossils found in the Pre-Cambrian Conception Group of South-eastern Newfoundland. Nature, **220**: 680-681.

Antcliffe, J.B., Hancy, A.D., and Brasier, M.D. 2015. A new ecological model for the ~565 Ma Ediacaran biota of Mistaken Point, Newfoundland. Precambrian Research, **268**: 227-242.

Bak, R.P.M., and Meesters, E.M. 1998. Coral population structure: the hidden information of colony size-frequency distributions. Marine Ecology Progress Series, **162**: 301–306.

Benus, A.P. 1988. Sedimentological context of a deep-water Ediacaran fauna (Mistaken Point Formation, Avalon Zone, Eastern Newfoundland). *In* E. Landing and G.M. Narbonne, and Paul Myrow. Trace fossils, small shelly fossils and the Precambrian-Cambrian boundary. Bulletin of the New York State Museum, **463**: 8-9.

Billet, D.S.M., and Hanson, B. 1982. Abyssal aggregations of *Kolga hyalina* Danielssen and Koren (Echinodermata: Holothurioidea) in the northeast Atlantic Ocean: a preliminary report. Deep Sea Research, **29**: 799–818.

Brasier, M.D., and Antcliffe, J.B. 2009. Evolutionary relationships within the Avalonian Ediacara biota: new insights from laser analysis. Journal of the Geological Society, **166**: 363-384.

Brasier, M.D., Antcliffe, J.B., and Liu, A.G. 2012. The architecture of Ediacaran fronds. Paleontology, **55**(5): 1105-1124.

Clapham, M.E., and Narbonne G.M. 2002. Ediacaran epifaunal tiering. Geology, **30**(7): 627-630.

Clapham, M.E., Narbonne, G.M., and Gehling, J.G. 2003. Paleoecology of the oldest known animal communities: Ediacaran assemblages at Mistaken Point, Newfoundland. Paleobiology, **29**(4): 527-544.

Clapham, M.E., Narbonne, G.M., Gehling, J.G., Greentree, C., and Anderson, M.M. 2004. *Thectardis avalonensis*: a new Ediacaran fossil from the Mistaken Point biota, Newfoundland. Journal of Paleontology, **76**(6): 1031-1036.

Clarke, K.R. 1993. Non-parametric multivariate analyses of changes in community structure. Australian Journal of Ecology, **18**: 117-143.

Hoyal Cuthill, J.F., and Conway Morris, S. 2014. Fractal branching organizations of Ediacaran rangeomorph fronds reveal a lost Proterozoic body plan. Proceedings of the National Academy of Sciences, **111**(6): 13122–13126.

Darroch, S.A., Laflamme, M., and Clapham, M.E. 2013. Population structure of the oldest known macroscopic communities from Mistaken Point, Newfoundland. Paleobiology, **39**(4): 591-608.

Darroch, S.A.F., Gutarra, S., Masaki, H., Olaru, A., Gibson, B.M., Dunn, F.S., Mitchell, E.G., Racicot, R.A., Burzynski, G., and Rahman, I.A. 2023. The rangeomorph *Pectinifrons abyssalis*: Hydrodynamic function at the dawn of animal life. iScience, **26**(2).

Dececchi, T.A., Narbonne, G.M., Greentree, C., and Laflamme, M. 2017. Relating Ediacaran fronds. Paleobiology, **43**(2): 171-180.

Dufour, S., and McIlroy, D. 2017. Ediacaran pre-placozoan diploblasts in the Avalonian biota: the role of chemosynthesis in the evolution of early animal life. Geological Society London Special Publications, **448**(1): 211-219.

Dufour, S.C., and McIlroy, D. 2017. An Ediacaran pre-placozoan alternative to the pre-sponge route towards the Cambrian explosion of animal life: a comment on Cavalier-Smith 2017. Philosophical Transactions of the Royal Society B, **373**: 1-4.

Dunn, F.S., Liu, A.G., and Donoghue, P.C. 2018. Ediacaran developmental biology. Biological Reviews, **93**(2): 914-932.

Erwin, D.H., Laflamme, M., Tweedt, S.M., Sperling, E.A., Pisani, D., and Peterson, K.J. 2011. The Cambrian conundrum: early divergence and later ecological success in the early history of animals. Science, **334**(6059): 1091-1097.

Fedonkin, M.A. 1980. New Precambrian Coelenterata in the north of the Russian Platform. Paleontological Journal, **14**(2): 1-10.

Ford, T.D. 1958. Pre-Cambrian fossils from Charnwood Forest. Proceedings of the Yorkshire Geological Society, **31**: 211–217.

Fraley, C., and Raftery, A.E. 2007. Bayesian regularization for normal mixture estimation and model-based clustering. Journal of Classification, **24**: 155–188.

Gehling, J.G. 1999. Microbial mats in terminal Proterozoic siliciclastics: Ediacaran death masks. Palaios, **14**(1): 40-57.

Gehling, J.G., Narbonne, G.M., and Anderson, M.M. 2000. The first named Ediacaran body fossil, *Aspidella Terranovica*. Paleontology, **43**(3): 427-456.

Gehling, J.G., and Narbonne, G.M. 2007. Spindle-shaped Ediacara fossils from the Mistaken Point assemblage, Avalon Zone, Newfoundland. Canadian Journal of Earth Sciences, **44**: 367-387.

Glaessner, M.F. 1984. The dawn of animal life: a biohistorical study. Cambridge University Press, Cambridge.

Hallam, A. 1967. The interpretation of size-frequency distributions in molluscan death assemblages. Palaeontology, **10**: 25-42.

Hammer, Ø., and Harper, D.A.T. 2006. Paleontological data analysis. Blackwell Publishing.

Hawco, J.B., Kenchington, C.G., and McIlroy, D. 2019. A quantitative and statistical discrimination of morphotaxa within the Ediacaran genus *Palaeopascichnus*. Papers in Paleontology.

Hintze, J.L., and Nelson, R.D. 1998. Violin plots: A box plot-density trace synergism. The American Statistician, **52**(2): 181-184.

Hofmann, H.J., O'Brien, S.J., and King, A.F. 2008. Ediacaran biota on Bonavista Peninsula, Newfoundland, Canada. Journal of Paleontology, **82**(1): 1-36.

Ichaso, A.A., Dalrymple, R.W., and Narbonne, G.M. 2007. Paleoenvironmental and basin analysis of the late Neoproterozoic (Ediacaran) Upper Conception and St. John's Groups, West Conception Bay, Newfoundland. Canadian Journal of Earth Sciences, **44**: 25-41.

Jenkins, R. J. F. 1985. The enigmatic Ediacaran (late Precambrian) genus *Rangea* and related forms. Paleobiology, **11**: 336-355.

Jenkins, R.J.F., and Gehling, J.G. 1978. A review of the frond-like fossils of the Ediacara assemblage. South Australian Museum Records, **17**: 347-359.

Kruskal, J.B. 1964. Multidimensional scaling by optimizing goodness of fit to a nonmetric hypothesis. Psychometrika, **29**: 1–27.

Laflamme, M., Schiffbauer, J., and Dornbos, S. 2011. Quantifying the evolution of early life, topics in geobiology. Springer Science + Business Media B.V.

Laflamme, M., Xiao, S., and Kowalewski, M. 2009. Osmotrophy in modular Ediacara organisms. Proceedings of the National Academy of Sciences of the United States of America, **106**(34): 14438-14443.

Liu, A.G.S.C. 2011. Understanding the Ediacaran assemblages of Avalonia: A paleoenvironmental, taphonomic and ontogenetic study. PhD thesis, Department of Earth Sciences, The University of Oxford.

Liu, A.G. 2016. Framboidal pyrite shroud confirms the 'Death Mask' model for moldic preservation of Ediacaran soft-bodied organisms. Palaios, **32**(3): 197-198.

Liu, A.G., and Dunn, F.S. 2020. Filamentous connections between Ediacaran fronds. Current Biology, **30**(7), 1322-1328.

Liu, A.G., Kenchington, C.G., and Mitchell, E.G. 2015. Remarkable insights into the paleoecology of the Avalonian Ediacaran macrobiota. Gondwana Research, **27**: 1355-1380.

Liu, A.G., and Matthews, J.J. 2017. Great Canadian lagerstätten 6. Mistaken Point Ecological Reserve, Southeast Newfoundland. Geoscience Canada, **44**: 63-76.

Liu, A.G., McIlroy, D., Antcliffe, J.B, and Brasier, M.D. 2011. Effaced preservation in the Ediacara biota and its implications for the early macrofossil record. Palaeontology, **54**(3): 607-630.

Lomas, S.A., and Joseph, P. 2004. Confined turbidite systems. Geological Society, London, Special Publications, **222**(1): 1-7.

Mason, S.J., and Narbonne, G.M. 2016. Two new Ediacaran small fronds from Mistaken Point, Newfoundland. Journal of Paleontology, **90**(2): 183-194.

Mason, S.J., Narbonne, G.M., Dalrymple, R.W., and O'Brien, S.J. 2013. Paleoenvironmental analysis of Ediacaran strata in the Catalina Dome, Bonavista Peninsula, Newfoundland. Canadian Journal of Earth Sciences, **50**: 197-212.

Matthews, J.J., Liu, A.G., Yang, C., McIlroy, D., Levell, B., and Condon, D.J. 2021. A chronostratigraphic framework for the rise of the Ediacaran macrobiota: new constraints from Mistaken Point Ecological Reserve, Newfoundland. The Geological Society of America Bulletin, **133**(3-4): 612-624.

McIlroy, D., Hawco, J., McKean, C., Nicholls, R., Pasinetti, G., and Taylor, R. 2020. Palaeobiology of the reclining rangeomorph *Beothukis* from the Ediacaran Mistaken Point Formation of southeastern Newfoundland. Geological Magazine, **159**(7): 1160-1174.

McIlroy, D., Dufour, S.C., Taylor, R., and Nicholls, R. 2021. The role of symbiosis in the first colonization of the seafloor by macrobiota: Insights from the oldest Ediacaran biota (Newfoundland, Canada). Biosystems, **205**: 1-16.

McIlroy, D., Pérez-Pinedo, D., Pasinetti, G., McKean, C., Taylor, R., and Hiscott, R. 2022. Rheotropic epifaunal growth, not felling by density currents, is responsible for many Ediacaran fossil orientations at Mistaken Point. Frontiers in Earth Science, **10**: 1-5.

Meesters, E.H., Hilterman, M., Kardinaal, E., Keetman, M., de Vries, M., and Bak, R.P.M. 2001. Colony size-frequency distributions of scleractinian coral populations: spatial and interspecific variation. Marine Ecology Progress Series, **209**: 43–54.

Mitchell, E.G., and Butterfield, N.J. 2018. Spatial analyses of Ediacaran communities at Mistaken Point. Paleobiology, **44**(1): 40-57.

Mitchell, E.G., Kenchington, C.G., Liu, A.G., Matthews, J.J., and Butterfield, N.J. 2015. Reconstructing the reproductive mode of an Ediacaran macro-organism. Nature, **524**: 343-346.

Narbonne, G.M. 2005. The Ediacara biota: Neoproterozoic origin of animals and their ecosystems. Annual Review of Earth and Planetary Sciences, **33**: 421-442.

Narbonne, G.M., Laflamme, M., Trusler, P.W., Dalrymple, R.W., and Greentree, C. 2014. Deep-water Ediacaran Fossils from Northwestern Canada: Taphonomy, Ecology and Evolution. Journal of Paleontology, **88**(2): 207-223

O'Brien, S.J., and King, A.F. 2005. Late Neoproterozoic (Ediacaran) stratigraphy of Avalon zone sedimentary rocks, Bonavista Peninsula, Newfoundland. Current Research (2005) Newfoundland and Labrador Department of Natural Resources Geological Survey, Report 05-1: 101-113.

Oksanen, J. 2013. Multivariate analysis of ecological communities in R: vegan tutorial.

Oksanen, J., Simpson, G., Blanchet, F., Kindt, R., Legendre, P., Minchin, P., O'Hara, R., Solymos, P., Stevens, M., Szoecs, E., Wagner, H., Barbour, M., Bedward, M., Bolker, B., Borcard, D., Carvalho, G., Chirico, M., De Caceres, M., Durand, S., Evangelista, H., FitzJohn, R., Friendly, M., Furneaux, B., Hannigan, G., Hill, M., Lahti, L., McGlinn, D., Ouellette, M., Ribeiro Cunha, E., Smith, T., Stier, A., Ter Braak, C., Weedon, J. 2022. vegan: Community Ecology Package. R package version 2.6-4, <https://CRAN.Rproject.org/package=vegan>.

Oxford University Press. 2008. Rose Diagram. In *A Dictionary of Earth Sciences* (3rd Ed.).

Pérez-Pinedo, D., McKean, C., Taylor, R., Nicholls, R., and McIlroy, D. 2022. *Charniodiscus* and *Arborea* are separate genera within the Arboreomorpha: Using the holotype of *C. concentricus* to resolve a taphonomic/taxonomic tangle. Frontiers in Earth Science, **9**.

Pérez-Pinedo, D., Neville, J., Pasinetti, G., McKean, C., Taylor, R., and McIlroy, D. 2023. Frond orientations with independent current indicators demonstrate the reclining rheotropic mode of life of several Ediacaran rangeomorph taxa. Paleobiology, 1-22.

Peterson K.J., Waggoner, B., and Hagadorn, J.W. 2003. A fungal analog for Newfoundland Ediacaran fossils? Integrative and Comparative Biology, **43**(1): 127-136.

R Core Team. 2022. R: A language and environment for statistical computing. R Foundation for Statistical Computing, Vienna, Austria.

Rasband, W.S. 1997-2018. Image J. U.S. National Institutes of Health, Bethesda, Maryland, USA.

Rhyland, J.S. "Taxes and tropisms of Bryozoans." Biology of Bryozoans, edited by Woollacott, R.M., and Zimmer, R.L., Academic Press, 1977, 411-436.

Scrucca, L., Fop, M., Murphy, T.B., and Raftery, A.E. 2016. Mclust 5: clustering, classification and density estimation using Gaussian finite mixture models. The R Journal, **8**(1): 289-317.

Seilacher, A. 1992. Vendobionta and Psammocorallia: lost constructions of Precambrian evolution. Journal of the Geological Society, London, **149**(4): 607-613.

Seilacher, A. 1999. Biomat-related lifestyles in the Precambrian. Palaios, **14**(1): 86-93.

Seilacher, A., Grazhdankin, D., and Legouta, A. 2003. Ediacaran biota: The dawn of animal life in the shadow of giant protists. Paleontological Research, **7**(1): 43-54.

Shao, Y., Chen, Z., Zhou, C., and Yuan, X. 2019. *Hiemalora stellaris* from the Ediacaran Dengying Formation in the Yangtze Gorges area, Hubei Province: affinity and taphonomic analysis. Acta Palaeontologica Sinica, **58**: 1–10.

Singer, A., Plotnick, R., and Laflamme, M. 2012. Experimental fluid mechanics of an Ediacaran frond. Palaeontologia Electronica, **15**(2): 1-14.

Sperling, E.A., Peterson, K.J., and Laflamme, M. 2011. Rangeomorphs, *Thectardis* (Porifera?) and dissolved organic carbon in the Ediacaran oceans. Geobiology, **9**: 24-33.

Suarez, P.A., and Leys, S.P. (2022). The sponge pump as a morphological character in the fossil record. Paleobiology, **48**(3): 446-461.

Taylor, R.S., Nicholls, R., Neville, J., and McIlroy, D. 2023. Morphological variation in the rangeomorph organism Fractofusus misrai from the Ediacaran of Newfoundland, Canada. Geological Magazine: **160**: 146-166.

Vixseboxse, P.B., Kenchington, C.G., Dunn, F.S., and Mitchell, E.G. 2021. Orientations of Mistaken Point fronds indicate morphology impacted ability to survive turbulence. Frontiers in Earth Science, **9**(762824).

Waggoner, B. 2003. The Ediacaran biotas in space and time. Integrative and Comparative Biology, **43**: 104-113.

Wood, D.A., Dalrymple, R.W., Narbonne, G.M., Gehling, J.G., and Clapham, M.E. 2003. Paleoenvironmental analysis of the late Neoproterozoic Mistaken Point and Trepassey Formations, Southeastern Newfoundland. Canadian Journal of Earth Sciences, **40**(10): 1375-1391.

Zhao, Y., Liu, Z., Zhang, Y., Li, J., Wang, M., Wang, W., and Xu, J. 2015. In situ observation of contour currents in the northern South China Sea: Applications for deepwater sediment transport. Earth and Planetary Science Letters, **430**: 477-485.

Appendix A – Data for E surface *F. misrai* specimens (282)

Specimen#	Shape	Length	Width	OrientationA	OrientationB	L/W ratio
2	curved	19.8	4.56	72	234	4.34
3	straight	9.11	3.31	24	204	2.75
4	straight	5.34	1.31	50	230	4.08
5	curved	6.57	1.67	76	216	3.93
6	curved	7.06	1.48	78	240	4.77
7	straight	7.54	1.84	52	232	4.10
8	curved	8.37	2.17	70	226	3.86
9	curved	14.39	2.72	88	236	5.29
10	kinked	12.13	2.69	42	228	4.51
11	straight	6.4	1.33	70	250	4.81
12	kinked	12.99	4.62	174	232	2.81
13	curved	10.71	2.05	60	252	5.22
15	straight	13.55	2.4	64	244	5.65
16	kinked	6.53	4.05	140	338	1.61
17	kinked	9.23	2.51	24	190	3.68
18	curved	21.19	6.09	64	274	3.48
19	straight	7.05	1.6	66	246	4.41
20	straight	9.83	2.41	56	236	4.08
21	straight	6.57	1.74	114	294	3.78
22	kinked	6.31	2.94	140	266	2.15
23	straight	17.54	3.45	86	266	5.08
24	kinked	11.34	4.52	36	226	2.51
27	curved	5.05	2.02	20	184	2.50
28	straight	15.1	3.04	62	242	4.97
29	curved	6.56	2.11	92	300	3.11
30	straight	16.78	4.18	32	212	4.01
31	straight	7.63	3.93	162	342	1.94
32	straight	12.44	1.84	40	220	6.76
33	straight	6.56	2.41	100	280	2.72
34	straight	11.57	2.62	68	248	4.42
35	straight	4.78	1.21	72	252	3.95
36	straight	9.16	3.24	96	276	2.83
37	straight	8.78	1.84	72	252	4.77
39	curved	5.07	1.93	84	286	2.63
40	straight	8.78	2.53	102	282	3.47
41	straight	10.16	1.87	62	242	5.43
42	kinked	20.35	4.73	100	246	4.30
43	straight	6.15	2.03	84	264	3.03

44	straight	5.2	1.79	66	246	2.91
45	curved	13.61	5.09	142	250	2.67
46	straight	8.31	2.67	44	224	3.11
47	straight	4.02	1.29	106	286	3.12
50	straight	5.36	2.25	122	302	2.38
51	straight	12.89	2.82	62	242	4.57
52	straight	8.51	2.74	92	272	3.11
53	kinked	4.27	2.66	150	306	1.61
54	curved	7.6	3.02	160	274	2.52
55	straight	5.62	2.31	126	306	2.43
56	straight	10.65	2.18	72	252	4.89
57	straight	9.76	2.29	78	258	4.26
58	straight	9.35	1.58	78	258	5.92
59	straight	13.11	3.05	20	200	4.30
61	straight	9.08	1.58	76	256	5.75
62	straight	8.74	1.87	42	222	4.67
63	straight	6.54	1.08	78	258	6.06
64	straight	12.67	3.69	24	204	3.43
65	straight	10.64	2.51	80	260	4.24
66	straight	7.91	2.41	86	266	3.28
68	straight	7.68	2.33	104	284	3.30
69	kinked	18.9	10.28	152	250	1.84
70	straight	21.5	4.04	66	246	5.32
71	straight	13.68	2.34	72	252	5.85
72	straight	3.78	1.1	52	232	3.44
73	curved	18	2.72	62	260	6.62
74	straight	33.37	5.13	56	236	6.50
76	curved	8.03	2.66	124	270	3.02
77	straight	15.98	3.3	70	250	4.84
79	straight	7.25	3.71	4	184	1.95
80	straight	4.63	2.87	160	340	1.61
81	straight	5.51	1.6	42	222	3.44
82	kinked	9.32	1.86	102	240	5.01
83	curved	17.7	6.22	104	250	2.85
84	curved	9.7	2.11	70	262	4.60
85	curved	8.59	1.87	62	256	4.59
86	straight	9.03	2.27	86	266	3.98
87	straight	14.2	3.48	70	250	4.08
88	curved	9.14	3.32	124	266	2.75
89	straight	5.94	2.12	14	194	2.80
90	straight	10.85	2.34	78	258	4.64
91	curved	10.33	1.92	68	240	5.38
92	straight	7.69	2.23	74	254	3.45

93	curved	12.89	2.94	82	248	4.38
94	straight	11.84	2.43	74	254	4.87
95	straight	7.28	1.59	38	218	4.58
96	straight	13.62	3.08	60	240	4.42
97	straight	9.58	1.97	76	256	4.86
100	curved	10.98	2.88	106	348	3.81
101	straight	9.31	3.47	116	296	2.68
102	straight	5.29	1.14	52	232	4.64
103	straight	9.45	1.99	82	262	4.75
104	curved	11.58	3.08	106	268	3.76
105	straight	4.86	1.7	32	212	2.86
106	straight	8.49	2.12	68	248	4.00
107	kinked	7.47	1.86	42	198	4.02
108	straight	10.05	2.07	48	228	4.86
109	straight	9.64	2.91	46	226	3.31
110	straight	8.09	3.51	166	346	2.30
111	straight	4.97	2.09	104	284	2.38
112	straight	14.55	2.88	78	258	5.05
113	curved	11.78	2.69	90	252	4.38
114	curved	18.72	3.56	66	222	5.26
116	curved	7.2	2.87	40	184	2.51
117	straight	9.65	1.94	14	194	4.97
118	straight	23.49	2.85	76	256	8.24
119	straight	14.95	2.99	48	228	5.00
120	straight	6.88	3.05	152	332	2.26
121	straight	12.94	3.04	38	218	4.26
122	kinked	7.86	1.56	98	226	5.04
123	straight	7.99	2.59	96	276	3.08
124	straight	13.87	4.27	82	262	3.25
125	straight	12.71	4.35	14	194	2.92
126	straight	3.69	1.91	179	359	1.93
127	curved	9.81	4.89	156	292	2.01
128	straight	3.55	0.88	64	244	4.03
129	curved	7.83	2.07	96	336	3.78
130	straight	6.18	2.26	42	222	2.73
131	kinked	16.55	3.47	60	280	4.77
132	straight	12.54	2.16	52	232	5.81
133	kinked	10.83	2.08	52	204	5.21
134	straight	8.26	2.44	90	270	3.39
135	straight	8.45	1.97	94	274	4.29
136	straight	6.01	2.73	160	340	2.20
137	curved	22	3.21	40	242	6.85
138	straight	4.85	1.47	58	238	3.30

139	curved	10.7	4.8	126	330	2.23
140	kinked	11.32	3.98	100	316	2.84
141	kinked	15.25	3.13	52	276	4.87
143	kinked	19.02	4.06	88	238	4.68
144	curved	6.95	2.27	112	322	3.06
145	straight	7.82	1.27	44	224	6.16
146	straight	4.26	2.07	146	326	2.06
147	kinked	11.17	3.53	106	262	3.16
148	straight	3.61	2.07	140	320	1.74
149	curved	14.59	3.29	86	238	4.43
150	straight	15.3	3.54	64	244	4.32
151	straight	13.05	1.93	94	274	6.76
152	straight	7.51	1.33	58	238	5.65
153	straight	11.55	1.76	66	246	6.56
154	curved	6.26	3.2	130	350	1.96
155	straight	13.15	2.82	58	238	4.66
156	curved	7.55	4.46	170	332	1.69
157	straight	12.6	3.15	78	258	4.00
158	straight	16.39	3.06	68	248	5.36
159	straight	6.51	2.64	132	312	2.47
160	straight	15.08	3.44	36	216	4.38
161	curved	9.98	1.64	80	248	6.09
162	straight	6.46	2.75	132	312	2.35
163	straight	9.34	3.09	34	214	3.02
164	straight	10.15	1.89	64	244	5.37
165	straight	11.9	3.71	34	214	3.21
166	straight	10.36	2.35	76	256	4.41
167	straight	5.24	1.85	122	302	2.83
168	curved	5.94	2.59	116	336	2.29
169	straight	8.23	2.03	28	208	4.05
170	curved	13.13	2.65	66	232	4.95
171	straight	5.51	2.58	6	186	2.14
172	curved	9.12	3.68	132	292	2.48
174	curved	13.23	2.56	32	248	5.17
175	straight	6.24	3.62	146	326	1.72
176	straight	8.82	1.32	48	228	6.68
177	straight	7.35	2.36	90	270	3.11
178	straight	7.25	2.82	100	280	2.57
179	straight	6.39	2.35	80	260	2.72
180	straight	14.3	2.69	74	254	5.32
181	curved	7.21	1.57	80	242	4.59
182	curved	13.93	2.21	60	226	6.30
183	straight	4.72	1.79	16	196	2.64

184	curved	5.03	2.1	176	330	2.40
185	curved	8.81	2.02	80	282	4.36
187	curved	17.63	3.76	82	278	4.69
189	straight	4.7	2.47	12	192	1.90
190	curved	8.59	4.01	140	338	2.14
191	curved	5.36	2.9	164	344	1.85
192	straight	20.18	4.07	82	262	4.96
193	straight	11.1	2.37	56	236	4.68
194	kinked	6.62	2.84	150	300	2.33
195	straight	8.54	2.35	42	222	3.63
196	curved	16.64	3.47	82	250	4.80
197	straight	12.61	4.67	176	356	2.70
198	straight	6.31	1.29	66	246	4.89
199	straight	8.92	3.38	116	296	2.64
200	kinked	6.39	2.41	104	322	2.65
201	straight	16.02	3.33	26	206	4.81
202	curved	9.56	2.54	112	276	3.76
203	straight	6.53	1.39	68	248	4.70
204	straight	7.31	2.51	16	196	2.91
205	straight	11.53	2.05	46	226	5.62
206	straight	8.77	2.46	22	202	3.57
207	straight	4.43	0.99	44	224	4.47
208	curved	6.55	2.04	166	276	3.21
209	straight	17.23	3.12	58	238	5.52
210	straight	11.17	2.29	56	236	4.88
212	curved	5.36	2.19	162	308	2.45
213	straight	6.58	3.4	162	342	1.94
214	straight	8.6	1.85	42	222	4.65
215	curved	14.85	2.9	78	240	5.12
216	straight	11.16	2.65	82	262	4.21
217	straight	10.48	2.7	92	272	3.88
218	straight	5.05	2.72	162	342	1.86
219	straight	4.41	2.35	176	356	1.88
220	straight	12.8	2.26	80	260	5.66
222	straight	9.84	1.56	52	232	6.31
224	straight	13.27	4.62	18	198	2.87
225	straight	7.29	2.85	8	188	2.56
226	curved	13.16	3.11	48	212	4.23
227	straight	11.96	2.54	84	264	4.71
229	straight	19.69	2.54	52	232	7.75
230	kinked	13.93	4.4	154	284	3.17
231	straight	6.2	2.12	112	292	2.92
232	curved	15	2.65	78	238	5.66

233	straight	5.34	1.15	80	260	4.64
234	curved	7.91	1.77	86	240	4.47
235	straight	6.09	2.88	148	328	2.11
236	straight	8.43	2.51	100	280	3.36
238	straight	10.39	1.68	58	238	6.18
239	curved	9.34	2.18	70	276	4.28
240	straight	12.06	2.61	50	230	4.62
241	straight	6.91	1.38	54	234	5.01
242	straight	10.34	2.41	40	220	4.29
243	curved	10.7	2.07	74	234	5.17
244	straight	14.65	2.77	68	248	5.29
245	straight	12.6	3.89	14	194	3.24
246	straight	13.8	2.28	80	260	6.05
247	straight	5.04	1.48	34	214	3.41
248	straight	7.29	1.63	46	226	4.47
249	straight	3.98	1.6	146	326	2.49
250	straight	10.76	2.34	84	264	4.60
251	straight	7.74	2.59	94	274	2.99
252	straight	12.3	2.2	62	242	5.59
253	straight	7.14	2.33	44	224	3.06
254	straight	8.03	2.07	68	248	3.88
255	straight	7.68	1.92	26	206	4.00
256	straight	7.42	1.6	102	282	4.64
257	straight	5.07	1.03	58	238	4.92
258	straight	8.11	1.47	58	238	5.52
259	straight	8.32	1.42	68	248	5.86
260	straight	5.8	1.23	44	224	4.72
261	straight	5	2.67	176	356	1.87
262	straight	2.67	0.89	78	258	3.00
263	straight	3.55	1.29	126	306	2.75
264	straight	18.68	3.63	68	248	5.15
265	straight	5.88	2.95	116	296	1.99
266	straight	5.01	1.6	94	274	3.13
267	straight	7.85	3.91	162	342	2.01
268	straight	6	2.29	116	296	2.62
269	curved	28.5	5.85	78	214	4.87
270	straight	8.69	4.43	24	204	1.96
271	straight	8.47	2.75	16	196	3.08
272	curved	20.5	3.79	50	192	5.41
273	curved	6.11	1.37	124	266	4.46
274	curved	11.7	3.2	56	268	3.66
275	straight	6.31	1.3	94	274	4.85
276	straight	9.8	3.18	102	282	3.08

277	curved	13.2	2.53	134	248	5.22
278	curved	7.98	3.4	142	334	2.35
279	straight	11.2	2.17	44	224	5.16
280	straight	4.96	1.6	122	302	3.10
281	straight	5.02	1.96	22	202	2.56
282	straight	3.9	1.1	78	258	3.55
283	curved	10.62	3.3	110	254	3.22
284	straight	10.48	1.33	56	236	7.88
285	straight	6	1.51	82	262	3.97
286	straight	7.1	1.39	82	262	5.11
287	straight	15.7	2.89	52	232	5.43
288	straight	9.12	1.36	60	240	6.71
290	straight	5.3	1.62	116	296	3.27
291	straight	5.07	0.83	72	252	6.11
292	straight	9.2	1.54	92	272	5.97
293	straight	14.5	2.2	60	240	6.59
294	straight	6.1	1.93	44	224	3.16
295	straight	7.44	1.53	90	270	4.86
296	straight	12.6	1.65	62	242	7.64
297	straight	5.75	1.54	38	218	3.73
298	curved	6.6	1.98	106	322	3.33
299	curved	12.8	3.68	88	338	3.48
300	straight	7.9	2.5	14	194	3.16
301	straight	4.8	2.15	126	306	2.23
302	straight	11.43	2.83	100	280	4.04
303	straight	3.35	1.4	132	312	2.39
304	straight	4.9	1	64	244	4.90
306	straight	7.11	1.2	78	258	5.93
307	straight	4.8	1.3	96	276	3.69

Appendix B – Data for H14 surface *F. andersoni* specimens (587)

Specimen#	Length	Width	OrientationA	L/W ratio
1	2.17	1.92	98	1.13
2	13.44	4.5	50	2.99
3	7.18	4.2	16	1.71
4	2.79	2.52	150	1.11
5	2.05	2.02	120	1.01
6	3.99	1.78	30	2.24
7	5.08	1.92	34	2.65
8	4.01	1.74	38	2.30
9	1.65	1.01	2	1.63
10	1.45	1.42	78	1.02
11	13.59	5.22	24	2.60
12	1.47	1.77	102	0.83
13	2.76	1.01	42	2.73
14	1.75	0.7	58	2.50
15	3.25	3.42	152	0.95
16	3.01	1.18	44	2.55
17	3.03	1.3	48	2.33
18	1.24	0.52	38	2.38
19	1.7	1.59	170	1.07
20	2.3	1.11	54	2.07
21	2.78	1.19	40	2.34
22	2.52	2.44	104	1.03
23	5.12	4.3	156	1.19
24	0.75	0.8	152	0.94
25	1.34	1.19	100	1.13
26	0.97	0.96	148	1.01
27	1.2	0.48	58	2.50
28	1.62	0.75	44	2.16
29	4.58	2.08	58	2.20
30	1.73	1.4	116	1.24
31	4.52	2.41	36	1.88
32	2.84	1.45	52	1.96
33	1.74	1.6	124	1.09
34	3.2	1.49	56	2.15
35	3.45	1.41	54	2.45
36	1.22	0.94	88	1.30
37	3.65	2.11	86	1.73
38	2.54	1.9	96	1.34

39	9.21	8.18	126	1.13
40	17.2	7.08	52	2.43
41	1.01	0.48	44	2.10
42	0.97	0.75	132	1.29
43	0.82	0.62	108	1.32
44	0.82	0.7	98	1.17
45	0.43	0.41	120	1.05
46	1.12	0.99	142	1.13
47	1.42	1.51	124	0.94
48	1.12	1.22	148	0.92
49	2.02	2.13	148	0.95
50	3.15	1.3	54	2.42
51	10.21	7.01	96	1.46
52	1.16	1.13	138	1.03
53	10.59	9.57	146	1.11
54	0.71	0.62	114	1.15
55	2.63	1.37	18	1.92
56	1.71	0.75	60	2.28
57	2.35	0.98	56	2.40
58	1.47	1.61	144	0.91
59	2.63	1.65	90	1.59
60	0.98	0.66	92	1.48
61	2.66	0.75	36	3.55
62	10.19	4.75	64	2.15
63	3.68	1.6	22	2.30
64	2.69	1.18	50	2.28
65	0.52	0.53	160	0.98
66	4.32	2.13	62	2.03
67	1.94	0.84	26	2.31
68	1.67	1.08	16	1.55
69	9.71	6.95	94	1.40
70	6.84	5.94	164	1.15
71	0.86	0.57	80	1.51
72	2.72	1.1	22	2.47
73	1.23	0.55	46	2.24
74	5.3	3.45	10	1.54
75	2.07	0.71	22	2.92
76	3.58	1.14	44	3.14
77	2.89	3	104	0.96
78	2.34	1.27	6	1.84
79	0.95	0.92	130	1.03
80	2.06	2.51	114	0.82
81	1.35	1.26	156	1.07

82	2.45	1.12	26	2.19
83	9.65	6.26	2	1.54
84	2.56	1.31	64	1.95
85	4.85	1.95	52	2.49
86	5.18	2.19	68	2.37
87	2.24	2.06	166	1.09
88	1.95	1.37	74	1.42
89	1.73	1.13	100	1.53
90	14.61	7.51	24	1.95
91	2.13	2.07	130	1.03
92	1.64	0.73	58	2.25
93	2.4	1.32	12	1.82
94	1.43	1.05	104	1.36
95	3.55	1.46	48	2.43
96	5.67	2.26	30	2.51
97	8.39	6.19	86	1.36
98	1.95	1.24	106	1.57
99	10.03	3.82	52	2.63
100	3.9	2.09	64	1.87
101	2.84	1.25	36	2.27
102	5.83	5.72	132	1.02
103	19.45	7.95	58	2.45
104	13.49	5.3	28	2.55
105	2.67	1.25	30	2.14
106	1.61	1.58	152	1.02
107	1.74	1.39	98	1.25
108	11.12	3.84	32	2.90
109	1.44	0.78	4	1.85
110	3.62	1.29	46	2.81
111	2.85	1.03	26	2.77
112	3.31	1.26	78	2.63
113	2.91	2.19	118	1.33
114	1.61	1.3	166	1.24
115	6.96	4.2	92	1.66
116	6.4	2.3	36	2.78
117	1.34	0.68	30	1.97
118	1.49	0.58	42	2.57
119	1.21	0.65	28	1.86
120	11.32	8.71	90	1.30
121	0.83	0.43	44	1.93
122	1.19	0.96	160	1.24
123	2.44	1.86	90	1.31
124	1.77	0.9	24	1.97

125	1.72	0.79	22	2.18
126	1.66	0.85	178	1.95
127	1.12	0.72	18	1.56
128	2.45	0.9	54	2.72
129	1.09	1.21	138	0.90
130	2.88	2.49	148	1.16
131	1.93	1.22	176	1.58
132	2.95	1.54	60	1.92
133	1.58	1.18	162	1.34
134	12.6	6.52	54	1.93
135	4.06	1.67	52	2.43
136	14.49	6.64	72	2.18
137	1.46	1.42	114	1.03
138	1.08	0.89	112	1.21
139	10.72	7.03	14	1.52
140	1.88	1.32	104	1.42
141	2.24	0.92	40	2.43
142	1.81	0.72	42	2.51
143	3.75	2.48	70	1.51
144	1.74	0.85	16	2.05
145	1.48	1.06	114	1.40
146	2.82	1.75	20	1.61
147	3.15	1.45	62	2.17
148	8.02	6.92	154	1.16
149	1.33	0.68	44	1.96
150	10.7	3.92	48	2.73
151	0.84	0.49	66	1.71
152	1.46	1.23	96	1.19
153	3.14	1.72	4	1.83
154	3.03	1.34	40	2.26
155	1.95	0.9	32	2.17
156	7.98	3.56	56	2.24
157	1.29	1.16	160	1.11
158	3.03	3.97	146	0.76
159	2.66	2.35	124	1.13
160	2.06	0.96	178	2.15
161	2.97	2.12	96	1.40
162	2.93	1.16	48	2.53
163	2.53	2.15	108	1.18
164	1.9	1.49	166	1.28
165	1.4	0.76	68	1.84
166	8.63	7.42	126	1.16
167	1.88	1.66	170	1.13

168	2.06	0.79	46	2.61
169	8.76	3.92	4	2.23
170	2.63	1.12	58	2.35
171	2.17	1.3	18	1.67
172	1.97	1.63	162	1.21
173	2.73	2.41	118	1.13
174	11.04	6.73	14	1.64
175	1.64	1.26	104	1.30
176	2.3	0.99	54	2.32
177	1.28	1.14	158	1.12
178	1.18	1.06	102	1.11
179	9.01	4.74	68	1.90
180	4.25	3.18	166	1.34
181	3.15	1.52	56	2.07
182	9.9	4.77	62	2.08
183	2.89	1.67	86	1.73
184	8.16	6.1	118	1.34
185	4.57	1.93	58	2.37
186	1.36	1.03	134	1.32
187	1.56	1.49	148	1.05
188	23.53	8.14	42	2.89
189	1.27	0.54	30	2.35
190	1.1	0.66	14	1.67
191	1.37	0.69	56	1.99
192	2.42	1.18	18	2.05
193	3.45	4.01	156	0.86
194	7.74	4.62	14	1.68
195	8.37	5.88	108	1.42
196	2.29	1.05	72	2.18
197	3.29	2.9	106	1.13
198	9.52	9.29	150	1.02
199	1.57	0.81	20	1.94
200	1.62	1.49	118	1.09
201	1.01	0.94	152	1.07
202	1.96	0.83	46	2.36
203	1.77	0.9	22	1.97
204	2.54	1.41	18	1.80
205	1.51	1.13	2	1.34
206	3.49	1.71	82	2.04
207	2.67	1.02	22	2.62
208	3.83	1.34	34	2.86
209	1.47	0.83	14	1.77
210	4.21	2.37	76	1.78

211	1.42	1.25	154	1.14
212	3.3	1.5	34	2.20
213	1.58	1.31	156	1.21
214	2.16	1.26	12	1.71
215	1.76	0.69	20	2.55
216	15.27	6.85	20	2.23
217	2.13	0.94	16	2.27
218	1.86	0.83	16	2.24
219	2.23	0.99	56	2.25
220	2.28	1.02	20	2.24
221	4.13	1.48	40	2.79
222	1.42	0.91	66	1.56
223	2.08	1.83	150	1.14
224	1.99	1.26	170	1.58
225	2.3	0.93	56	2.47
226	11.7	9.71	110	1.20
227	2.24	2.1	152	1.07
228	9.89	9.15	162	1.08
229	2.68	1.2	42	2.23
230	9.35	4.34	52	2.15
231	2.94	1.55	88	1.90
232	7.51	3.8	70	1.98
233	3.76	1.95	88	1.93
234	2.97	1.52	80	1.95
235	3.96	1.64	18	2.41
236	11.06	7.97	174	1.39
237	14.66	9.04	16	1.62
238	3.07	1.02	34	3.01
239	2.13	1.92	140	1.11
240	11.94	6.49	2	1.84
241	2.06	1.6	102	1.29
242	4.06	1.74	24	2.33
243	2.38	1.67	158	1.43
244	2.32	2.06	130	1.13
245	7.89	5.54	166	1.42
246	10.82	9.45	126	1.14
247	1.65	1.52	146	1.09
248	1.76	1.48	94	1.19
249	2.71	1.12	54	2.42
250	6.52	3.11	10	2.10
251	2.24	0.7	38	3.20
252	9.61	8.17	128	1.18
253	1.96	0.86	18	2.28

254	4.68	2.7	74	1.73
255	1.77	0.88	54	2.01
256	2.71	1.46	80	1.86
257	3.28	1.63	66	2.01
258	8.81	4.82	52	1.83
259	10.27	3.84	64	2.67
260	2.82	1.48	28	1.91
261	3.05	2.24	170	1.36
262	6.39	1.91	36	3.35
263	1.37	0.52	30	2.63
264	3.51	1.78	40	1.97
265	1.61	1.33	138	1.21
266	3.28	2.08	172	1.58
267	1.25	1.51	128	0.83
268	2.77	2.88	156	0.96
269	7.77	6.25	136	1.24
270	2.13	1.78	158	1.20
271	2.36	0.74	42	3.19
272	1.43	0.79	72	1.81
273	2.9	0.83	36	3.49
274	1.34	1	68	1.34
275	2.98	1.24	30	2.40
276	7.68	7.86	118	0.98
277	3.66	1.89	88	1.94
278	3.54	1.34	52	2.64
279	1.49	1.17	102	1.27
280	3.02	2.24	88	1.35
281	2.24	1.25	56	1.79
282	2.25	1.83	142	1.23
283	16.27	5.69	56	2.86
284	5.77	2.51	56	2.30
285	1.96	0.76	50	2.58
286	1.38	0.68	26	2.03
287	3.52	1.5	60	2.35
288	10.24	8.58	114	1.19
289	3.71	1.93	20	1.92
290	6.22	5.23	158	1.19
291	3.15	2.02	174	1.56
292	2.13	1.91	118	1.12
293	2.11	1.59	92	1.33
294	2.76	2.64	122	1.05
295	7.92	4.53	28	1.75
296	1.83	0.79	40	2.32

297	1.32	1.39	138	0.95
298	3.84	2.05	68	1.87
299	7.52	7.25	122	1.04
300	2.05	0.95	36	2.16
301	1.86	2.34	136	0.79
302	2.86	1.19	54	2.40
303	8.42	3.16	44	2.66
304	11.16	7.04	92	1.59
305	2.46	1.37	10	1.80
306	7.79	7.92	148	0.98
307	1.28	0.98	154	1.31
308	2.14	2.06	146	1.04
309	8.54	3.51	38	2.43
310	0.95	1.01	116	0.94
311	1.47	1.39	90	1.06
312	0.83	0.8	136	1.04
313	2.26	0.9	38	2.51
314	2.3	0.63	42	3.65
315	2.69	1.42	12	1.89
316	10.9	5.54	6	1.97
317	2.14	1.09	44	1.96
318	1.04	0.94	142	1.11
319	1.13	0.58	82	1.95
320	1.27	1.02	154	1.25
321	2.11	0.99	52	2.13
322	3.92	1.86	26	2.11
323	0.9	0.85	122	1.06
324	2.12	0.68	36	3.12
325	1.84	1.3	92	1.42
326	2.15	1.01	32	2.13
327	1.15	1.04	128	1.11
328	9.96	6.25	10	1.59
329	3.35	1.33	16	2.52
330	2.42	1.34	10	1.81
331	2.02	0.67	36	3.01
332	2.32	1.26	18	1.84
333	1.4	1.02	174	1.37
334	1.28	0.91	86	1.41
335	1.26	0.56	32	2.25
336	1.28	0.6	18	2.13
337	1.5	0.82	178	1.83
338	1.32	0.97	114	1.36
339	1.82	1.14	80	1.60

340	10.22	5.78	32	1.77
341	2.42	1.91	174	1.27
342	11.48	8.18	94	1.40
343	2.22	1.3	12	1.71
344	0.6	0.53	148	1.13
345	2.3	1.28	20	1.80
346	7.24	7.95	166	0.91
347	2.23	1.09	60	2.05
348	3.61	3.02	158	1.20
349	5.97	2.32	26	2.57
350	2.52	1.82	168	1.38
351	1.85	0.62	32	2.98
352	5.12	3.37	174	1.52
353	2.62	1.19	20	2.20
354	12.53	7.45	2	1.68
355	1.76	0.93	30	1.89
356	1.68	0.74	38	2.27
357	3.51	1.84	82	1.91
358	1.31	1.07	96	1.22
359	2.3	2.11	136	1.09
360	1.55	0.98	86	1.58
361	1.01	1.03	118	0.98
362	3.52	1.48	56	2.38
363	1.55	1.29	160	1.20
364	7.98	7.91	164	1.01
365	1.23	0.84	164	1.46
366	1.67	1.25	162	1.34
367	2.21	1.32	22	1.67
368	1.14	0.76	98	1.50
369	1.67	1.36	160	1.23
370	2.19	0.7	84	3.13
371	3.71	1.34	58	2.77
372	1.24	0.71	20	1.75
373	1.96	1.1	74	1.78
374	1.59	1.21	160	1.31
375	1.29	0.75	66	1.72
376	1.64	0.91	16	1.80
377	3.93	2.51	2	1.57
378	7.19	5.31	176	1.35
379	1.94	1.61	118	1.20
380	1.46	0.73	20	2.00
381	1.18	0.9	88	1.31
382	1.43	1.08	172	1.32

383	2.15	1.91	134	1.13
384	2.62	1.42	82	1.85
385	2.76	1.38	20	2.00
386	3.75	1.44	24	2.60
387	1.75	1.13	8	1.55
388	2.35	0.77	32	3.05
389	9.45	7.83	98	1.21
390	2.97	1.97	164	1.51
391	3.2	1.67	20	1.92
392	5.2	2.52	34	2.06
393	2.25	1.31	6	1.72
394	1.22	1.09	126	1.12
395	4.14	2.01	44	2.06
396	2.35	1.05	32	2.24
397	2.78	2.5	148	1.11
398	1.8	0.95	4	1.89
399	5.58	3.12	178	1.79
400	3.15	1.65	32	1.91
401	3.48	1.6	20	2.18
402	1.99	1.12	32	1.78
403	6.71	6.01	108	1.12
404	6.41	2.98	52	2.15
405	2.8	2.67	148	1.05
406	11.26	4.47	60	2.52
407	3.19	1.62	82	1.97
408	2.5	2.32	156	1.08
409	2.82	1.41	18	2.00
410	9.25	4.65	32	1.99
411	2.45	2.51	112	0.98
412	3.95	2.14	22	1.85
413	7.37	4.76	116	1.55
414	1.72	1.81	152	0.95
415	1.44	0.68	14	2.12
416	2.2	0.93	18	2.37
417	2.31	0.98	42	2.36
418	8.4	3.55	61	2.37
419	2.23	1.5	174	1.49
420	2.2	1.66	158	1.33
421	2.59	1.32	72	1.96
422	1.13	0.54	68	2.09
423	4.05	1.82	40	2.23
424	1.95	1.01	44	1.93
425	1.59	0.6	36	2.65

426	3.1	1.29	36	2.40
427	9.24	4.09	30	2.26
428	1.97	0.92	52	2.14
429	1.75	0.98	4	1.79
430	2.26	1.06	32	2.13
431	2.34	0.96	38	2.44
432	1.01	0.92	144	1.10
433	1.98	1.14	10	1.74
434	9.35	4.59	8	2.04
435	3.85	1.65	78	2.33
436	1.15	0.86	102	1.34
437	3.79	1.69	36	2.24
438	2.67	1.59	2	1.68
439	2.3	2.01	122	1.14
440	1.28	0.94	172	1.36
441	2.69	1.26	20	2.13
442	10.45	4.07	46	2.57
443	2.15	1.68	154	1.28
444	1.01	0.81	130	1.25
445	3.89	1.79	38	2.17
446	1.31	0.57	46	2.30
447	5.35	1.9	38	2.82
448	2.76	1.22	30	2.26
449	5.88	1.31	76	4.49
450	1.73	0.61	54	2.84
451	18.92	5.25	38	3.60
452	5	2.8	10	1.79
453	3.8	1.54	68	2.47
454	2.43	1.55	22	1.57
455	3.47	1.5	56	2.31
456	3.37	1.46	40	2.31
457	1.47	0.51	174	2.88
458	2.4	1.07	66	2.24
459	14.9	12.89	128	1.16
460	3.3	1.43	34	2.31
461	2.77	2	6	1.39
462	4.7	2.06	34	2.28
463	2.76	1.99	166	1.39
464	1.48	0.74	96	2.00
465	12.52	4.8	32	2.61
466	3.54	1.81	48	1.96
467	1.85	0.76	34	2.43
468	1.17	0.96	170	1.22

469	1.17	0.96	26	1.22
470	2.22	1.42	10	1.56
471	1.52	1.44	116	1.06
472	1.45	1.2	82	1.21
473	1.55	1.01	68	1.53
474	2.07	1.69	98	1.22
475	2.5	1.46	92	1.71
476	2.38	1.97	110	1.21
477	3.49	1.51	40	2.31
478	2.09	1.67	176	1.25
479	1.22	0.56	48	2.18
480	1.77	0.87	24	2.03
481	1.89	1.63	92	1.16
482	2.31	1.65	108	1.40
483	1.92	1.4	138	1.37
484	1.24	0.48	38	2.58
485	1.78	1.31	74	1.36
486	1.62	1.62	94	1.00
487	3.73	1.23	42	3.03
488	2.64	1.72	78	1.53
489	2.42	0.97	28	2.49
490	1.22	1.12	124	1.09
491	1.8	1.93	124	0.93
492	1.32	1.02	116	1.29
493	1.06	1.07	138	0.99
494	1.53	1.56	140	0.98
495	4.09	1.97	24	2.08
496	1.85	1.1	176	1.68
497	1.28	1.21	102	1.06
498	1.81	1.48	158	1.22
499	1.99	1.3	138	1.53
500	3.55	1.4	40	2.54
501	2.27	2.08	120	1.09
502	2.3	1	18	2.30
503	3.27	1.11	28	2.95
504	1.16	0.53	62	2.19
505	3.82	2.28	148	1.68
506	4.28	3.66	158	1.17
507	8.52	7.38	136	1.15
508	0.97	0.83	94	1.17
509	1.21	0.55	18	2.20
510	3.39	1.64	2	2.07
511	2.37	1.18	12	2.01

512	1.7	0.8	168	2.13
513	5.3	4.17	82	1.27
514	1.78	1.57	106	1.13
515	2.46	1.05	38	2.34
516	2.4	1.6	172	1.50
517	2.88	1.49	72	1.93
518	1.74	1.63	120	1.07
519	2.33	1.89	132	1.23
520	2.05	0.82	28	2.50
521	14.94	4.82	30	3.10
522	3.36	1.32	36	2.55
523	2.63	1.1	42	2.39
524	2.24	1.97	122	1.14
525	1.1	0.69	76	1.59
526	1.26	0.62	56	2.03
527	3.87	1.36	34	2.85
528	1.64	1.48	128	1.11
529	1.61	1.12	14	1.44
530	2.79	1.04	54	2.68
531	2.77	1.73	76	1.60
532	2.93	0.97	16	3.02
533	1.54	1.14	66	1.35
534	2.5	1.65	68	1.52
535	2.15	0.9	22	2.39
536	6.74	3.75	4	1.80
537	1.5	1.02	102	1.47
538	3.29	1.26	26	2.61
539	4.08	1.7	48	2.40
540	1.94	1.78	116	1.09
541	9.35	4.28	10	2.18
542	1.92	1.08	58	1.78
543	1.43	0.94	156	1.52
544	1.78	1.24	90	1.44
545	1.46	0.8	76	1.83
546	2.41	1.02	60	2.36
547	1.95	0.82	52	2.38
548	2.57	1.4	54	1.84
549	5.12	4.96	114	1.03
550	6.31	2.27	28	2.78
551	2.19	0.99	36	2.21
552	6.67	5.12	74	1.30
553	3.46	1.73	62	2.00
554	2.26	1.05	62	2.15

555	1.74	1.71	146	1.02
556	2.34	2.01	162	1.16
557	1.72	1.06	92	1.62
558	5.99	6.5	132	0.92
559	5.06	2.42	68	2.09
560	2.54	1.09	42	2.33
561	2.06	0.96	70	2.15
562	2.36	1.91	160	1.24
563	2.2	0.94	46	2.34
564	2.75	2.25	116	1.22
565	1.82	0.74	18	2.46
566	1.8	0.84	28	2.14
567	5.2	3.61	78	1.44
568	1.76	0.62	20	2.84
569	1.5	1.37	144	1.09
570	3.5	1.89	6	1.85
571	3.66	1.08	36	3.39
572	12.92	5.46	60	2.37
573	2.38	1.51	166	1.58
574	2.46	0.91	16	2.70
575	1.92	0.88	62	2.18
576	0.81	0.83	104	0.98
577	1.32	1.38	120	0.96
578	2.44	1.33	40	1.83
579	1.4	0.68	58	2.06
580	1.43	1.07	104	1.34
581	3.42	1.43	38	2.39
582	2.57	0.85	30	3.02
583	20.42	6	40	3.40
584	2.41	2.26	144	1.07
585	1.65	1.37	102	1.20
586	3.14	1.83	6	1.72
587	1.54	1.11	4	1.39

Appendix C – R script used for statistical analyses

```
#Examining the population structure, orientation and implications of
Fractofusus on two Ediacaran fossiliferous surfaces in Newfoundland
#Jenna M. Neville
#Department of Earth Sciences, Memorial University of Newfoundland, St.
John's, NL, Canada
#Correspondence: jmn345@mun.ca (Neville, J)
#Load and explore datasets (make sure variables are read as numeric,
factors etc.)
setwd("~/Desktop/MUN PHD/Our papers/MP and Hofmann
paper/Methods/Datasets/MP datasets")
dir()
MP <- read.csv("MP.csv")
MPunder180 <- read.csv("MPunder180.csv")
MPover180 <- read.csv("MPover180.csv")
MPon360 <- read.csv("MPon360.csv")
#Example to explore the dataset
dim(MPover180)
colnames(MPover180) # or names()
head(MPover180)
summary(MPon360)
#Download and load packages. Alternative packages might be required.
Download as indicated by R.
# e,g., install.packages("ggplot2")
#e,g., library(ggplot2)
library(mclust)
library(ggplot2)
library(vegan)
library(circular)
#1. Morphometric quantitative size-frequency distributions analysis
#1.1 Normality analysis
#Shapiro Wilks test. H0 = Normally distributed.If p-value < alpha (0.05).
H0 rejected. Not normally distributed.
#Logarithmic transformation of the data when required.
#Width
shapiro.test(MP$Width) #Not normal
shapiro.test(log(MP$Width)) #Normal after transformation
LOGWIDTH <- log(MP$Width)
MP$LOGWIDTH <- LOGWIDTH
#Length
shapiro.test(MP$Length) #Not normal
shapiro.test(log(MP$Length)) #Normal after transformation
LOGLENGTH <- log(MP$Length)
MP$LOGLENGTH <- LOGLENGTH
#Inspection of histograms before and after transformation
#For width:
par(mfrow=c(1,2))
hist(MP$Width, # histogram
    col="white", # column color
    border="black",
    prob = TRUE, # show densities instead of frequencies
```

```
      xlab = "Width",
      ylim=c(0,0.6),
      main = "Non-transformed")
lines(density(MP$Width), # density plot
       lwd = 2, # thickness of line
       col = "chocolate3")
curve(dnorm(x, mean=mean(MP$Width), sd=sd(MP$Width)), add=TRUE,
col="blue")
hist(MP$LOGWIDTH, # histogram
      col="white", # column color
      border="black",
      prob = TRUE, # show densities instead of frequencies
      xlab = "Width",
      ylim=c(0,1.2),
      main = "Transformed")
lines(density(MP$LOGWIDTH), # density plot
       lwd = 2, # thickness of line
       col = "chocolate3")
curve(dnorm(x, mean=mean(MP$LOGWIDTH), sd=sd(MP$LOGWIDTH)), add=TRUE,
col="blue")
dev.off()
#For length:
par(mfrow=c(1,2))
hist(MP$Length, # histogram
      col="white", # column color
      border="black",
      prob = TRUE, # show densities instead of frequencies
      xlab = "Length",
      ylim=c(0,0.13),
      main = "Non-transformed")
lines(density(MP$Length), # density plot
       lwd = 2, # thickness of line
       col = "chocolate3")
curve(dnorm(x, mean=mean(MP$Length), sd=sd(MP$Length)), add=TRUE,
col="blue")
hist(MP$LOGLENGTH, # histogram
      col="white", # column color
      border="black",
      prob = TRUE, # show densities instead of frequencies
      xlab = "Length",
      ylim=c(0,1),
      main = "Transformed")
lines(density(MP$LOGLENGTH), # density plot
       lwd = 2, # thickness of line
       col = "chocolate3")
curve(dnorm(x, mean=mean(MP$LOGLENGTH), sd=sd(MP$LOGLENGTH)), add=TRUE,
col="blue")
dev.off()
#1.2 Size-frequency distributions on mclust
par(mfrow=c(1,2))
#Univariate size-frenquency distribution: Width
gaus1 = Mclust(MP$LOGWIDTH, G=1)
summary(gaus1)
gaus2 = Mclust(MP$LOGWIDTH, G=2)
```

```
summary(gaus2)
gaus3 = Mclust(MP$LOGWIDTH, G=3)
summary(gaus3)
BIC(gaus1,gaus2,gaus3)
mb1 = Mclust(MP$LOGWIDTH)
mb1$modelName
mb1$G
head(mb1$z)
mb1$bic
summary(mb1, parameters = TRUE)
BIC <- mclustBIC(MP$LOGWIDTH)
plot(BIC) #BIC solution for 1 age/size group
#Univariate size-frenquency distribution: Length
gaus1 = Mclust(MP$LOGLENGTH, G=1)
summary(gaus1)
gaus2 = Mclust(MP$LOGLENGTH, G=2)
summary(gaus2)
gaus3 = Mclust(MP$LOGLENGTH, G=3)
summary(gaus3)
BIC(gaus1,gaus2,gaus3)
mb = Mclust(MP$LOGLENGTH)
mb$modelName
mb$G
head(mb$z)
mb$bic
summary(mb, parameters = TRUE)
BIC <- mclustBIC(MP$LOGLENGTH)
plot(BIC) #BIC solution for 1 age/size group
dev.off ()
#Multivariate size-frequency distribution: Length and Width
par(mfrow=c(1,1))
MP <- MP[,-c(1:5)]
gaus1 = Mclust(MP, G=1)
summary(gaus1)
gaus2 = Mclust(MP, G=2)
summary(gaus2)
gaus3 = Mclust(MP, G=3)
summary(gaus3)
BIC(gaus1,gaus2,gaus3)
mb = Mclust(MP)
mb$modelName
mb$G
head(mb$z)
mb$bic
summary(mb, parameters = TRUE)
BIC <- mclustBIC(MP)
plot(BIC) #BIC solution for 2 age/size group
dev.off()
mb$classification
MP <- read.csv("MP.csv")
MP$sizeclass <- mb$classification
MP$sizeclass <- as.factor(MP$sizeclass)
ggplot(MP, aes(x=sizeclass, y= MP$orientation.A)) +
  geom_violin()
```

```
pairs(MP[,c(2,3,4)], pch = 19,  cex = 0.5,
      col = MP$sizeclass,
      lower.panel=NULL)
ggplot(MP, aes(sizeclass, orientation.A, colour = sizeclass,
fill=sizeclass)) +
  geom_violin(alpha = 0.5) +
  labs(x = "Size class",
       y = "Orientation",
       colour = "Size class",
       fill= "Size class") +
  theme_bw(base_size = 15)
wilcox.test(orientation.A ~ sizeclass, data=MP)
#We cooroborate that the distiction in clustering algorithms are due to
shape-related parameters
#Alternative part of the script: clustering algorithms of mclust on L/W
ratio
LWratio <- (MP$Length/MP$Width)
shapiro.test(LWratio)
shapiro.test(log(LWratio)) #Both non normal. Non normal after logarithmic
transformation.
LogLWratio <- log(LWratio)
MP$LWratio <- LWratio
gaus1 = Mclust(LogLWratio, G=1)
summary(gaus1)
gaus2 = Mclust(LogLWratio, G=2)
summary(gaus2)
gaus3 = Mclust(LogLWratio, G=3)
summary(gaus3)
BIC(gaus1,gaus2,gaus3)
mb = Mclust(LogLWratio)
mb$modelName
mb$G
head(mb$z)
mb$bic
summary(mb, parameters = TRUE)
BIC <- mclustBIC(LogLWratio)
plot(BIC) #BIC solution for 2 age/size group
#plot(mb)
mod3dr <- MclustDR(mb)
summary(mb)
summary(mod3dr)
plot(mb, what = "classification")
plot(mod3dr, what = "classification")
plot(mod3dr, what = "density", type = "persp")
plot(mb, what = "density", type = "persp")
plot(mod3dr, what = "density", type = "hdr")
plot(mb, what = "density", type = "hdr")
mb$classification
MP$Shape <- mb$classification
MP$Shape <- as.factor(MP$Shape)
dev.off
summary(MP$sizeclass)
summary(MP$Shape)
ggplot(MP, aes(x=Shape, y= orientation.A)) +
```

```r
  geom_violin()
pairs(MP[,2:4], pch = 19,  cex = 0.5,
      col = MP$Shape,
      lower.panel=NULL)
ggplot(MP, aes(Shape, orientation.A, colour = Shape, fill=Shape)) +
  geom_violin(alpha = 0.5) +
  labs(x = "Shape",
       y = "Orientation",
       colour = "Shape",
       fill= "Shape") +
  theme_bw(base_size = 10)
#THe clusters picked up on length and width are the clusters on
length/width ratio. They differ in only one specimen.
#Ordination analysis NMDS
com = MP [,c(2:4)]
m_com = as.matrix(com)
NMDS1=metaMDS(m_com, k=2)
NMDS1=metaMDS(m_com,k=2,trymax=100)
stressplot(NMDS1)
plot(NMDS1)
orditorp(NMDS1,display="species",col="red",air=0.01)
ordihull(NMDS1,groups=MP$Shape,draw="polygon",col="lightblue",label=F)
ordihull(NMDS1,groups=MP$sizeclass,draw="polygon",col="lightgreen",label=F
)
a <-as.data.frame(NMDS1$points)
NMDS1.a <- a$MDS1
NMDS2.a <- a$MDS2
MP$NMDS1 <- NMDS1.a
MP$NMDS2 <- NMDS2.a
plot(MP$NMDS1,MP$NMDS2, col=MP$sizeclass)
ggplot(MP, aes(x=Shape, y= orientation.A)) +
  geom_violin()
pairs(MP[,c(2,3,4)], pch = 19,  cex = 0.5,
      col = MP$Shape,
      lower.panel=NULL)
ggplot(MP, aes(Shape, orientation.A, colour = Shape, fill=Shape)) +
  geom_violin(alpha = 0.5) +
  labs(x = "Shape",
       y = "Orientation",
       colour = "Shape",
       fill= "Shape") +
  theme_bw(base_size = 10)
MPShape1 <- subset(MP, Shape == 1)
MPShape2 <- subset(MP, Shape == 2)
shapiro.test(MP$orientation.A)
shapiro.test(log(MP$orientation.A))
shapiro.test(MPShape1$orientation.A)
shapiro.test(log(MPShape1$orientation.A))
shapiro.test(MPShape2$orientation.A)
shapiro.test(log(MPShape2$orientation.A))
wilcox.test(orientation.A ~ Shape, data=MP)
t.test(MPShape1$orientation.A, MPShape2$orientation.A)
#Roseplots for each shape
#2.1 Angular histograms, roseplots and density lines
```

```
par(mfrow=c(1,2))
#Over 180°:
MPShape1 <- subset(MP, Shape == 1)
MPShape2 <- subset(MP, Shape == 2)
control.circ <- circular(MPShape1$orientation.A, units = "degrees",
template = "geographics")
plot.circular(control.circ,stack = TRUE, pch = 20, sep = 0.05, shrink =
1.6) #plots experimental data
lines(density.circular(control.circ, bw=10, fill=red))
rose.diag(control.circ,bins=30, add=TRUE)
control.circ <- circular(MPShape2$orientation.A, units = "degrees",
template = "geographics")
plot.circular(control.circ,stack = TRUE, pch = 20, sep = 0.05, shrink =
1.6) #plots experimental data
lines(density.circular(control.circ, bw=10, fill=red))
rose.diag(control.circ,bins=30, add=TRUE)
dev.off()
summary(MPShape1$LWratio)
summary(MPShape2$LWratio)
#-----------------------------------
#New Dataset: Hofmann 14.
setwd("~/Desktop/MUN PHD/Our papers/MP and Hofmann
paper/Methods/Datasets/H14  dataset")
dir()
H14 <- read.csv("H14.csv")
H14under180 <- read.csv("H14under180.csv")
H14over180 <- read.csv("H14over180.csv")
H14on360 <- read.csv("H14on360.csv")
#Example to explore the dataset
dim(H14under180)
colnames(H14under180) # or names()
head(H14under180)
summary(H14under180)
#1. Morphometric quantitative size-frequency distributions analysis
#1.1 Normality analysis
#Shapiro Wilks test. H0 = Normally distributed.If p-value < alpha (0.05).
H0 rejected. Not normally distributed.
#Logarithmic transformation of the data when required.
#Width
shapiro.test(H14$Width) #Not normal
shapiro.test(log(H14$Width)) #non-Normal after transformation
LOGWIDTH <- log(H14$Width)
H14$LOGWIDTH <- LOGWIDTH
#Length
shapiro.test(H14$Length) #Not normal
shapiro.test(log(H14$Length)) #non-Normal after transformation
LOGLENGTH <- log(H14$Length)
H14$LOGLENGTH <- LOGLENGTH
#Inspection of histograms before and after transformation
#For width:
par(mfrow=c(1,2))
hist(H14$Width, # histogram
     col="white", # column color
     border="black",
```

```
      prob = TRUE, # show densities instead of frequencies
      xlab = "Width",
      ylim=c(0,0.6),
      main = "Non-transformed")
lines(density(H14$Width), # density plot
       lwd = 2, # thickness of line
       col = "chocolate3")
curve(dnorm(x, mean=mean(H14$Width), sd=sd(H14$Width)), add=TRUE,
col="blue")
hist(H14$LOGWIDTH, # histogram
      col="white", # column color
      border="black",
      prob = TRUE, # show densities instead of frequencies
      xlab = "Width",
      ylim=c(0,1.2),
      main = "Transformed")
lines(density(H14$LOGWIDTH), # density plot
       lwd = 2, # thickness of line
       col = "chocolate3")
curve(dnorm(x, mean=mean(H14$LOGWIDTH), sd=sd(H14$LOGWIDTH)), add=TRUE,
col="blue")
dev.off()
#For length:
par(mfrow=c(1,2))
hist(H14$Length, # histogram
      col="white", # column color
      border="black",
      prob = TRUE, # show densities instead of frequencies
      xlab = "Length",
      ylim=c(0,0.37),
      main = "Non-transformed")
lines(density(H14$Length), # density plot
       lwd = 2, # thickness of line
       col = "chocolate3")
curve(dnorm(x, mean=mean(H14$Length), sd=sd(H14$Length)), add=TRUE,
col="blue")
hist(H14$LOGLENGTH, # histogram
      col="white", # column color
      border="black",
      prob = TRUE, # show densities instead of frequencies
      xlab = "Length",
      ylim=c(0,1),
      main = "Transformed")
lines(density(H14$LOGLENGTH), # density plot
       lwd = 2, # thickness of line
       col = "chocolate3")
curve(dnorm(x, mean=mean(H14$LOGLENGTH), sd=sd(H14$LOGLENGTH)), add=TRUE,
col="blue")
dev.off()
#1.2 Size-frequency distributions on mclust
par(mfrow=c(1,2))
#Univariate size-frenquency distribution: Width
gaus1 = Mclust(H14$LOGWIDTH, G=1)
summary(gaus1)
```

```
gaus2 = Mclust(H14$LOGWIDTH, G=2)
summary(gaus2)
gaus3 = Mclust(H14$LOGWIDTH, G=3)
summary(gaus3)
BIC(gaus1,gaus2,gaus3)
mb1 = Mclust(H14$LOGWIDTH)
mb1$modelName
mb1$G
head(mb1$z)
mb1$bic
summary(mb1, parameters = TRUE)
BIC <- mclustBIC(H14$LOGWIDTH)
plot(BIC) #BIC solution for 1 age/size group
#Univariate size-frenquency distribution: Length
gaus1 = Mclust(H14$LOGLENGTH, G=1)
summary(gaus1)
gaus2 = Mclust(H14$LOGLENGTH, G=2)
summary(gaus2)
gaus3 = Mclust(H14$LOGLENGTH, G=3)
summary(gaus3)
BIC(gaus1,gaus2,gaus3)
mb = Mclust(H14$LOGLENGTH)
mb$modelName
mb$G
head(mb$z)
mb$bic
summary(mb, parameters = TRUE)
BIC <- mclustBIC(H14$LOGLENGTH)
plot(BIC) #BIC solution for 1 age/size group
dev.off ()
#Multivariate size-frequency distribution: Length and Width
par(mfrow=c(1,1))
H14 <- H14[,-c(1:5)]
gaus1 = Mclust(H14, G=1)
summary(gaus1)
gaus2 = Mclust(H14, G=2)
summary(gaus2)
gaus3 = Mclust(H14, G=3)
summary(gaus3)
BIC(gaus1,gaus2,gaus3)
mb = Mclust(H14)
mb$modelName
mb$G
head(mb$z)
mb$bic
summary(mb, parameters = TRUE)
BIC <- mclustBIC(H14)
plot(BIC) #BIC solution for 3 age/size group
dev.off()
mb$classification
H14 <- read.csv("H14.csv")
H14$sizeclass <- mb$classification
H14$sizeclass <- as.factor(H14$sizeclass)
ggplot(H14, aes(x=sizeclass, y= Orientation)) +
```

```
  geom_violin()
pairs(H14[,c(2,3,4)], pch = 19,  cex = 0.5,
      col = H14$sizeclass,
      lower.panel=NULL)
ggplot(H14, aes(sizeclass, Orientation, colour = sizeclass,
fill=sizeclass)) +
  geom_violin(alpha = 0.5) +
  labs(x = "Size class",
       y = "Orientation",
       colour = "Size class",
       fill= "Size class") +
  theme_bw(base_size = 15)
#Kruskal-Wallis tets. Non-parametric equivalent to the One-way ANOVA
kruskal.test(Orientation ~ sizeclass, data = H14)
#We corroborate that the disctiction in clustering algorithms are due to
shape-related parameters
#Alternative part of the script: clustering algorithms of mclust on L/W
ratio
LWratio <- (H14$Length/H14$Width)
shapiro.test(LWratio)
shapiro.test(log(LWratio)) #Both non normal. Non normal after logarithmic
transformation.
LogLWratio <- log(LWratio)
H14$LWratio <- LWratio
gaus1 = Mclust(LogLWratio, G=1)
summary(gaus1)
gaus2 = Mclust(LogLWratio, G=2)
summary(gaus2)
gaus3 = Mclust(LogLWratio, G=3)
summary(gaus3)
BIC(gaus1,gaus2,gaus3)
mb = Mclust(LogLWratio)
mb$modelName
mb$G
head(mb$z)
mb$bic
summary(mb, parameters = TRUE)
BIC <- mclustBIC(LogLWratio)
plot(BIC) #BIC solution for 2 age/size group
#plot(mb)
mod3dr <- MclustDR(mb)
summary(mb)
summary(mod3dr)
plot(mb, what = "classification")
plot(mod3dr, what = "classification")
plot(mod3dr, what = "density", type = "persp")
plot(mb, what = "density", type = "persp")
plot(mod3dr, what = "density", type = "hdr")
plot(mb, what = "density", type = "hdr")
mb$classification
H14$Shape <- mb$classification
H14$Shape <- as.factor(H14$Shape)
dev.off
summary(H14$sizeclass)
```

```
summary(H14$Shape)
ggplot(H14, aes(x=Shape, y= Orientation)) +
  geom_violin()
pairs(H14[,2:4], pch = 19,  cex = 0.5,
      col = H14$Shape,
      lower.panel=NULL)
ggplot(H14, aes(Shape, Orientation, colour = Shape, fill=Shape)) +
  geom_violin(alpha = 0.5) +
  labs(x = "Shape",
       y = "Orientation",
       colour = "Shape",
       fill= "Shape") +
  theme_bw(base_size = 10)
ggplot(H14, aes(sizeclass, Orientation, colour = sizeclass,
fill=sizeclass)) +
  geom_violin(alpha = 0.5) +
  labs(x = "Size class",
       y = "Orientation",
       colour = "Size class",
       fill= "Size class") +
  theme_bw(base_size = 15)
#Ordination analysis NMDS
com = H14 [,c(2:4)]
m_com = as.matrix(com)
NMDS1=metaMDS(m_com, k=2)
NMDS1=metaMDS(m_com,k=2,trymax=100)
stressplot(NMDS1)
plot(NMDS1)
orditorp(NMDS1,display="species",col="red",air=0.01)
ordihull(NMDS1,groups=H14$Shape,draw="polygon",col="lightblue",label=F)
ordihull(NMDS1,groups=H14$sizeclass,draw="polygon",col="lightgreen",label=
F)
a <-as.data.frame(NMDS1$points)
NMDS1.a <- a$MDS1
NMDS2.a <- a$MDS2
H14$NMDS1 <- NMDS1.a
H14$NMDS2 <- NMDS2.a
plot(H14$NMDS1,H14$NMDS2, col=H14$sizeclass)
ggplot(H14, aes(x=Shape, y= Orientation)) +
  geom_violin()
pairs(H14[,c(2,3,4)], pch = 19,  cex = 0.5,
      col = H14$Shape,
      lower.panel=NULL)
ggplot(H14, aes(Shape, Orientation, colour = Shape, fill=Shape)) +
  geom_violin(alpha = 0.5) +
  labs(x = "Shape",
       y = "Orientation",
       colour = "Shape",
       fill= "Shape") +
  theme_bw(base_size = 10)
H14Shape1 <- subset(H14, Shape == 1)
H14Shape2 <- subset(H14, Shape == 2)
shapiro.test(H14$Orientation)
shapiro.test(log(H14$Orientation))
```

```
shapiro.test(H14Shape1$Orientation)
shapiro.test(log(H14Shape1$Orientation))
shapiro.test(H14Shape2$Orientation)
shapiro.test(log(H14Shape2$Orientation))
wilcox.test(Orientation ~ Shape, data=H14)
#Roseplots for each shape
#2.1 Angular histograms, roseplots and density lines
par(mfrow=c(1,2))
#Over 180°:
H14Shape1 <- subset(H14, Shape == 1)
H14Shape2 <- subset(H14, Shape == 2)
control.circ <- circular(H14Shape1$Orientation, units = "degrees",
template = "geographics")
plot.circular(control.circ,stack = TRUE, pch = 20, sep = 0.05, shrink =
1.6) #plots experimental data
lines(density.circular(control.circ, bw=10, fill=red))
rose.diag(control.circ,bins=30, add=TRUE)
control.circ <- circular(H14Shape2$Orientation, units = "degrees",
template = "geographics")
plot.circular(control.circ,stack = TRUE, pch = 20, sep = 0.05, shrink =
1.6) #plots experimental data
lines(density.circular(control.circ, bw=10, fill=red))
rose.diag(control.circ,bins=30, add=TRUE)
dev.off()
summary(H14Shape1$LWratio)
summary(H14Shape2$LWratio)
#Visualize a dissimilarity matrix (E.g., MP)
dist_m <- as.matrix(dist(MP [,c(2:3)]))
dist_mi <- 1/dist_m
library(qgraph)
qgraph(dist_mi, layout='spring', vsize=3)
qgraph(dist_mi, layout='spring', vsize=3, groups= MP$sizeclass, alpha=0.5)
library(factoextra)
# Correlation-based distance method
res.dist <- get_dist(MP [,c(2:3)], method = "pearson")
fviz_dist(res.dist, lab_size = 2)
res.dist <- dist(MP [,c(2:3)], method = "euclidean")
# Compute hierarchical clustering
res.hc <- hclust(res.dist, method = "ward.D2")
# Visualize
plot(res.hc, cex = 0.5)
library("factoextra")
# Enhanced k-means clustering
res.km <- eclust(MP [,c(2,3,4,7)], "kmeans", nstart = 25)
fviz_gap_stat(res.km$gap_stat)
res.hc <- eclust(MP [,c(2,3,4,7)], "hclust") # compute hclust
fviz_dend(res.hc, rect = TRUE) # dendrogam
```

Appendix D – Data for E surface retrodeformed *F. misrai* specimens (282)

Specimen#	Length	Width	OrientationA
2	15.09371	2.012202	62.53136
3	5.67214	1.631946	15.55018
4	3.366559	0.642616	36.68044
5	5.191683	0.71614	68.25172
6	5.676832	0.625048	71.21732
7	4.819851	0.897354	38.65853
8	6.264238	0.970377	59.78552
9	12.52356	1.055718	86.80202
10	7.348345	1.340289	29.36874
11	4.78986	0.594747	59.78552
12	10.97212	1.857434	176.2416
13	7.31014	0.96922	47.26947
15	9.591431	1.112149	52.03251
16	4.116784	1.986713	152.3258
17	5.746855	1.237518	15.55018
18	14.99944	2.822079	52.03251
19	5.083827	0.733212	54.53522
20	6.48233	1.159016	42.81821
21	6.478482	0.541686	125.4648
22	3.978087	1.442207	152.3258
23	15.04322	1.363113	83.61613
24	6.804	2.26	24.42228
27	3.228149	0.985139	12.81563
28	10.4941	1.423463	49.61102
29	5.866981	0.789578	93.19798
30	10.11145	2.086743	21.3328
31	5.816415	1.734201	168.5208
32	7.496215	0.918566	27.67419
33	6.143368	0.837443	105.755
34	8.499984	1.186457	57.11968
35	3.643836	0.53394	62.53136
36	8.395279	1.168199	99.54593
37	6.69307	0.811941	62.53136
39	4.282422	0.775941	80.45407
40	8.302194	0.863429	108.7827
41	7.060932	0.875617	49.61102
42	19.05755	1.643613	105.755
43	5.194654	0.816145	80.45407

44	3.749773	0.820281	54.53522
45	8.700023	2.482354	153.9736
46	5.071118	1.3267	31.11331
47	3.866593	0.425341	114.6453
50	5.351647	0.677913	134.994
51	8.95821	1.32045	49.61102
52	7.610976	1.025329	93.19798
53	2.9145	1.257622	160.1583
54	5.687958	1.350479	167.1844
55	5.62	0.693	139.2966
56	8.118588	0.961974	62.53136
57	7.847859	0.967135	71.21732
58	7.518184	0.667281	71.21732
59	8.380404	1.487462	12.81563
61	7.175111	0.677545	68.25172
62	5.294686	0.931725	29.36874
63	5.258709	0.456116	71.21732
64	7.888695	1.8193	15.55018
65	8.701622	1.043363	74.24501
66	6.784029	0.952204	83.61613
68	7.327013	0.781342	111.7483
69	13.135	4.813554	161.6174
70	15.50387	1.851361	54.53522
71	10.42838	1.032577	62.53136
72	2.416318	0.536462	38.65853
73	12.50953	1.273625	49.61102
74	22.00563	2.467117	42.81821
76	8.02687	0.798863	137.1818
77	11.95968	1.475689	59.78552
79	5.326265	1.680059	2.502477
80	3.465164	1.283402	167.1844
81	3.337954	0.797198	29.36874
82	8.812807	0.634774	108.7827
83	16.88647	2.085814	111.7483
84	7.259631	0.943546	59.78552
85	5.969823	0.875617	49.61102
86	7.7446	0.896889	83.61613
87	10.6275	1.556181	59.78552
88	9.136437	0.997078	137.1818
89	3.983837	1.01128	8.857167
90	8.72431	0.988251	71.21732
91	7.589009	0.869465	57.11968
92	5.969466	0.97038	65.35469

93	10.7163	1.202198	77.32696
94	9.19096	1.05741	65.35469
95	4.372726	0.79469	26.02642
96	9.296368	1.456193	47.26947
97	7.570216	0.844787	68.25172
100	10.56099	0.949599	114.6453
101	9.219728	1.068538	127.9675
102	3.381566	0.555969	38.65853
103	7.8564	0.813732	77.32696
104	11.1381	1.015543	114.6453
105	2.928585	0.848675	21.3328
106	6.23724	0.960034	57.11968
107	4.525321	0.926743	29.36874
108	6.25741	1.020583	34.76578
109	5.937006	1.440892	32.9112
110	6.392803	1.50518	171.1428
111	4.741569	0.70086	111.7483
112	11.69942	1.216309	71.21732
113	10.39638	1.025305	90
114	13.49918	1.631397	54.53522
116	4.338645	1.432764	27.67419
117	6.472059	0.925417	8.857167
118	18.56204	1.222154	68.25172
119	9.308287	1.474175	34.76578
120	4.781418	1.428146	161.6174
121	7.772401	1.519407	26.02642
122	7.284578	0.552127	102.673
123	7.322956	0.933838	99.54593
124	11.53103	1.746049	77.32696
125	8.524339	2.075033	8.857167
126	3.234183	0.734665	179.375
127	7.074092	2.24088	164.4498
128	2.512884	0.407788	52.03251
129	7.176314	0.746349	99.54593
130	3.74384	1.126042	29.36874
131	11.29625	1.640582	47.26947
132	8.016039	1.053416	38.65853
133	6.922942	1.0144	38.65853
134	7.289821	0.930017	90
135	7.653101	0.723637	96.38387
136	4.497978	1.220797	167.1844
137	13.25697	1.602499	27.67419
138	3.252797	0.701218	45.00599

139	10.7	1.44	139.2966
140	10.60106	1.382997	105.755
141	9.748372	1.526477	38.65853
143	16.55303	1.575815	86.80202
144	6.818595	0.715551	122.8803
145	4.772099	0.631052	31.11331
146	2.809229	0.995503	157.1413
147	10.74374	1.163918	114.6453
148	2.275895	1.015431	152.3258
149	12.51315	1.299896	83.61613
150	10.83018	1.64042	52.03251
151	11.81929	0.708944	96.38387
152	5.036805	0.634435	45.00599
153	8.328823	0.806533	54.53522
154	3.772211	1.597507	143.3196
155	8.819438	1.345194	45.00599
156	6.174553	1.853944	173.7111
157	10.13146	1.330338	71.21732
158	12.04103	1.385709	57.11968
159	3.943753	1.315377	145.2342
160	9.048	1.72	24.42228
161	8.16186	0.681719	74.24501
162	3.913463	1.370184	145.2342
163	5.610064	1.544398	22.85872
164	7.184725	0.875818	52.03251
165	7.147726	1.854277	22.85872
166	8.18658	1.007741	68.25172
167	5.231834	0.557395	134.994
168	5.882405	0.797554	127.9675
169	5.022298	1.008689	18.3826
170	9.468178	1.214383	54.53522
171	3.973318	1.182305	3.758368
172	5.524889	1.833555	145.2342
174	7.97226	1.278005	21.3328
175	4.114928	1.740929	157.1413
176	5.491578	0.650806	34.76578
177	6.486705	0.899524	90
178	6.789545	0.979913	105.755
179	5.22588	0.976854	74.24501
180	11.10057	1.170548	65.35469
181	5.896494	0.652622	74.24501
182	9.507959	1.044866	47.26947
183	3.112573	0.860846	10.16045

184	4.313991	0.829721	177.4975
185	7.205008	0.839679	74.24501
187	14.65697	1.537505	77.32696
189	3.207998	1.167791	7.567311
190	5.415494	1.967091	152.3258
191	4.160772	1.261929	169.8395
192	16.77695	1.664267	77.32696
193	7.319823	1.139779	42.81821
194	4.518499	1.342724	160.1583
195	5.173526	1.170885	29.36874
196	13.83391	1.41892	77.32696
197	10.815	1.845141	177.4975
198	4.550206	0.591152	54.53522
199	8.83351	1.040824	127.9675
200	6.096304	0.808169	111.7483
201	9.86627	1.648856	16.95294
202	9.379248	0.800661	122.8803
203	4.797312	0.629456	57.11968
204	4.820532	1.207108	10.16045
205	7.101005	1.015061	32.9112
206	5.528974	1.206744	14.17186
207	2.703376	0.491922	31.11331
208	5.175879	0.874805	171.1428
209	11.55581	1.488299	45.00599
210	7.365984	1.101306	42.81821
212	4.085975	0.966387	168.5208
213	5.015991	1.500326	168.5208
214	5.209874	0.92176	29.36874
215	11.94065	1.224756	71.21732
216	9.278034	1.083614	77.32696
217	9.372859	1.010361	93.19798
218	3.849659	1.200261	168.5208
219	3.782247	0.928497	177.4975
220	10.46812	0.939443	74.24501
222	6.290097	0.7608	38.65853
224	8.611346	2.2383	11.47923
225	5.160261	1.320677	5.019864
226	8.193783	1.533339	34.76578
227	10.10212	1.021187	80.45407
229	12.58659	1.238739	38.65853
230	9.860416	2.03894	163.0471
231	6.082776	0.668268	122.8803
232	12.06126	1.119173	71.21732

233	4.367167	0.478035	74.24501
234	6.784029	0.699336	83.61613
235	4.084439	1.373815	158.6672
236	7.894602	0.872192	105.755
238	6.968362	0.801392	45.00599
239	6.990202	0.974849	59.78552
240	7.603127	1.280326	36.68044
241	4.48413	0.668583	40.70339
242	6.230776	1.203122	27.67419
243	8.306019	0.900756	65.35469
244	10.76273	1.254384	57.11968
245	8.450564	1.855604	8.857167
246	11.28594	0.947756	74.24501
247	3.027272	0.739712	22.85872
248	4.489707	0.807098	32.9112
249	2.624585	0.769471	157.1413
250	9.088533	0.940778	80.45407
251	7.010059	0.951381	96.38387
252	8.548175	1.030138	49.61102
253	4.357133	1.157757	31.11331
254	5.899297	0.937392	57.11968
255	4.729897	0.950692	16.95294
256	7.016205	0.546042	108.7827
257	3.400346	0.49133	45.00599
258	5.439212	0.701218	45.00599
259	6.112348	0.643042	57.11968
260	3.539408	0.611176	31.11331
261	4.288261	1.054931	177.4975
262	2.146904	0.375873	71.21732
263	3.55	0.387	139.2966
264	13.7234	1.643832	57.11968
265	5.822986	0.908411	127.9675
266	4.537519	0.587726	96.38387
267	5.984123	1.725375	168.5208
268	5.941823	0.705173	127.9675
269	22.91639	2.470628	71.21732
270	5.410636	2.184146	15.55018
271	5.585487	1.322529	10.16045
272	12.92406	1.859171	36.68044
273	6.107618	0.411445	137.1818
274	7.715489	1.538942	42.81821
275	5.714919	0.477527	96.38387
276	9.266685	1.085259	108.7827

277	8.055205	1.257135	147.0888
278	5.101115	1.658154	153.9736
279	6.834719	1.078254	31.11331
280	4.952271	0.482072	134.994
281	3.164817	0.961471	14.17186
282	3.135927	0.464563	71.21732
283	10.35859	1.054742	120.2145
284	6.910968	0.639623	42.81821
285	4.98819	0.617455	77.32696
286	5.902692	0.568386	77.32696
287	10.03603	1.409431	38.65853
288	6.224881	0.642994	47.26947
290	5.24861	0.498856	127.9675
291	3.864905	0.366256	62.53136
292	8.228083	0.57628	93.19798
293	9.897014	1.040138	47.26947
294	3.722481	0.959	31.11331
295	6.566134	0.583166	90
296	8.756668	0.772603	49.61102
297	3.453733	0.7697	26.02642
298	6.348137	0.652849	114.6453
299	11.13979	1.428325	86.80202
300	5.29837	1.192548	8.857167
301	4.8	0.645	139.2966
302	10.70407	0.983388	105.755
303	2.029428	0.697548	145.2342
304	3.468488	0.463396	52.03251
306	5.717036	0.506796	71.21732
307	4.399273	0.468722	99.54593